تحضير ودراسة بعض أكاسيد المعادن الثانوية وثرايتاتها

مقدمة من

زينة محمد علي عباس رسول البنا

وهي جزء من متطلبات نيل شهادة الماجستير علوم الفيزياء
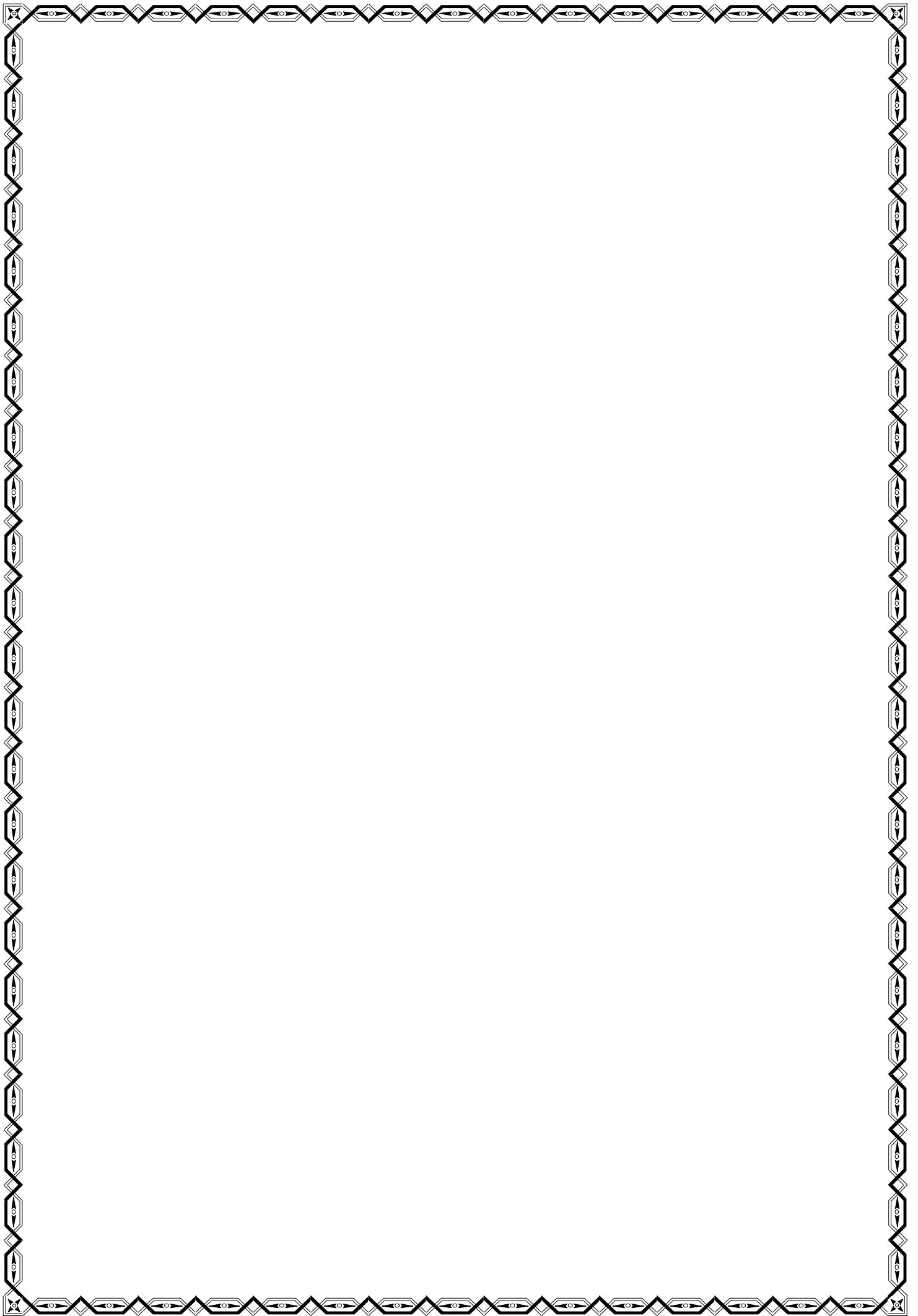
إشراف

أستاذ المساعد   أستاذ المساعد

د.كريم منيكش حسن   د. تحسين حسين مبارك

1433 هـ   2012 م

بسم الله الرحمن الرحيم

لَقَدْ أَرْسَلْنَا رُسُلَنَا بِالْبَيِّنَاتِ وَأَنزَلْنَا مَعَهُمُ الْكِتَابَ وَالْمِيزَانَ لِيَقُومَ النَّاسُ بِالْقِسْطِ وَأَنزَلْنَا الْحَدِيدَ فِيهِ بَأْسٌ شَدِيدٌ وَمَنَافِعُ لِلنَّاسِ وَلِيَعْلَمَ اللَّهُ مَن يَنصُرُهُ وَرُسُلَهُ بِالْغَيْبِ إِنَّ اللَّهَ قَوِيٌّ عَزِيزٌ .

صدق الله العظيم

بسم الله الرحمن الرحيم

لَقَدْ أَرْسَلْنَا رُسُلَنَا بِالْبَيِّنَاتِ وَأَنزَلْنَا مَعَهُمُ الْكِتَابَ وَالْمِيزَانَ لِيَقُومَ النَّاسُ بِالْقِسْطِ وَأَنزَلْنَا الْحَدِيدَ فِيهِ بَأْسٌ شَدِيدٌ وَمَنَافِعُ لِلنَّاسِ وَلِيَعْلَمَ اللَّهُ مَن يَنصُرُهُ وَرُسُلَهُ بِالْغَيْبِ إِنَّ اللَّهَ قَوِيٌّ عَزِيزٌ .

صدق الله العظيم

الآية 25(سورة الحديد)

Contents

List of Symbols

Symbol	Definition	Unit
H	Magnetic field	A/m
B	Magnetic Flux density	T
μ_0	Absolute vacuum permeability	-
μ	Relative permeability	-
d	Density	g/cm^3
N	Number of turns	-
ρ	Resistivity	Ω.cm
λ	Wavelength	Å
d	Interplaner spacing	Å
D	Crystallite size	nm
β	Full width at half maximum	rad
θ	Diffraction angle	degree
P	Porosity	%
R	Electrical resistance	Ω
A	Area	m^2
ℓ	Thickness	m
E	Electron energy	eV
T	Temperature	°C
k	Boltzmann constant	eV .k^{-1}
N	Avogadro's number	mol^{-1}
M	Molecular weight	g/mol
a	Lattice constant	Å
n	Integer	-
(hkl)	Miller indices	-
D	Bulk density	g/cm^3
*D*x	X-ray density	g/cm^3
n_D	Refractive index	-
N1	Number of turns in primary coils	-
N2	Number of turns in secondary coils	-
L	Inductance of a coil	H
I	Current	A
ϕ	Induced magnetic flux	Wb
F	Load hanging	Kg
ρ_o	Constant	-
J	Magnetic polarization	T
Br	Remnant flux density	T

List of Abbreviations

SEM	Scanning electron microscope
XRD	X-ray diffraction
TEM	Transmission electron microscope
TMAH	Tetramethylammonium hydroxide
CTAB	Hexadecy trimethylammonium bromide
TGA	Thermo-gravimetric analysis
EDS	Energy dispersive spectrometry
MPS	Methacryloxy propyltrimethoxy silane
PL	Photoluminescence
FWHM	Full Width at Half Maximum
PM	Powder Metallurgy
V.H	Vickers Hardness
ICDD	International Centre for Diffraction Data
JCPDS	Joint Committee on Powder Diffraction Standards

List of Figures

List of Tables

ACKNOWLEDGEMENT

Praise is for almighty Allah, the most merciful and compassionate ,the creator of the universe, who enable me to complete this research successfully .

I offer my humblest and sincerest words of thanks to the prophet Muhammad (peace be upon him) who is forever a torch of guidance and knowledge for the humanity.

I express my sincere thanks to my supervisor, Dr. **Tahseen H. Mubarak** in the Department of Physics, for his esteemed supervision, incessant support, inspiration and constructive criticism throughout my project work.

I would like to thank my supervisor, Dr. **karim H.Hassan**, for his guidance through my graduate studies including this thesis. His knowledge, patience, and enthusiasm for research proved to be very valuable in assisting me in this endeavor.

Finally I would also express my deep sense of gratitude to my parents and family especially my brother Ahssan for their unlimited encouragement and support.
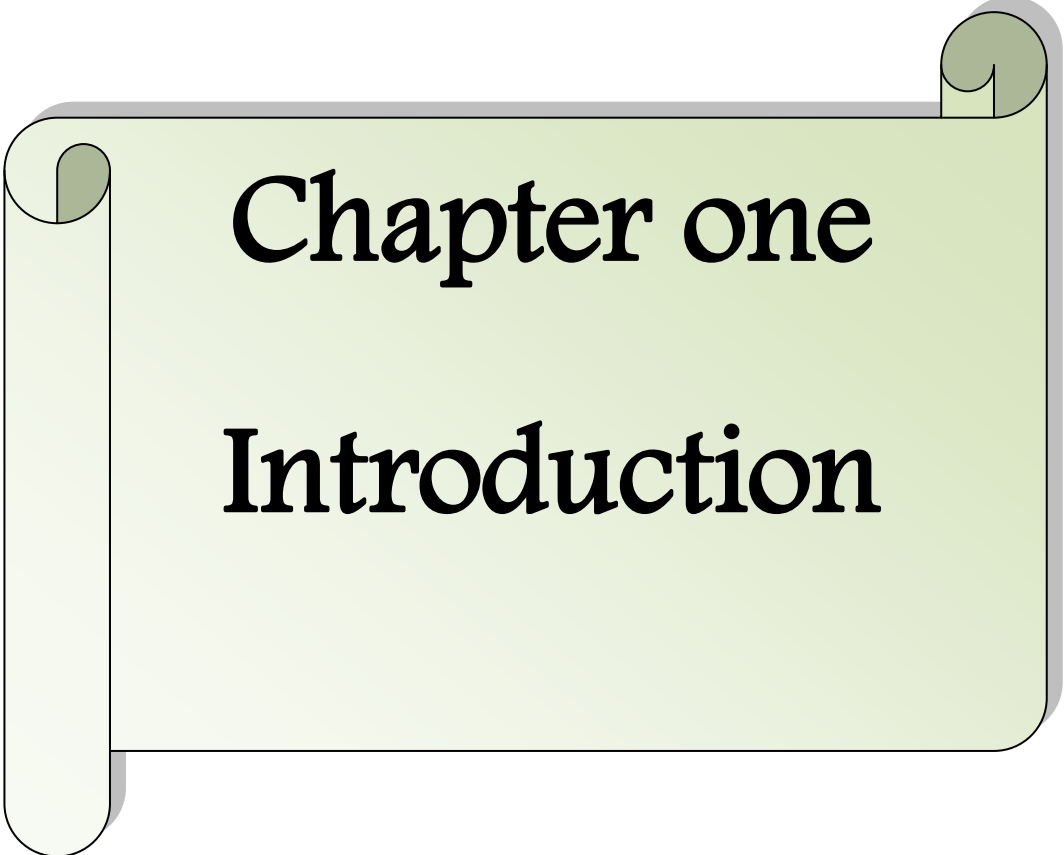
Dedication

I would like to dedicate my thesis to my family: parents, brothers and sisters.

Zena

2012

Chapter one

Introduction
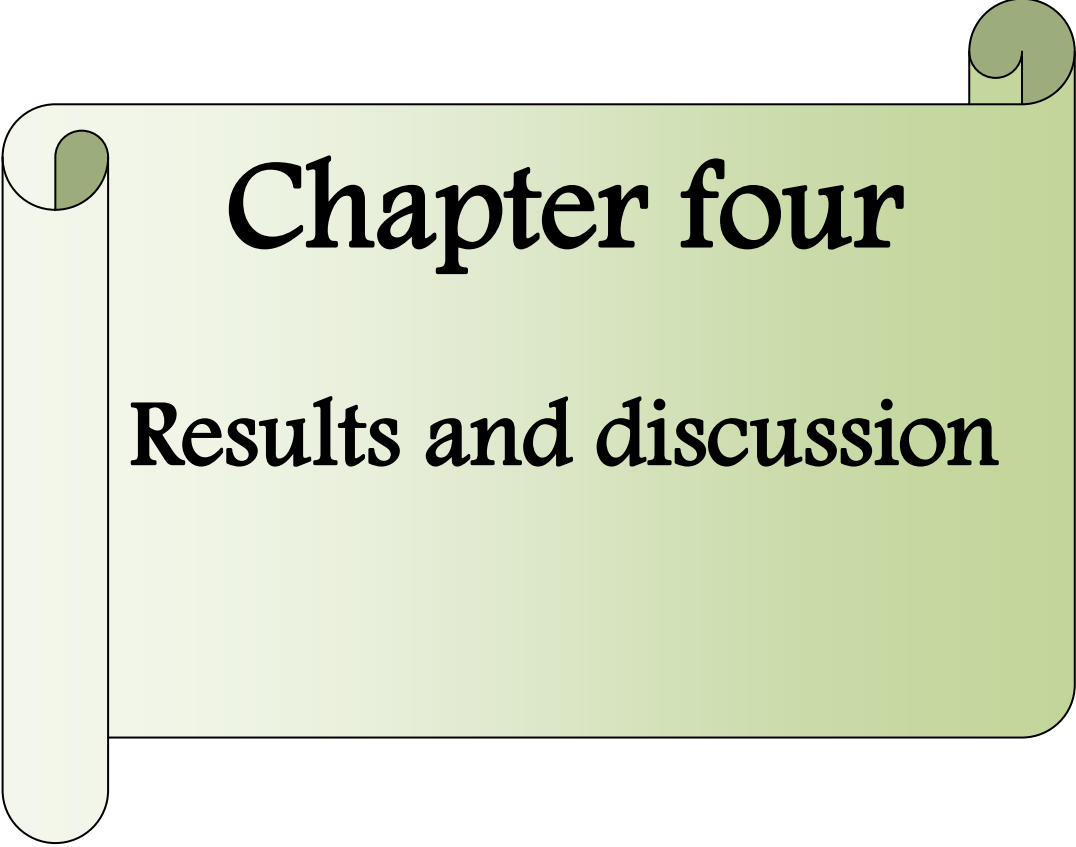
Chapter two

Theoretical part

Chapter three

Experimental part

Chapter four

Results and discussion

References

1-1 Introduction

Today, magnetic materials are found in numerous products around us- home appliances, electronic products, automobiles, communication equipments and data processing devices and equipments. These materials have now become a vital part of everyday life in modern industries. The magnetic materials used in early applications were metallic magnetic materials, but for frequencies exceeding MHz, metals and alloys are generally not suitable as soft magnets, as the eddy current losses are very high.

According to George G.Orenchak's work, "Measuring soft ferrite core properties", soft ferrites are ceramic electromagnetic (magnetically soft) material primarily used as cores for high frequency inductors and transformers. Using ferrite is not a new concept before Christ was born, ferrite gained attention because it attracted iron. Quantities of ferrite were first discovered in Asia, in the magnesia region; ferrite's first name magnetite, came from this region. Commercial use of ferrite did not begin until the 1940s, and it is still used today. Ferrite has distinct properties which make it valuable and useful [1].

The development of ferrites since 1946 reported that electrical resistivities of ferrites over a million times those of metals and has an enormous impact in the application of magnetic materials particularly at high frequencies. Ferrites are used today in radio , television, microwave ,satellite communication, bubble devices, audio, video ,digital recording and as permanent magnets [2].

Powder metallurgy (PM) products are today used in a wide range of industries, from automotive and aerospace applications to power tools and household appliances. Each year the international PM awards highlight the developing capabilities of the technology, as well as the less influence of the PM companies activity than of the traditional, especially metallurgical, ones on the ecological system. As PM applications cover very diversified domains of the

modern industry, their development continuously stimulate the research efforts for PM progress [3].

In the last two decades, new terms with the prefix "nano" have rushed into the scientific vocabulary nanoparticle, nanostructure, nanotechnology, nanomaterial, nanocluster, nanochemistry, nanocolloids, nanoreactor and so on. A series of new journals are devoted particularly to this subject, monographs with the corresponding names have appeared, "nano"-specialized institutes, chairs and laboratories have been founded; and numerous conferences are held. In most cases new names were applied to long known objects or phenomena; however, new objects inaccessible to researchers some 20 years ago have also appeared these include fullerenes, quantum dots, nanotubes, nanofilms and nanowires, i.e., the objects with at least one nanometer (10^{-7}-10^{-9}m) dimension. The enhanced interest of the researchers in nanoobjects is due to the discovery of unusual physical and chemical properties of these objects, which is related to the manifestation of the so-called "quantum size effects", these arise in the case where the size of the system is commensurable with the de-Broglie wavelengths of the electrons, phonons or exciting propagating in them [4].

The research of nanocrystalline magnetic materials has undergone a huge development in the last years. This is due to the properties common to both amorphous and crystalline materials and the ability of these alloys to compete with their crystalline counterparts. The benefits found in the nanocrystalline alloys stem from their chemical and structural variations on a nanoscale, which are important for developing optimal magnetic properties. It is well known that the microstructure, especially the crystallite size, essentially determines the hysteresis loop of the soft ferromagnetic materials. The reduction of crystallite size to the dimensions of the domain wall width increases the coercivity towards an extreme value controlled by the anisotropy. However, the lowest coercivity is found again for crystallite smaller than the correlation lengths like in amorphous and nanocrystalline alloys [5].

Metal oxides are of interest to many scientific and technological disciplines. In particular, nanostructures of these materials have attracted considerable interest as they exhibit materials properties that differ strongly from those of the bulk phases. These particle size effects enable tailoring the materials to a wide range of applications including magnetic ferrofluids, electronics and catalysis. Typical metal oxides of interest include semiconducting or metallic oxides of the type ZnO, TiO_2, NiO, Fe_2O_3, doped Fe_2O_3 and Cr_2O_3 [6].

Ferrite nanoparticles are very important magnetic materials because of their high electric resistivity. They have wide applications in technology. Particularly at high frequencies. Ferrite nanoparticles are widely used due to the following properties [7]:

1. High frequencies application.
2. High coercivity in selective ferrites.
3. Mechanical stiffness.
4. Wide selection of materials.
5. Cheap to assemble.

1-3 Aims of the research

The manufacturing of electrical converter using powder metallurgy can be considered as complex subject due to the several variables which include, for example, selection of raw materials, purity and grain size. There are many researches that have been used to study ferrites iron-nickel, iron-silicon, and so on, but the researches on iron-zinc and iron-zinc –copper in our country are limited and due to the significance of core-industrial in electrical converters, barometer and computer devices...etc, this work has been done and included:

1. Preparation of nanomaterials such as (ZnO), (CuO)and (Fe_2O_3) in a chemical process.

2. Preparing compacted-materials of $(ZnO)_x(Fe_2O_3)_{1-x}$, $(ZnO)_x(CuO)_{1-x}(Fe_2O_3)$ by using powder metallurgy at different weight ratios (x=0, 0.2, 0.4, 0.6, 0.8, 1).

3. Studying the effect of time and temperature of sintering on crystal size , electric and magnetic properties (hystersis loop) for materials being prepared by using precipitation method.

4. Studying the effect of different ratios of pure zinc oxide-and copper oxide powder added on magnetic properties and nanostructure of prepared materials.

5. Prepare and study the magnetic and electric properties of compacted: $[(ZnO)_x(Fe_2O_3)_{1-x}]$ and $[(ZnO)_x (CuO)_{1-x}(Fe_2O_3)]$

6. Studying the effect of density ,porosity and hardness for all the models prepared.

1-4 Outline of the thesis

1. The first chapter includes an introduction to the research, a historical background, literature review, the aims of the research and outline of the thesis.

2. Chapter two contains a detailed description of magnetic materials and their properties and ferrites and how they work and nanotechnology.

3. Chapter Three includes the experimental part from to the selection of raw materials and their methods of preparation and the compaction models of sintering at different temperatures and testing of syntheses (X-ray diffraction, scanning electron microscope) and mechanical (measuring density, porosity, hardness test) and electrical measurements (electrical resistivity) and tests of magnetic (hysteresis loop).

4. Chapter four contains the extracted results and discusses the synthetic tests, mechanical, electrical and magnetic influence and change the various transactions such as temperature, mole fraction and size.

2-1 Introduction

This chapter shows the theoretical part which includes the explanation of nanotechnology and it contains explanation methods of preparation of nanomaterials and shows the properties of oxides (ZnO,CuO,Fe_2O_3) in addition to studying ferrites and explaining their (Structure, Electrical and Magnetic) properties.

2-2 Nanotechnology

One of the most exciting and fastest growing area in science and engineering today is nanotechnology, materials science and electronics to create new function systems of nanoscale dimensions of the order of a billionth of a meter, nanotechnology refers to the study manipulation and utilization of nano size materials (sizes of atoms and molecules). Materials whose crystallites, particle sizes are smaller than 100 nm are commonly named nanocrystalline, nanostructured, nanosized materials [5].

The progress of technology and quality of life of mankind have always been closely knit with the progress in material science and material processing technology. Most material processing techniques are based on breaking up a large chunk of material into desired shapes and sizes, inducing strain, lattice defects and other deformations in the processed material. Recent developments in nanotechnology and the demonstration of various quantum size effects in nanoscale particles imply that most of the novel devices of the future will be based on the properties of nanomaterials , each nanoparticle contains only about $3-10^7$ atoms/molecules. Lattice defects and other imperfections induced by the traditional material processing techniques will no longer be diluted by sheer number of atoms, when used for synthesizing nanoparticles. Furthermore, it is difficult to achieve size selective synthesis of such small particles, by using the traditional approach. The alternative synthetic technique for nanoparticles involves controlled precipitation of nanoparticles from precursors dissolved in a solution [30]. Nanoparticle preparation and study of nanoparticle are important in the recent research. The characters of metal nano particles like optical,

electronic, magnetic, and catalytic depend on their size, shape and chemical surroundings . In nanoparticle preparation, it is very important to control the particle size, particle shape and morphology [31].

Nanomaterials and nanoparticles are used in a broad spectrum of applications. Today they are contained in many products and used in various technologies. Most nanoproducts produced on an industrial scale are nanoparticles, although they also arise as by products in the manufacture of other materials.

2-3 Production of nanoparticles and nanomaterials

Two basic strategies are used to produce nanoparticles: "top-down" and "bottom -up". The term "top-down" refers here to the mechanical crushing of source material using a milling process. In the "bottom-up" strategy, structures are built up by chemical processes [32].The selection of the respective process depends on the chemical composition and the desired features specified for the nanoparticles, this is shown in Figure (2-1).
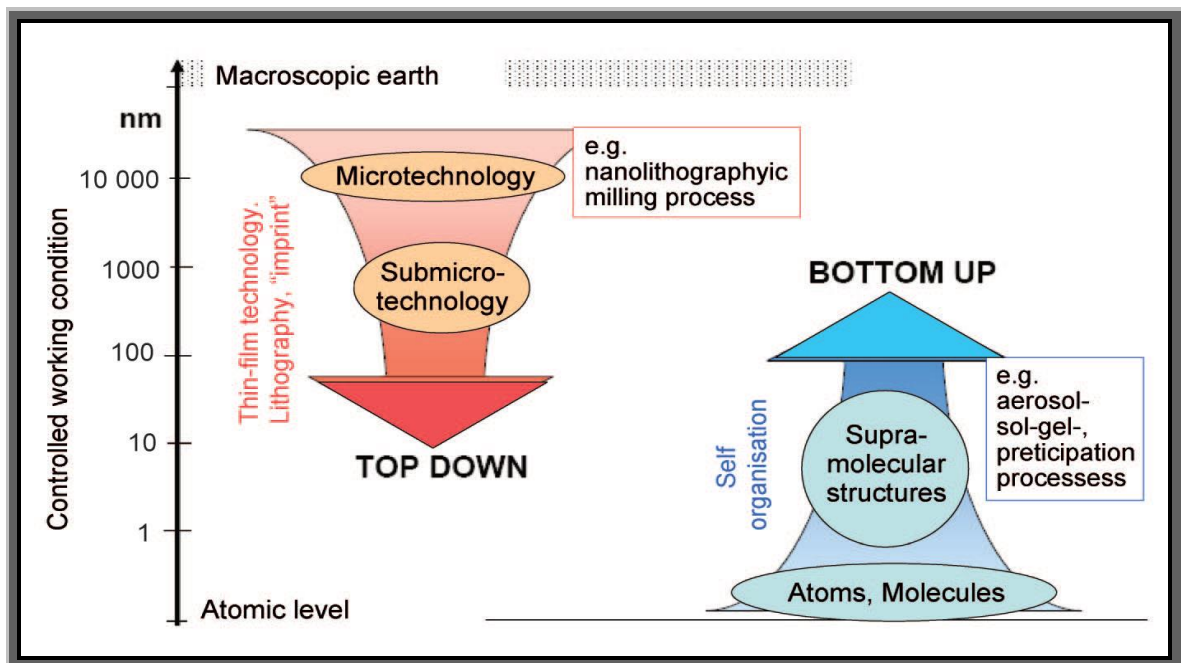
Figure (2-1) Methods of nanoparticle production [33].

"Top-down" refers to mechanical-physical particle production processes based on principles of microsystem technology.The traditional mechanical-physical crushing methods for producing nanoparticles involve various milling techniques [32]. This method does not allow full control of particle shape and is shown in Figure (2- 2).
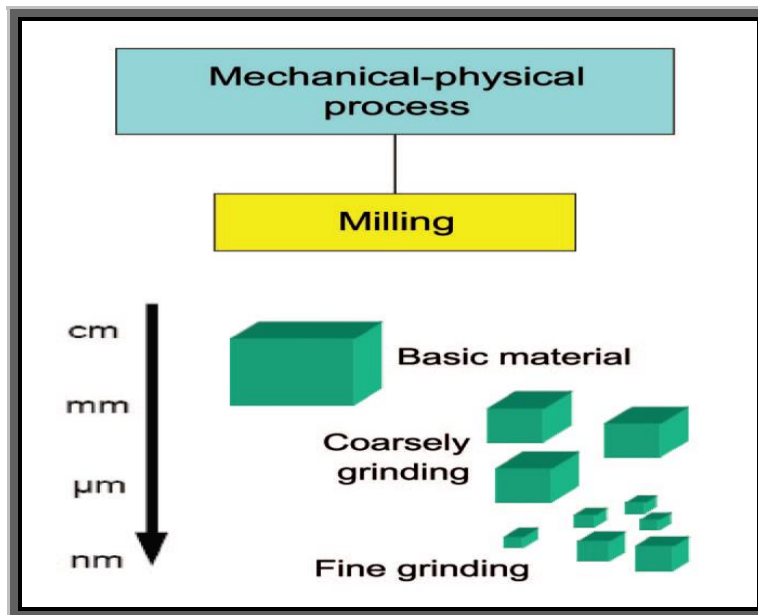
Figure (2-2) Mechanical-physical nanoparticle production processes [33].

Bottom-up methods are based on physicochemical principles of molecular or atomic self-organization. This approach produces selected, more complex structures from atoms or molecules, better controlling of shapes and size ranges. It includes aerosol precipitation reactions and sol-gel processes [32].

2-3-1 Precipitation processes

The precipitation of solids from a metal ion containing solution is one of the most frequently employed production processes for nanomaterials. Metal oxides as well as non-oxides or metallic nanoparticles can be produced by this approach, the process is based on reactions of salts in solvents. A precipitating agent is added to yield the desired particle precipitate, and the precipitate is filtered out and thermally post-treated. In precipitation processes, particle size , size distribution, crystallinity and morphology (shape) are determined by

reaction kinetics (reaction speed). The influencing factors include, beyond the concentration of the source material, the temperature, pH value of the solution, the sequence in which the source materials are added, and mixing processes [33]. Chemo-physical methods is shown in Figure (2-3).
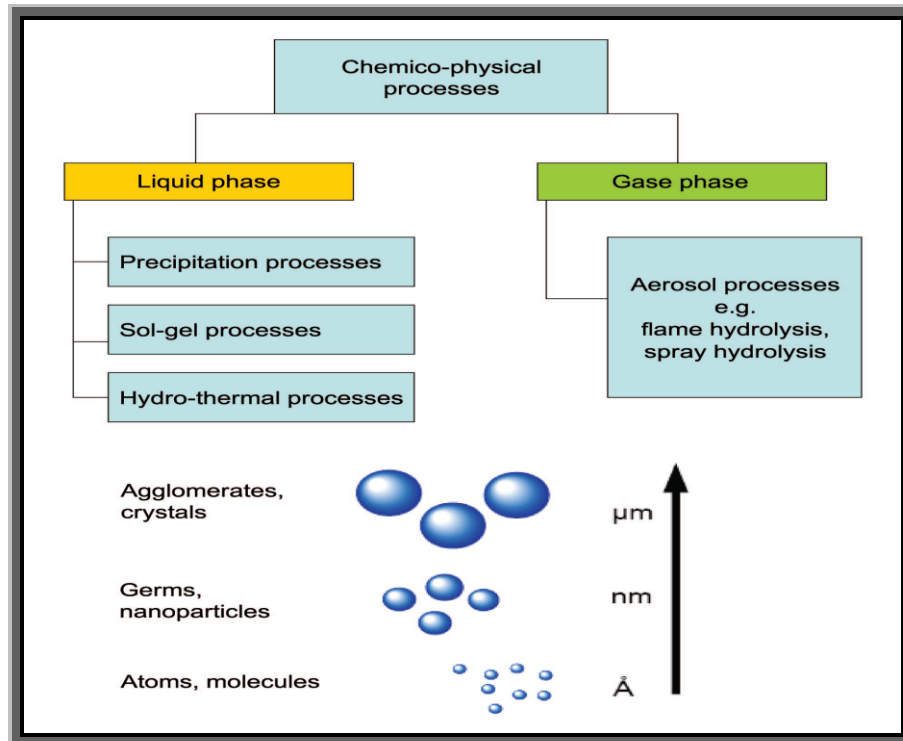
Figure (2-3) Chemo-physical processes in nanoparticle production [33].

2-4 Nanomaterials

In the materials world, particularly in ceramics, the trend is always to prepare finer powder for the ultimate processing and better sintering to achieve dense materials with dense fine-grained microstructure of the particulates with better and useful properties for various applications. The fineness can reach up to a molecular level **(1 nm – 100 nm),** by special processing techniques. More is the fineness, more is the surface area, which increases the 'reactivity' of the material. So, the densification or consolidation occurs very well at lower temperature than that of conventional ceramic systems, which is finally' cost-effective' and also improves the properties of materials like abrasion resistance,

18

corrosion resistance, mechanical properties, electrical properties, optical properties, magnetic properties, and a host of other properties for various useful applications in diverse fields [34].

Nanoparticle is a quasi-zero-dimensional (0D) nano-objection in which all characteristic linear dimensions are of the same order of magnitude (not more than 100 nm). Nanoparticles can basically differ in their properties from larger particles, for example,from long- and well-known ultra dispersed powders with a grain size above 0.5 mm. As a rule, nanoparticles are shaped like spheroids. Nanoparticles with a clearly ordered arrangement of atoms (or ions) are called nanocrystallites and nanoparticles with a clear-cut discontinuity of the system of electronic energy levels are often referred to as "quantum dots" or "artificial atoms"(most often, they have compositions of typical semiconductor materials) [4]. Figure (2-4) shows ZnO nanoparticles .

A   B
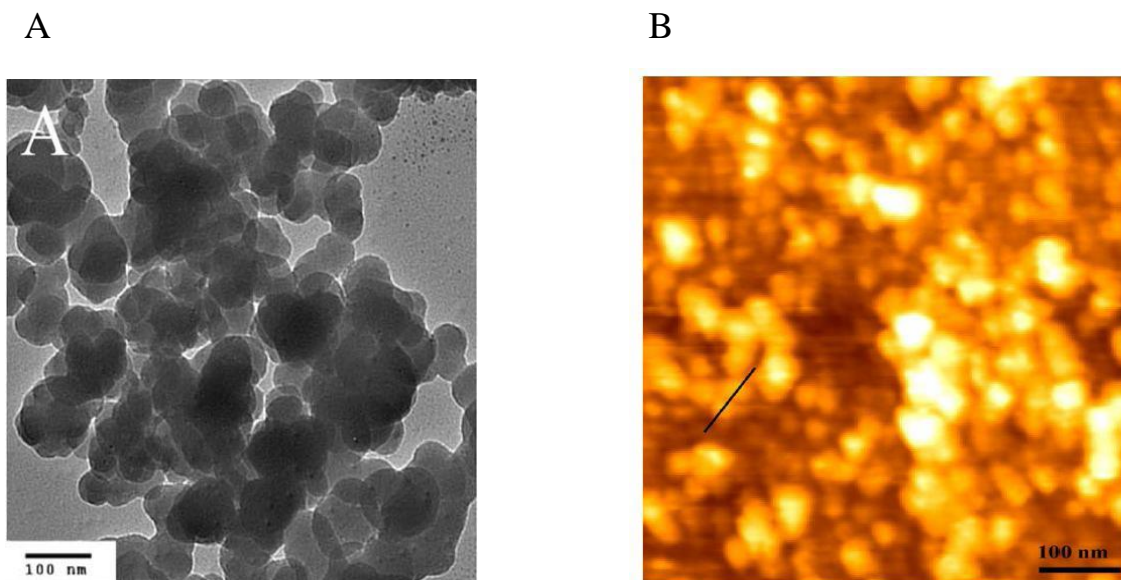
Figure (2-4) ZnO nanoparticles images A- (SEM) ,B- (AFM) [35].

2-5 Properties of nanoparticles

Nanoparticles are of interest because as size decreases (<100 nm), surface properties such as chemical, electrical, optical, magnetic and mechanical ,begin to dominate over the bulk material. Incorporation of these 'designer' particles into other materials, exploiting the properties of the nanoparticle surface atoms, allows the formation of novel products with enhanced or entirely different properties. Metals can be made stronger and harder; ceramics can have enhanced ductility and formability, normally insulating materials can be made to conduct heat or electricity, and protective coatings can become transparent [36].

2-6 Scope of Applications

The deviations from the bulk phase diagram may be exploited to form certain compositions of alloys that are otherwise unstable in the bulk form. In addition, the thermal stability of interfacial regions is typically less than that of the bulk material : thus the nano-phase materials are often sintered or undergo phase transformation at temperatures below those of the bulk material. This is a characteristic which has numerous applications to material processing. By improving material properties, we are able to find the applications as varied as semiconductor electronics, sensors, special polymers, magnetics, advanced ceramics, and membranes, we need to improve our current understanding of particle size control and methodologies for several classes of nanophase materials and address the issues of their characterization, we should also explore the fields in which there are foreseeable application of nano-phase materials to long standing materials problems, since these 'issues' have to be tackled by us. As said earlier, there is a scope of wider applications in different fields such as : (a) Electronics in terms of thin films, electronic devices and in electrical ceramics,(b)Bionics,(c)Photonics,(d)Bio-ceramics,(e)Bio-technology,(f)Medical instrumentation, etc [34].

2-7   Zinc oxide

Zinc oxide is an inorganic compound with the formula ZnO. It usually appears as a white powder, nearly insoluble in water. The powder is widely used as an additive into numerous materials and products including plastics, ceramics, glass, cement ,rubber and lubricants [37].

In materials science, ZnO is often called a II-VI semiconductor because zinc and oxygen belong to the 2nd and 6th groups of the periodic table, respectively. This semiconductor has several favorable properties: good transparency, high electron mobility, wide band gap, strong room temperature luminescence, etc. Those properties are already used in emerging applications for transparent electrodes in liquid crystal displays and in energy-saving or heat-protecting windows [38].

2-7-1   Crystal structures

Zinc oxide crystallizes in three forms:

1- hexagonal wurtzite

2- cubic zincblende

3- cubic rock salt.

The wurtzite structure is most stable and thus most common at ambient conditions and is shown in figure (2-5).
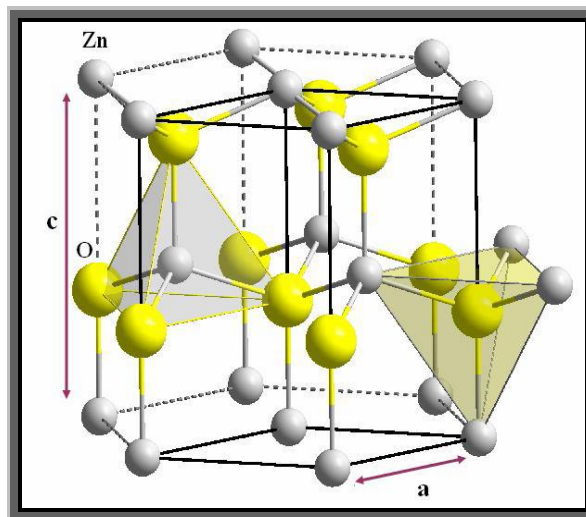
Figure (2-5) Hexagonal wurtzite structures of ZnO [39].

The bonding in ZnO is largely ionic, which explains its strong piezoelectricity. Due to this ionicity, zinc and oxygen planes bear electric charge (positive and negative, respectively).Therefore, to maintain electrical neutrality, those planes reconstruct at atomic level in most relative materials, but not in ZnO - its surfaces are atomically flat, stable and exhibit no reconstruction. This anomaly of ZnO is not fully explained yet [40].

2-7-2 Chemical properties

ZnO exists as white powder commonly known as white zinc or as the mineral zincite. The mineral usually contains a certain amount of manganese and other elements and is of yellow to red color [41]. Crystalline zinc oxide is thermo-chromic, changing from white to yellow when heated and in air reverting to white on cooling [42]. This is caused by a very small loss of oxygen at high temperatures to form the non-stoichiometric $Zn_{1+x}O$, where at 800 °C, x= 0.00007 [30].Table (2-1) Shows ZnO properties.

Table (2-1) ZnO Properties [43].

Molecular formula	ZnO
Molar mass	81.408 g/mol
Appearance	White solid
Odor	Odorless
Density	5.606 g/cm^3
Melting point	1975 °C (decomposes)
Boiling point	2360 °C
Solubility in water	0.16 mg/100 mL at (30 °C)
Band gap	3.3 eV (direct)
Refractive index (n_D)	2.0041

2-7-3 Electronic properties

ZnO has a relatively large direct band gap of (3.3 eV) at room temperature; therefore, pure ZnO is colorless and transparent, advantages associated with a large band gap including higher breakdown voltages, ability to sustain large electric fields, lower electronic noise, and high temperature and high-power operation. The band gap of ZnO can further be tuned from (3–4 eV) by its alloying with magnesium or cadmium oxides [44]. Most ZnO has (n-type) character, even in the absence of intentional doping, native defects such as oxygen vacancies or zinc interstitials are often assumed to be the origin of this , but the subject remains controversial [45]. An alternative explanation has been proposed, based on theoretical calculations, that unintentional substitution hydrogen impurities are responsible [46]. Controllable n-type doping is easily achieved by substituting Zn with group-III elements Al, Ga, In or by substituting oxygen with group-VII elements chlorine or iodine [47].

2-8 Copper (II) oxide

Copper oxide is formed when copper is exposed to oxygen and oxidized. There are two types of copper oxide: copper (I) oxide and copper (II) oxide. Cupric oxide (CuO) is a black material which melts above 1200°C with some loss of oxygen ,and is used as a pigment in clay glazes. Several colors, including red, blue, and green, can be derived from it. As a mineral, it is known as tenorite. It is red in color and does not dissolve in water or any organic solvents.

Copper (II) oxide has application as a p-type semiconductor. It is used an abrasive to polish optical equipment, and to produce dry cell batteries in addition to its use in wet cell batteries as cathode [48].

Cupric oxide (CuO) is an important transition metal oxide with a narrow bandgap (Eg 1·2 eV) and forms the basis of several high temperature superconductors and giant magnetoresistance materials [49].Table (2-2) shows CuO properties.

Table (2-2) CuO Properties[48].

Molecular formula	CuO
Molar mass	79.545 g/mol
Appearance	black to brown powder
Density	6.315 g/cm^3
Melting point	1326 °C
Boiling point	2000 °C
Solubility in water	insoluble
Band gap	1.2 eV
Refractive index (n_D)	2.63

2-8-1 Crystal structure

Copper (II) oxide belongs to the monoclinic crystal system, with a crystallographic point group of 2/m or C_{2h}. The space group of its unit cell is C2/c, and its lattice parameters are a = 4.6837, b = 3.4226, c = 5.1288, α = 90°, β = 99.54°, γ = 90°. The copper atom is coordinated by 4 oxygen atoms in an approximately square planar configuration [50] as shown in figure (2-6) below.
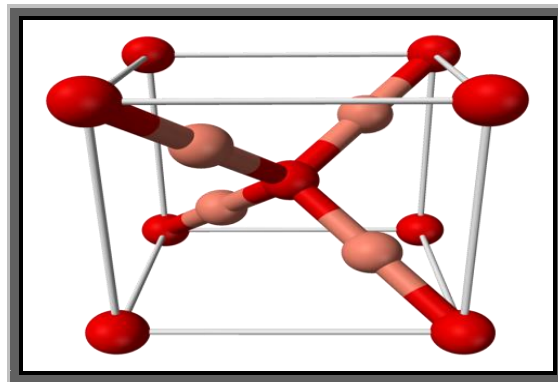
Figure (2- 6) The crystal structure of CuO [48].

2-9   Iron (III) oxide

Iron (III) oxide or ferric oxide is inorganic compound with the formula Fe_2O_3. It is one of the three main oxides of iron, the other two being iron (II) oxide (FeO), which is rare, and iron (II,III) oxide (Fe_3O_4), which also occurs naturally as the mineral magnetite. As the mineral known as hematite, Fe_2O_3 is the main source of iron for steel industry. Fe_2O_3 is ferromagnetic, dark red, and readily attacked by acids. Rust is often called iron (III) oxide, and to some extent this label is useful, because rust shares several properties and has a similar composition. To a chemist, rust is considered an ill-defined material, described as hydrated ferric oxide [51]. Figure (2-7) shows crystal structure of Fe_2O_3. Table (2-3) shows Fe_2O_3 Properties.
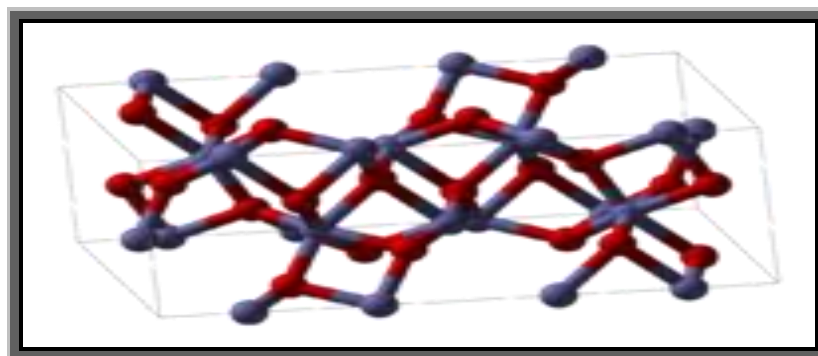
Figure (2-7) Part of the crystal structure of Fe_2O_3[52].

Table (2-3) Fe_2O_3 Properties[42].

Molecular formula	Fe_2O_3
Molar mass	159.69 g/mol
Appearance	red-brown solid
Density	5.242 g/cm^3, solid
Melting point	1566 °C
Solubility in water	insoluble

2-10 Ferrite (magnet)

Ferrites are ceramic, homogeneous materials composed of various oxides with iron oxide as their main constituent. Ferrites can have several distinct crystal structures. Many of them are magnetic materials and they are used to make permanent magnets, ferrite cores for transformers, and in various other applications. Ferrites are usually non-conductive ferrimagnetic ceramic compounds derived from iron oxides such as hematite (Fe_2O_3) or magnetite (Fe_3O_4) as well as oxides of other metals, and are like most other ceramics, hard and brittle. In terms of their magnetic properties, the different ferrites are often classified as "soft" or "hard", which refers to their low or high magnetic coercivity [53].

2-10-1 Ferrite's Structure

Ferrite has a three-dimensional, crystalline structure. Its chemical formula is $MO.Fe_2O_3$, which means that it has two elements of iron and three elements of oxygen. The MO refers to other metal oxides which could be manganese, zinc or nickel oxide, by adding the other metal oxides you are able to change the property of ferrite to make it suitable for various applications. Ferrite is a material that can be magnetized easily and can hold this property indefinitely. Even there is an ability to magnetize ferrite so that it has multiple poles [54].

2-10-2 Magnetic material types

Magnetic materials are grouped into two types, soft and hard. This is the classification based on their ability to be magnetized and demagnetized , not their ability to withstand penetration or abrasion. Soft materials are easy to magnetize and demagnetize and hard ferrite magnets are made in two different magnetic forms isotropic and oriented. The isotropic magnets are formed to desired shapes, sintered and then magnetized [55].

2-10-3 Soft ferrites

Ferrites that are used in transformer or electromagnetic cores contain nickel, zinc, and manganese compounds. They have a low coercivity and are called soft ferrites. The low coercivity means the materials magnetization can easily reverse direction without dissipating much energy (hysteresis losses), while the material's high resistivity prevents eddy currents in the core, another source of energy loss, because of their comparatively low losses at high frequencies. They are extensively used in the cores of RF transformers and inductors in applications such as switched-mode power supplies [56].

The most common soft ferrites are:

- **Manganese-zinc ferrite (MnZn)**, with the formula $(Mn_aZn_{(1-a)}Fe_2O_4)$. MnZn have higher permeability and saturation induction than NiZn.

- **Nickel-zinc ferrite (NiZn)**, with the formula $(Ni_aZn_{(1-a)}Fe_2O_4)$. NiZn ferrites exhibit higher resistivity than MnZn, and are therefore more suitable for frequencies above 1 MHz.

In ceramic industries, powder metallurgy method of manufacturing is extensively used. Soft ferrites are also manufactured by this method. Soft ferrites are magnetically soft materials, being used as core of electronic transformers and other electromagnetic applications, where the frequency ranges from 100 KHz to a few GHz for soft ferrites [29].

2-10-4 Hard ferrites

Permanent ferrite magnets are made of hard ferrites, which have a high coercivity and high remanence after magnetization. These are composed of iron and barium or strontium oxides. The high coercivity means the materials are very resistant to become demagnetized, an essential characteristic for a permanent magnet. They also conduct magnetic flux well and have a high magnetic permeability. This enables these so-called ceramic magnets to store stronger magnetic fields than iron itself. They are cheap, and are widely used in household products such as refrigerator magnets. The maximum magnetic field B is about 0.35 tesla and the magnetic field strength H is about 30 to 160

kiloampere turns per meter (400 to 2000 Oersteds). The density of ferrite magnets is about 5g/cm^3 [56].

2-11   Structure Properties of ferrites

X-ray diffraction has long been used to determine the atomic scale structure of materials. The technique is based on the fact that the wavelength of X-rays is comparable in size to the distances between atoms in condensed matter. Thus, when a bulk material that exhibits a long-range, periodic atomic order, such as a crystal, is irradiated with X-rays, it acts as an extended, almost perfect grating and produces a diffraction pattern showing numerous sharp spots, called Bragg diffraction peaks. By measuring and analyzing the positions and intensities of Bragg peaks, it is possible to determine the spatial characteristics of the grating, i.e. to determine the three-dimensional (3D) atomic arrangement in bulk crystals. This is the essence of the so-called "crystal structure" [57].

2-11-1 Debye-Scherrer-Method

The Debye-Scherrer method uses a crystalline powder and illuminates it with monochromatic X-rays. The diffracted signal is detected by a Geiger-Muller-Tube. The powder sample contains small single-crystals, so-called crystallites. A set of parallel lattice planes (hkl) in a crystallite leads to a constructive interference of reflected X-rays if its alignment fulfills the Bragg condition [58].

nλ=2dsinθ …………………………………………………………..…..(2-1)

Where λ- wavelength of X-ray**,** d-interplaner spacing, θ-diffraction angle**,**

n = 1, 2, 3….

The crystallite size can be found out by using the Scherrer's formula [66].

D = 0.9λ / β cos θ …………………………………………………………..(2-2)

Where   D - crystallite size , λ -wavelength (1.54 Å), β -Full width at half maximum (FWHM), θ- Diffraction angle.

2-11-2 Spacing of Lattice Planes

The perpendicular distance separating each lattice plane in a stack is denoted by the letter *d*, *d* spacing and the relationship to the particular lattice plane is d_{hkl} (i.e., d_{001}, d_{101}, d_{103}) with the Miller indices for the particular plane shown in the subscript, this is the common notation used in crystallography and X-ray diffraction. The values of d spacing in terms of Hexagonal (ZnO, Fe_2O_3) systems are shown in the relationship [59].

$$d = \left[\frac{4}{3a^2}(h^2 + hk + k^2) + \frac{l^2}{c^2} \right] \quad \dots\dots\dots\dots\dots\dots\dots\dots\dots\dots\dots\dots\dots\dots\dots(2\text{-}3)$$

The values of d spacing for monoclinic (CuO) is shown in the relationship :

$$d = \left[\frac{\frac{h^2}{a^2} + \frac{l^2}{c^2} - \frac{2hl\cos\beta}{ac}}{\sin^2\beta} + \frac{k^2}{b^2} \right] \quad \dots\dots\dots\dots\dots\dots\dots\dots\dots\dots\dots\dots\dots\dots(2\text{-}4)$$

2-12 Mechanical properties of ferrites

Mechanical properties are most important in ferrites. The ceramic nature of a ferrite makes it vulnerable to impact, thermal shock ,and tensile failure. It is important for the ferrite designer to know the internal structure of his material, their mechanical workability, hardness, density and amount of porosity [55].

2-12-1 Densities of ferrites

Ferrites, being ceramic formed by sintering, have mechanical properties similar to those of pottery and in particular the properties depend on the sintered density. The pressed core before firing consists of relatively porous compact of oxides and during sintering the oxides react to form crystallites, or grains, of the required composition, the grains nucleate at discrete centres and grow outwards until the boundaries meet those of neighboring crystallites. During this process the density of the mass rises. Although there are some differences in X-ray densities owing to differences in divalent ions, the major contribution to effective density of ferrite part is its porosity [60].

2-12-2 Porosity in ferrites

The porosity has an important effect on the mechanical and magnetic properties of ferrites and low porosities are usually preferable ,if the porosity is denoted by *P* then :

P% = (1 − D/Dx) …………………………………………………………….(2-5)

where *D* is the bulk density and *D*x is the X-ray density.

In normal production the porosity might range from 1% to 15% depending on the grade of ferrite [61,62].

2-13 Electrical properties of ferrites

The electrical properties of ferrite substances play an important role in many electrotechnical applications. The factors that have the most influence on these properties are the purity of the constituent oxides and the effect of impurities on the final ferrite produced, the proportions and homogeneity in the powder mix and the control of temperature and atmosphere during sintering[55].

2-13-1 Resistivity of ferrites

High resistivity ferrites with low eddy current losses are required from the technological applications point of view. The electrical resistivity of ferrites has been normally found to increase on doping or substituting with other oxides occurring at high frequencies in ferromagnetic materials[56]. This resistivity varies with applied field, temperature, and frequency. Generally for ferrite materials, it decreases slightly as frequency increases. The characteristic tables of the materials indicate the mean DC - resistivity values for the various ferrite materials measured at low frequency and with a low field by using the formula [54].

$$\rho = R\frac{A}{\ell}$$ …………………………………………………………….(2-6)

where (R) is electrical resistance, (A) represents the surface area, and (ℓ) is the thickness of the model.

The resistivity depends on temperature as in the relationship [54].

$$\rho = \rho_o \exp(E/kT) \ldots\ldots\ldots\ldots\ldots\ldots\ldots\ldots\ldots\ldots\ldots\ldots\ldots\ldots\ldots\ldots(2\text{-}7)$$

where E activation energy, T temperature, k is the Boltzmann constant
(k =8.62 $*10^{-5}$ eV .k^{-1}) and (ρ_o is a constant).

2-14   Magnetic properties of ferrites

2-14-1 Permeability

The magnetic flux density inside a ferrite core can be described by the formula

$$B = \mu_0 H + J \quad \ldots\ldots\ldots\ldots\ldots\ldots\ldots\ldots\ldots\ldots\ldots\ldots\ldots\ldots\ldots..(2\text{-}8)$$

where B is magnetic flux density, H is magnetic field ,μ_0 is absolute vacuum permeability, J is magnetic polarization of ferrite material [56].

This relation introduces the relative permeability μ of a ferrite material which may be defined as :

$$\mu = \frac{1}{\mu_0} * \frac{B}{H} \quad \ldots\ldots\ldots\ldots\ldots\ldots\ldots\ldots\ldots\ldots\ldots\ldots\ldots\ldots(2\text{-}9)$$

2-14-2 Magnetism in ferrites

A sintered ferrite consists of small crystals, typically 10 to 20 μm in dimension. Domains exist within these crystals (weiss domains) in which the molecular magnets are already aligned (ferrimagnetism).When a driving magnetic field (H) is applied to the material, the domains progressively align with it, as shown in figure (2-8).
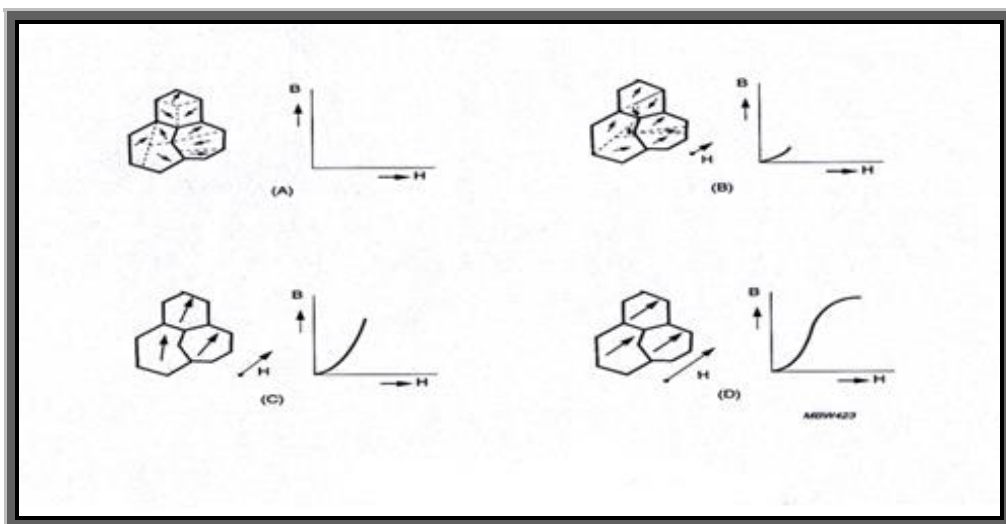
Figure (2-8) Alignment of domains [63] .

2-14-3 Hysteresis loop

The static hysteresis loops, (BH) curves, are obtained by measuring the resulting flux density B inside the core under test with increasing values of H field until saturation. B-H curves and hysteresis loops are valuable tools for comparing the characteristics and behavior of different magnetic materials in order to select them for an appropriate application. During this magnetization process, energy barriers have to be overcome. Therefore the magnetization will always lag behind the field. If the resistance against magnetization is small, a large induced flux will result in a given magnetic field. The value of the permeability is high. The shape of the hysteresis loop also has a marked influence on other properties, for example, power losses [64]. Figure (2-9) shows the hysteresis loop.
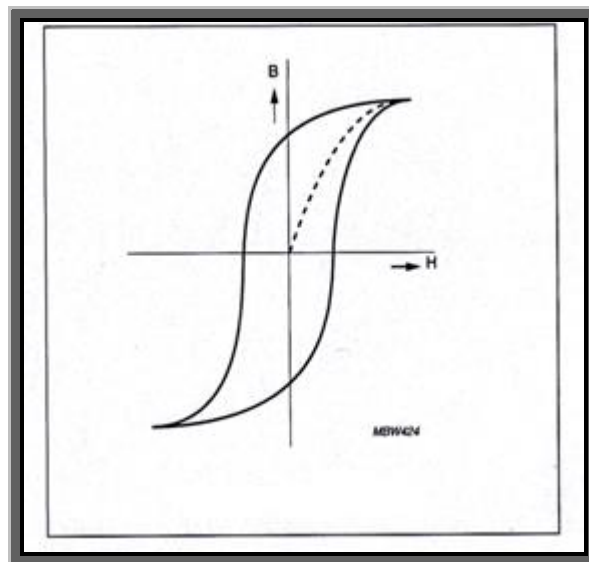
Figure (2-9) Hysteresis loop [56].

For each ferrite material, measurements were made on reference toroids (previously demagnetized) at 25 and 100°C. Remnant flux density Br is defined as the intersection of the hysteresis loop with B axis (H = 0). Br is an important factor for unipolar operating systems. Coercive force Hc is the intersection of the hysteresis loop with H axis (B = 0). It is representative of static hysteresis loss of the considered material, which is recorded in the ferrite materials section [63].

3-1   Introduction

This chapter shows the experimental part and includes the explanation of powder metallurgy, the process of preparation of nano (ZnO, CuO and Fe_2O_3) oxides, and the manufacturing of ferrites $(ZnO)_x(Fe_2O_3)_{1-x}$, $(ZnO)_x(CuO)_{1-x}(Fe_2O_3$) then testing methods such as (XRD, SEM, Electrical, Magnetic and Mechanical) properties.

3-2   Powder metallurgy

Powder metallurgy has been defined as the art and science of producing fine metal powders (raw materials) and objects finished or semi-finished shaped from individual mixed or alloyed metal powder with or without the inclusion of non metallic constituents. It is that branch of metal working process, which in its simplest form, consists of preparing and mixing of metal powder compacting and simultaneous or subsequent heating (or sintering) at elevated temperature in a furnace under a protective atmosphere (non-oxidising atmosphere or vacuum) with or without fusion of low melting point [65].

Compacting is generally performed at room temperature, and the elevated-temperature process of sintering is usually conducted at atmospheric pressure. Optional secondary processing often follows to obtain special properties or enhanced precision. The two main techniques used to form and consolidate the powder are sintering and metal injection molding. Recent developments have made it possible to use rapid manufacturing techniques which use the metal powder for the products, because with this technique, the powder is melted and not sintered, better mechanical strength can be accomplished [66].

3-3   Characteristics and testing of metal powder

The processes of manufacturing powder metallurgy depend largely on the physical and chemical characteristics of the initial metal powders. The characteristics of metal powders in turn depend upon the method used in producing these metal powders. There are various methods of manufacturing metal powders and consequently there is a wide range in their characteristics.

A choice regarding the suitability of manufacturing techniques of metal powder can be made only after considering the required finished product for a specific job. The basic characteristics of metal powder are: chemical composition and purity, particle size and its distribution , particle shape, particle porosity, particle micro structure specific surface [65].

The term "impurity" refers to the same elements or compounds which have an undesirable effect. Impurities influence not only the mechanical properties of the powder compacts but also their chemical, electrical and magnetic properties. It may also exert a decisive effect on pressing sintering and other post –sintering operation which are essential for the production of finished product from powder. The particle size has a great importance in powder metallurgy because it affects most of the properties such as mould strength, density of compact, porosity, expulsion of trapped (occluded), gases dimensional stability, agglomerations and flow and mixing characteristics. Particle size effect on porosity is shown in Figure (3-1).
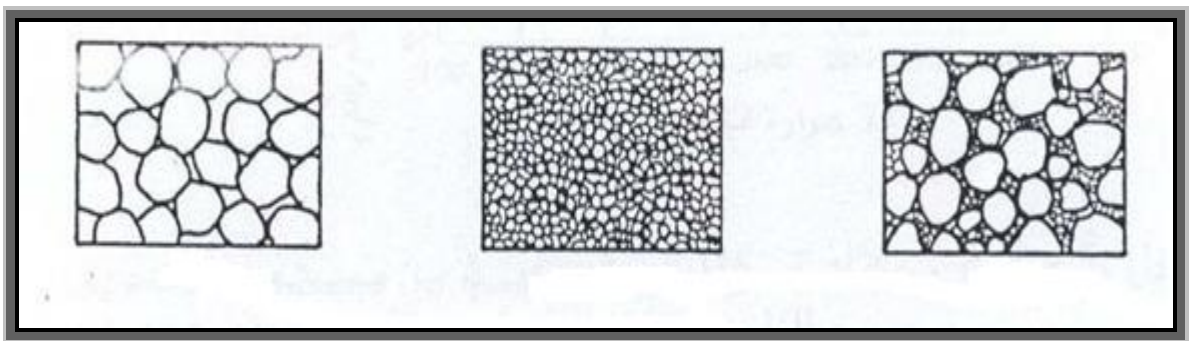
Figure (3-1) The effect of particle size on porosity [65].

3-4 Powder preparation

These powders can be produced by various methods such as milling , reduction and other methods, but the most versatile among these are based on precipitation from sols and gels.

3-5 Pressing properties

These are represented by the term compressibility which is one of the most important characteristics of a metal powder since it affects the densification process. It is a measure of the powder ability to deform under applied pressure and is represented by the pressure/density or pressure/porosity. Figure (3-2) illustrates the reduction in porosity after pressing.
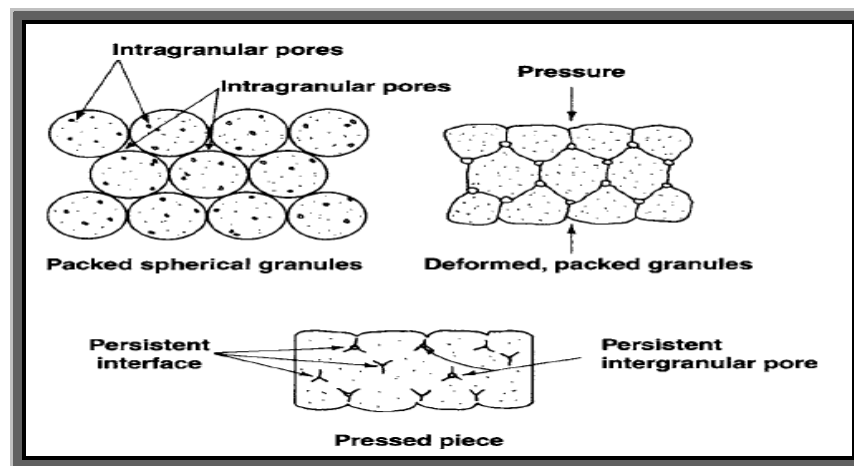
Figure (3-2) Reduction in porosity after pressing [65].

3-5-1 Powder compaction

The main purpose of the compaction process is to form metal powder into compacts of desired shape with sufficient strength to withstand ejection from the tool and subsequent handling up to the completion of sintering without breakage or damage. It is the subsequent sintering operation which imparts the final strength. The density of the compacted powder is directly proportional to the amount of pressure applied. There is 25 to 45 % shrinkage of the powder after compacting. Figure (3-3) illustrates the mechanism of powder consolidation.
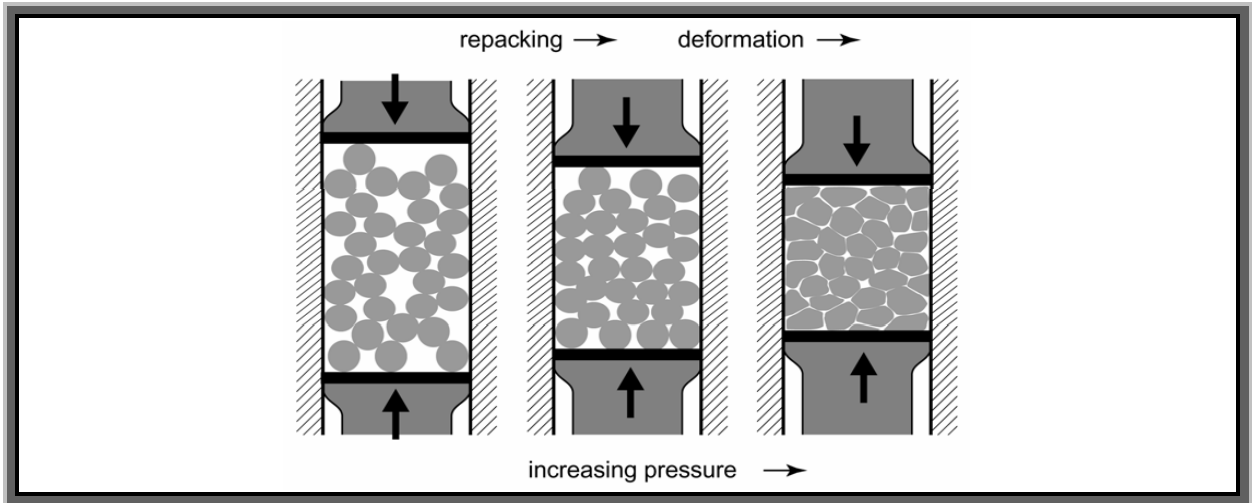
Figure (3-3) Mechanism of powder consolidation [67].

3-5-2 Pellet formation

Die is the part for making pellets. Dies are commonly made of hard steel. Most of the dies make circular pellets of varying diameter, depending upon amount of the material used. A die made of steel was used and finally ground powder was cold pressed into pellets of 10 mm diameter under a uniaxial pressure of 500 psi using hydraulic press. Figure (3-4) shows the transformation of powder to compact sample.
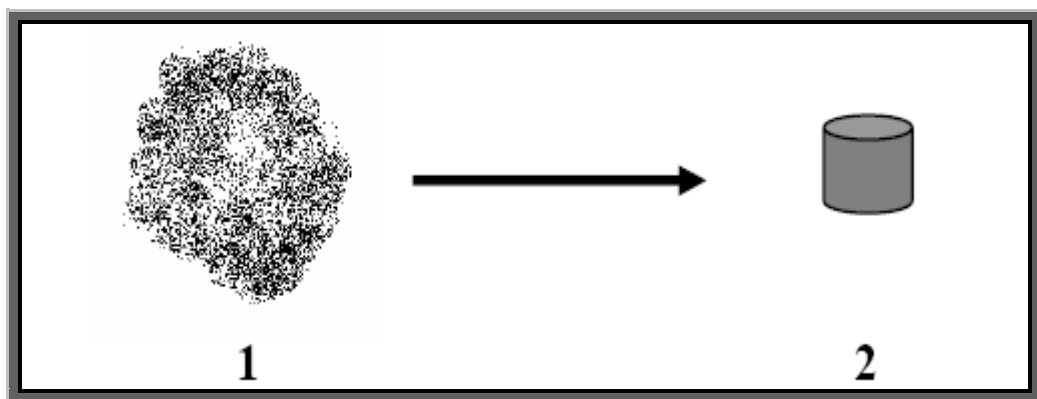
Figure (3-4) Transformation of powder to compact sample .

3-5-3 Toroid formation

This design is based on a toroid (the same shape as a doughnut). The coil is wound through the hole in the torus and around the outside. Toroid outside diameter is 10 mm and inside diameter 4 mm and the height of toroid is 5 mm as shown in Figure (3-5).
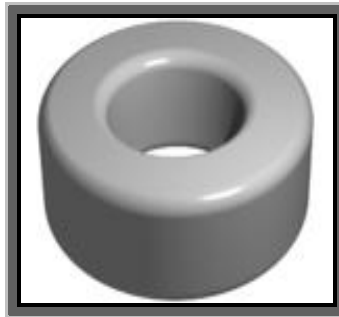
Figure (3-5) Toroid shape

3-5-4 Cold compaction

Cold compaction is a process in which powder is compressed at a temperature where deformation mechanics like dislocation or diffusion creep can be neglected. Cold compressing is the most important compaction method in powder metallurgy. It starts from bulk powders containing very small amounts and sometimes even no lubricants or binder additions. The cold pressure shaping techniques have the largest scope for shaping metal powder. Included in this class are cold die compaction, isostatic pressing, explosive forming, high energy rate forming, powder rolling, cyclic compaction, vibratory compacting, centrifugal compaction, powder extrusion and cold working of preformed blanks. Compaction ejection of the pressed part is effected by the movement of the die or punch. The density and strength of the unsintered compact are called "green density".

3-6   Green density

In general, green density has been found to increase with:

1- The increase of compaction pressure.

2- The increase of particle size or apparent density .

3- The decrease of particle hardness (and strength) .

4-The decrease of compacting speed.

Improvement in green density may also be affected by employing smooth and regularly shaped annealed particles with high particle densities (possessing no internal or interconnected porosity). Green strength of a powder is defined as the mechanical strength of a green compact required to withstand without damage to sharp edges and fracture. Figure (3-6) shows green compact and pressing mechanism.
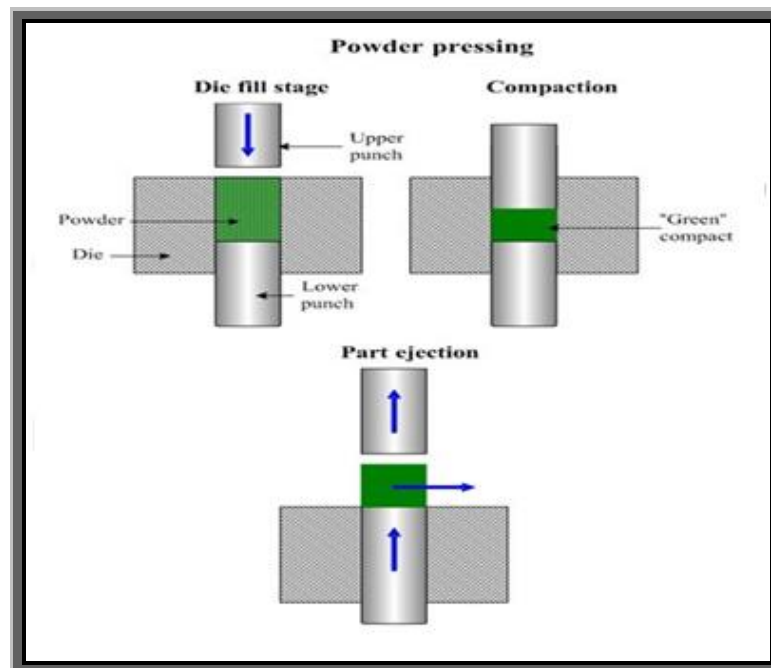
Figure (3-6) Pressing mechanism [68].

3-7 Sintering

Sintering may be defined as the heating of loose or compacted aggregate of metal powder below the melting point of the base metal with or without the application of external pressure in order to transform it to a more dense material by interparticle bonding. Sintering process is concerned with the diffusion of particle to particle , the formation of grain boundary and the closing of voids present in the green briquettes. Sintering is a rather very complex process in which physical, chemical and metallurgical effects interact because of the numerous changes occurring simultaneously within the material. It is very difficult to define and analyse sintering under heat; bonding takes place between the porous aggregate particles and once cooled powder has also bonded to form a solid piece. Sintering can be considered to proceed in three stages:

1- Neck growth proceeds rapidly but powder particles remain discrete.

2- Most densification occurs, the structure recrystallizes and particles diffuse into each other.

3- Isolated pores tend to become spheroidal and densification continues at a much lower rate. Figure (3-7) shows compact powder before and after sintering:
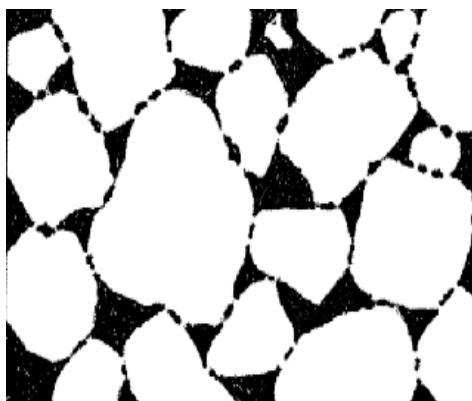
        Before Sintering   After Sintering

Figure (3-7) Powder metal compact before and after sintering [69].

3-8   Preparation of nanomaterials

This part includes the selection of raw materials and the preparation of nano ZnO , nano CuO and nano Fe_2O_3 by precipitation method and finally Production of ferrites with two series as:

1- $(ZnO)_x(Fe_2O_3)_{1-x}$

2- $(ZnO)_x(CuO)_{1-x}(Fe_2O_3$). Where x = (0, 0.2, 0.4, 0.6, 0.8, 1).
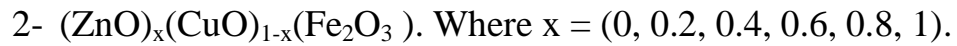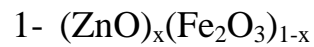
3-8-1   Selection of raw materials

Raw materials of high purity are used, because the presence of impurities affect the properties of prepared   materials. The preparation of nanomaterials through a chemical precipitation shown in figure (3-8).
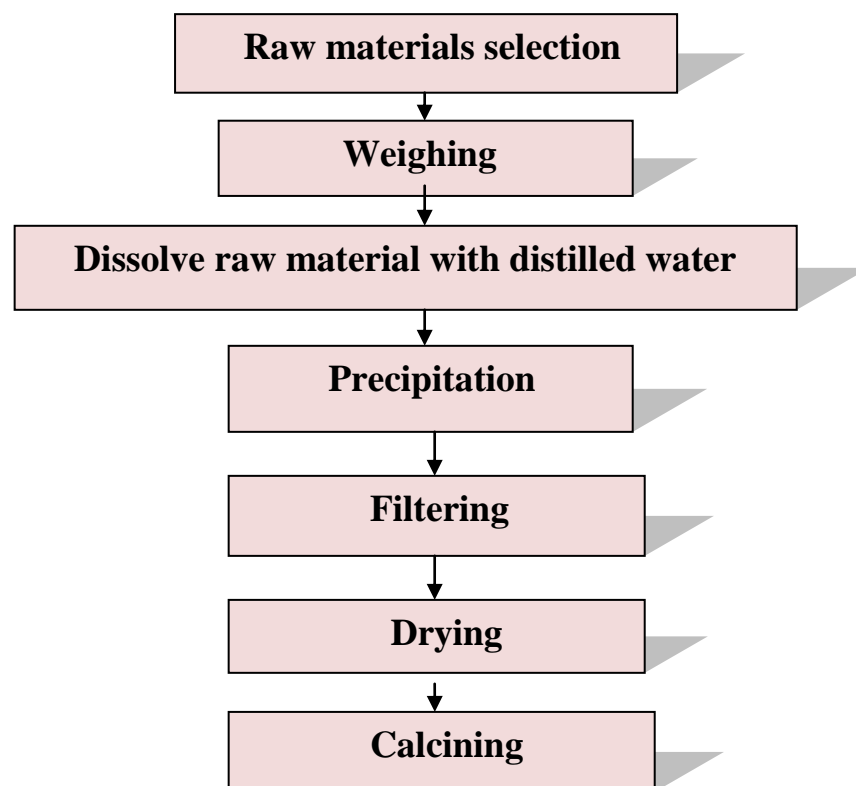
Figure (3-8) Nanomaterials preparation steps

3-9 The preparation of nano zinc oxide

There are many methods used for the preparation of ZnO material, the one we use is a method which is easy if compared to other methods and the chemicals required for these methods are available and cheap.

3-9-1 Materials

All the chemical materials used are commercial one and are of analytical grade. The chemical materials used for preparation are shown in table (3-1) together with their properties.

Table (3-1) Raw materials used

Name	Chemical formula	Molecular weight g/mol	Origin	Color	Purity %
Zinc nitrate	$Zn(NO_3)_2.6H_2O$	297	India	White	98%
Sodium bicarbonate	$NaHCO_3$	84	India	White	99%

3-9-2 Tools and equipment used

Volumetric flasks, filter paper, burette, balance, PH meter, beakers, hot plate magnetic stirrer, funnel, distilled water, oven, furnace.

3-9-3 Method of preparation:

The schematic representation of the main steps employed in the preparation is shown in figure (3-9)

```
      ┌───────────────────┐      ┌─────────────────────────┐
      │  (0.1M) NaHCO₃     │      │ (0.1M) Zn(NO₃)₂6H₂O     │
      └───────────────────┘      └─────────────────────────┘
                    ┌──────────────────┐
                    │  Precipitation   │
                    └──────────────────┘
                             │
                    ┌──────────────────┐
                    │   Zn(HCO₃)₂      │
                    └──────────────────┘
                             │
                    ┌──────────────────┐
                    │   Decantation    │
                    └──────────────────┘
                             │
                    ┌──────────────────┐
                    │    Filtering     │
                    └──────────────────┘
                             │
                    ┌──────────────────┐
                    │     Washing      │
                    └──────────────────┘
                             │
                    ┌──────────────────┐
                    │  Drying at 80 °C │
                    └──────────────────┘
                             │
                    ┌──────────────────┐
                    │Calcining at 450 °C│
                    └──────────────────┘
                             │
                    ┌──────────────────┐
                    │ Nano ZnO Powder  │
                    └──────────────────┘
```
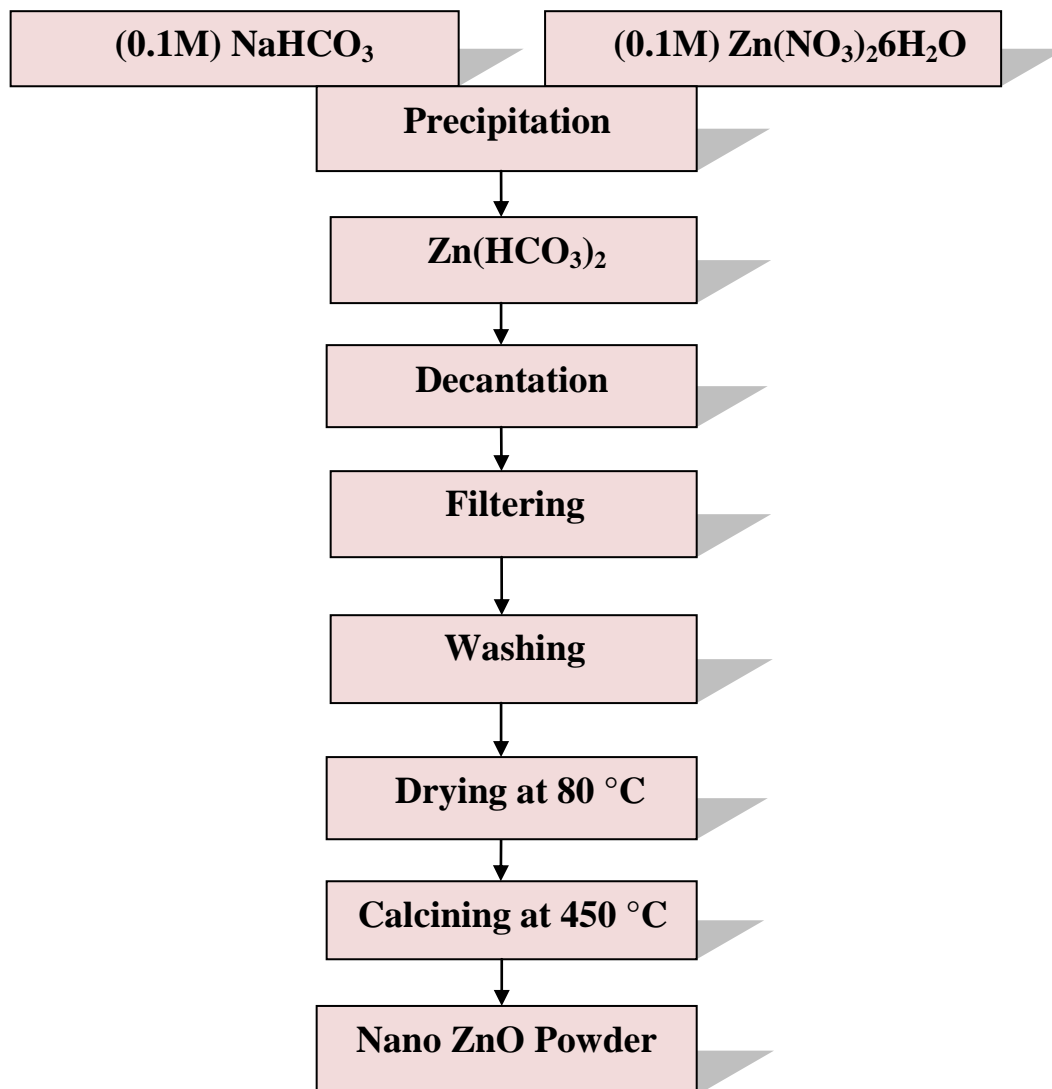
Figure (3-9) Steps of process nano ZnO preparation

3-9-4 Preparation of solution :

(0.1M) Zinc nitrate and sodium bicarbonate are prepared by dissolution (29.7 g) Zinc nitrate hexahydrate and (8.4 g) sodium bicarbonate in (1 L) of distilled water respectively.

3-9-5 Precipitation procedure:

(0.1M) Zinc nitrate was placed in 500 ml beaker placed on a hot plate magnetic stirrer. A magnetic bar is used in order to obtain homogeneous mixing of the material. The two electrodes of pH meter were inserted in the solution. Measure and monitor the pH value of the solution during the addition of the

sodium bicarbonate drop by drop from burette. The temperature of the solution was fixed at 80°C. The addition continued until the pH of the solution reaches (6.8) where the precipitation was completed.

3-9-6 Decantation and filtration:

The precipitate was allowed to settle over night and then filtered off and then washed several times with distilled water until it became free from excess bicarbonate that may exist.

3-9-7 Drying and calcinations:

The precipitates were dried at 80°C for 3 hours in an oven and then calcined at 450 °C for 2 hours in a furnace.

3-10   preparation of nano copper oxide

There are several ways to prepare (nano CuO) but we use the same one of nano ZnO.

3-10-1 Material:

All the chemical materials used are commercial and are of analytical grade. Table (3-2) shows the properties of these materials:

Table (3-2) Raw materials used

Name	Chemical formula	Molecular weight g/mol	Origin	Color	Purity %
Cupric nitrate	$Cu(NO_3)_2.3H_2O$	241	England	Blue	99%
Sodium bicarbonate	$NaHCO_3$	84	India	White	99%

3-10-2 Tools and equipment used

Volumetric flasks, filter paper, burette, a sensitive balance, pH meter, beakers, hot plate magnetic stirrer, funnel, distilled water, oven, furnace.

3-10-3 Preparation of solution:

(0.1M) copper nitrate and sodium bicarbonate are prepared by dissolution of (24.1 g) zinc nitrate and (8.4 g) sodium bicarbonate in (1 L) of distilled water respectively.

3-10-4 Precipitation procedure:

(0.1M) copper nitrate are placed in 500 ml beaker and placed on a hot plate magnetic stirrer. A magnetic bar is used in order to obtain homogeneous mixing of the material. The two electrodes of pH meter are inserted in the solution, the solution during addition of the sodium bicarbonate gradually drop by drop from burette and the temperature of the solution is measured and monitored and fixed at 80°C. The addition continues until the pH of the solution reaches 6.8 where the precipitation was completed.

3-10-5 Decantation and filtration:

The precipitate is allowed to settle over night and then filtered off and the precipitate is washed several times with distilled water until it becomes free from excess bicarbonate that may exist. A pale blue color precipitate is observed and the supernatant solution is then discarded carefully.

3-10-6 Drying and calcinations:

The precipitate is dried at 80°C for 3 hours in an oven and then calcined at 450 °C for 2 hours in a furnace.

3-11 Preparation of Fe_2O_3 nano particle

Fe_2O_3 Nano particles are prepared chemically by a modified sol-gel method from Iron(III) nitrate and Citric acid.

3-11-1 Materials:

Table (3-3) shows the properties of the material used in preparation :

Table (3-3) Raw materials used

Name	Chemical formula	Molecular weight g/mol	Origin	Color	Purity%
Ferric nitrate	$Fe(NO_3)_3. 9H_2O$	403.84	India	Red	98%
Citric acid	$C_6H_8O_7$	192	India	White	99%

3-11-2 Tools and equipments used:

The tools to be used include volumetric flasks, filter paper, burette, a sensitive balance, pH meter, beakers, hot plate magnetic stirrer, funnel, distilled water, oven, furnace.

3-11-3   Preparation of solution :

(0.2M) ferric nitrate and citric acid are prepared by dissolving (8.04 g) of ferric nitrate in (200 ml) of distilled water and (33.6 g) citric acid in (800ml) of distilled water respectively.

3-11-4 Fe_2O_3 preparation:

These particles have been prepared by a slightly modified method for simplicity (200 ml) of iron nitrate. $Fe(NO_3)_3.9H_2O$ is used as a precursor solution, and was gelated by using 800 ml of monohydrated citric acid solution (0.05 to 0.2M) as ligand molecules. The iron solution is added to the citric acid solution drop wise with vigorous stirring by magnetic stirrer . The solution was then heated to a temperature of 80°C, while maintaining vigorous stirring until the gel is formed and then the contained water is evaporated, and the dried gel is annealed at temperatures of 200 °C.

3-12 The preparation of the ferrites

The following description process is typical for the manufacture of our range of soft ferrites.

3-12-1 Ferrite formulas

Several samples of ferrites are prepared using the following formulas:

$(ZnO)_x(Fe_2O_3)_{1-x}$

$(ZnO)_x(CuO)_{1-x}(Fe_2O_3)$ where the value of x being (0-1).
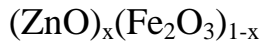
3-12-2 Stoichiometric calculations

The appropriate weight percentage of each oxide to be mixed for different composition is calculated by the following formula;

Weight % of oxide = (molecular weight of oxide X required weight of the sample)/(sum of the molecular weight of the given composition).

2-12-3 Proportions of the composition

The weights of oxides powder needed to prepare the required formula are given in table (3-4).

Table (3-4) Symbols of ferrites prepared

Sample	Chemical formula	Sample	Chemical formula
F1	(Fe_2O_3)	C1	$(CuO) (Fe_2O_3)$
F2	$(ZnO)_{0.2} (Fe_2O_3)_{0.8}$	C2	$(ZnO)_{0.2} (CuO)_{0.8} (Fe_2O_3)$
F3	$(ZnO)_{0.4} (Fe_2O_3)_{0.6}$	C3	$(ZnO)_{0.4} (CuO)_{0.6} (Fe_2O_3)$
F4	$(ZnO)_{0.6} (Fe_2O_3)_{0.4}$	C4	$(ZnO)_{0.6} (CuO)_{0.4} (Fe_2O_3)$
F5	$(ZnO)_{0.8} (Fe_2O_3)_{0.2}$	C5	$(ZnO)_{0.8} (CuO)_{0.2} (Fe_2O_3)$
F6	(ZnO)	C6	$(ZnO) (Fe_2O_3)$

3-12-4 Mixing

Weighing of raw materials is very important and should be done with great care. For weighing, electronic analytical balance with accuracy up to 10^{-4} g is used. The care is taken to check the zero setting before weighing the powders on the balance. A small error in weighing may change moler ratios of raw material and finally the properties. The powders are mixed to obtain a uniform distribution of the components. These are mixed using a variable speed electric mixer for two hours for the purpose of obtaining a homogeneous mixture and the non-agglomerated mixtures are then dried in an oven at 80 °C for 2 hours.

3-12-5 Equipment (mold)

There are many types of equipments used in powder compacting. These are the molds. A mold is designed for the manufacture of samples in the form of pellet in diameter (9mm) and thickness (5mm) and the weight of the sample is (1.3 g) . It uses hydraulic press with a pressure of 500-700 psi, and the diameter of the mold used (1cm) with a hight of (3cm).

3-12-6 Forming

Since ferrite parts are formed by pressing. The granules are poured in to a suitable die and then compressed, and a so-called (green) product is formed. It is still very fragile and requires sintering to obtain the final ferrite properties. It is preferable to have a powder of various sizes of particles which increases the durability and fills in the spaces between the big Particles.

3-12-7 Sintering

The (green) cores are loaded on refractory plates (pure alumina container) and sintered at temperature of (800, 900 and 1000 °C) depending on the ferrite grade for four hours. A linear shrinkage of up to 20% (50% in volume) takes place. The sintering can be done in tunnel kilns having a fixed temperature in box kilns. Ferrites are usually made by sintering them at the sintering temperature so that the reactions take place between the carefully mixed raw materials, mostly oxides or carbonates, which lead to ferrite formation where O_2

exchange between ferrite and the furnace atmosphere affects its magnetic, electrical and mechanical properties. Figure (3-10) shows the ceramic method of ferrite preparation .

.

```
                    ┌─────────────────────┐
                    │   Raw material      │
                    └─────────────────────┘
                              ↓
                    ┌─────────────────────┐
                    │     Weighing        │
                    └─────────────────────┘
                              ↓
                    ┌─────────────────────┐
                    │      Mixing         │
                    └─────────────────────┘
                              ↓
                    ┌─────────────────────┐
                    │  Drying of powder   │
                    └─────────────────────┘
                              ↓
                ┌─────────────────────────┐
                │  Compaction of samples  │
                └─────────────────────────┘
                              ↓
            ┌─────────────────────────────────┐
            │ Sintering at (800,900 and 1000 °C) │
            └─────────────────────────────────┘
                              ↓
    ┌──────────────────────────────────────────────────┐
    │ Complementary processes (smoothing and polishing) │
    └──────────────────────────────────────────────────┘
```
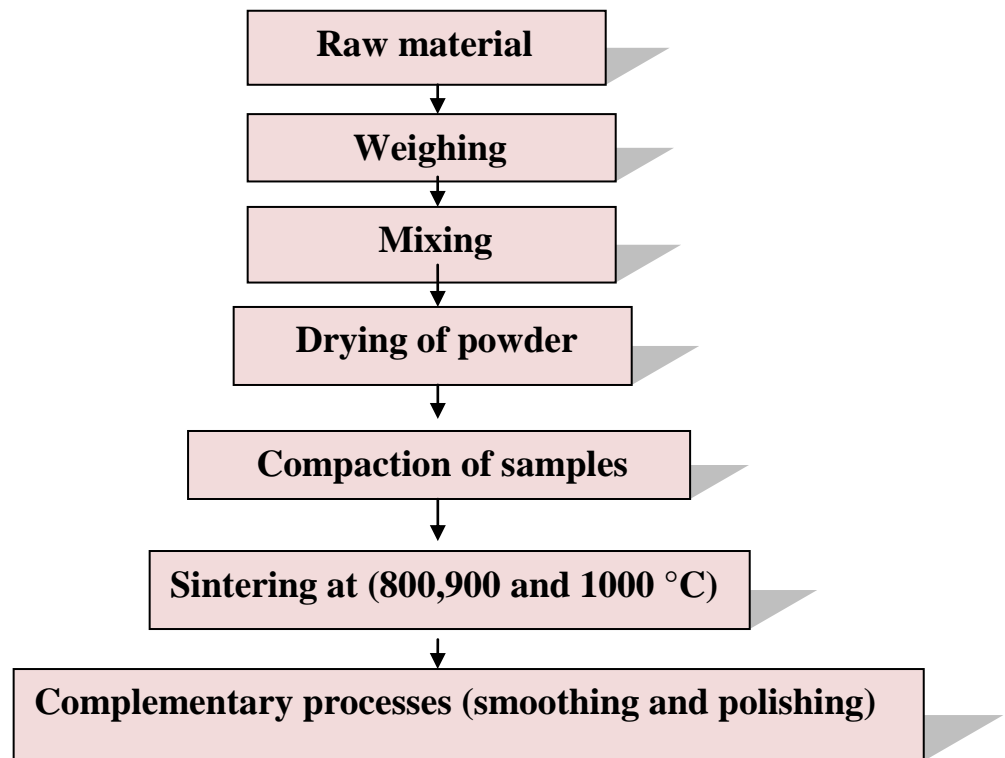
Figure (3-10) Method for ceramic ferrites preparation

3-13 Measurements and testing

3-13-1 X-ray diffraction

Testing of X-ray diffraction of the oxides prepared by using a diffraction X-ray type (XRD-6000) with an accelerating voltage of (60 KV), of the SHIMADZU company (JAPAN) that generates X-ray wavelength (1.5406 Å) to the source of the target (Cu) and within range of angular (2θ =20º-60º).

3-13-1-2 Calculation of crystallite size from X-ray diffraction

Detailed knowledge of crystallite size, shape and strain in a finely divided powder often helps to correlate many physical properties of a system undergoing transformation in a solid-state reaction. X-ray line broadening analysis provides a method of finding bulk average size of coherently diffracting

domains and root mean square (r.m.s) strain. The average crystallite size (D) from X-ray line broadening has been calculated using (2-2) equation [70,71].

3-13-1-3 Density measurement from X-ray diffraction

The X-ray density of the samples have been computed from the values of lattice parameters using the formula [6]:

$$d = \frac{8M}{N\,a^3} \quad \dots\dots\dots\dots\dots\dots\dots\dots\dots\dots\dots\dots\dots\dots\dots\dots\dots\dots\dots\dots\dots.(3\text{-}1)$$

where 8 represents the number of molecules in a unit cell of a spinal lattice, M the molecular weight of the sample, N the Avogadro's number and (a) represents the lattice constant of the sample. The lattice constant (a) of the structure was calculated using the equation [59]:

$$a = d\,(h^2 + k^2 + l^2)^{1/2} \quad \dots\dots\dots\dots\dots\dots\dots\dots\dots\dots\dots\dots\dots\dots\dots...(3\text{-}2)$$

3-13-2 Scanning electron microscope (SEM)

The scanning electron microscope (SEM) uses a focused beam of high-energy electrons to generate a variety of signals at the surface of solid specimens. The signals that derive from electron sample interactions reveal information about the sample including external morphology (texture), chemical composition, and crystalline structure and orientation of materials making up the sample. In most applications, data are collected over a selected area of the surface of the sample, and a 2-dimensional image is generated that displays spatial variations in these properties. Areas ranging from approximately 1 cm to 5 microns in width can be imaged in a scanning mode using conventional SEM techniques (magnification ranging from 20X to approximately 30,000X, spatial resolution of 50 to 100 nm).The SEM is also capable of performing analyses of selected point locations on the sample, this approach is especially useful in qualitatively or semi-quantitatively determining chemical compositions[31].

The scanning electron microscope used in imaging the nanoparticles is a VEGA//EasyProbe which is a favorable combination of a scanning electron microscope and a fully integrated energy dispersive X-ray microanalyser produced by TESCAN, s.r.o., Libušina trída 21.

3-13-3 Electrical tests

To study the electrical properties of the prepared ferrite especially at high frequencies, we have to test the electrical resistivity of the prepared samples.

3-13-3-1 measurement of electrical resistivity

Resistivity: This is the electrical resistance of a ferrite core, having a constant cross-sectional area and its unit is ohm-cm. In the present work The surface of the pellets is cleaned by grinding with SiC paper in order to remove any contamination and then used to study the room temperature resistivity, silver paste is used to coat the polished pellets to provide electrical contacts. DC - resistivity is measured by a two-probe method using LCR meter. We apply the relationship (2-6) to measure The electrical resistivity.

3-13-4 Magnetic test

Magnetic flux density(B)- this is defined as the number of magnetic lines if force passing through a unit area of cross-section.

Coercive force (Hc)-it is the magnetizing field strength (H) required to bring the magnetic flux density (B) of a magnetizes material to zero. It's unit is oersted [29]. To measure the hysteresis loop The values of magnetic field strength and magnetic induction can be measured indirectly by monitoring the applied current **I** in the transformer coil and the induced magnetic flux ϕ through the core and taking into account the relations [63].

$$H = \frac{N_1}{L} I \dots\dots\dots\dots\dots\dots\dots\dots\dots\dots\dots\dots\dots\dots\dots\dots\dots\dots\dots(3\text{-}3)$$

$$B = \frac{\phi}{N_2 A} \dots\dots\dots\dots\dots\dots\dots\dots\dots\dots\dots\dots\dots\dots\dots\dots\dots.(3\text{-}4)$$

where N1, N2 are the number of turns in primary and secondary coils respectively, L is the inductance of a coil, A is the cross-section of a ferromagnet. The magnetic flux ϕ is calculated as the integral of the voltage us induced in the secondary coil.

3-13-5 Mechanical test (Hardness)

Vickers hardness test is used to measure the hardness of ferrite samples , it inserts a tool sutures (indenter) in several regions of the surface of the sample . Hardness test a very small diamond indenter having pyramidal geometry is forced into the surface of the specimen [67,72]. The angle between the faceted (136º) are calculated through the Vickers hardness as follows:

$$V.H = \frac{F}{d^2/2 \ sin*\frac{1}{2}(136°)} \quad \text{...(3-5)}$$

F Represents the load hanging, d Represents the average impact of diameter.

$$V.H = 1.854\frac{F}{d^2} \quad \text{..(3-6)}$$

4-1 Introduction

This chapter includes results and discussions, calculations for the tests (X-ray diffraction, scanning electron microscope (SEM), density, porosity, hardness, electrical resistivity, hysteresis loop).

4-2 Structures Test

X-Ray Diffraction method:

X-ray diffraction is a versatile, non-destructive analytical method for identification and quantitative determination of various crystalline forms, known as 'phases' of compound present in powder and solid samples. X-Ray diffraction patterns are recorded from 20° to 60° (XRD-6000) using Cu Kα (λ=1.5406 Å) with an accelerating voltage of(60 KV), of the SHIMADZU company (JAPAN). Data are collected with a counting rate of 5°/min. From XRD the crystallite size can be found out by using the scherrer's formula.

4-2-1 XRD pattern of ZnO powder

The XRD pattern is obtained by using X-ray diffractometer. The crystal planes of (100), (002) and (101) belong to hexagonal system. The crystal parameters are (a = 3.249Å and c = 5.206 Å) by using equation (2-3) . All diffraction data are in good agreement with JCPDS files No.361451, no other phases are detected, and the diffraction peaks are sharp, and the crystal grows completely with high purity. The powders are calcined at (a) 350 and (b) 450 °C for 2 hours. The XRD pattern of the synthesized ZnO powders are shown in Figure (4-1).
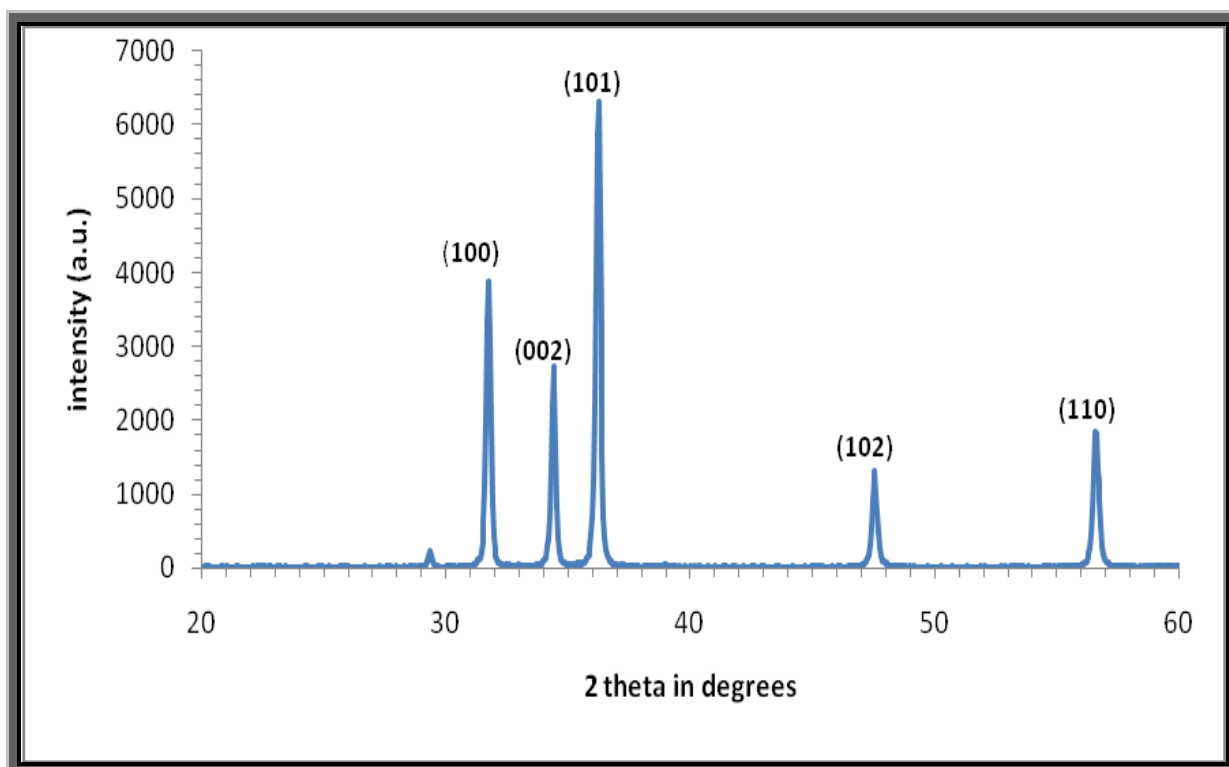
(a) calcined at 350 °C
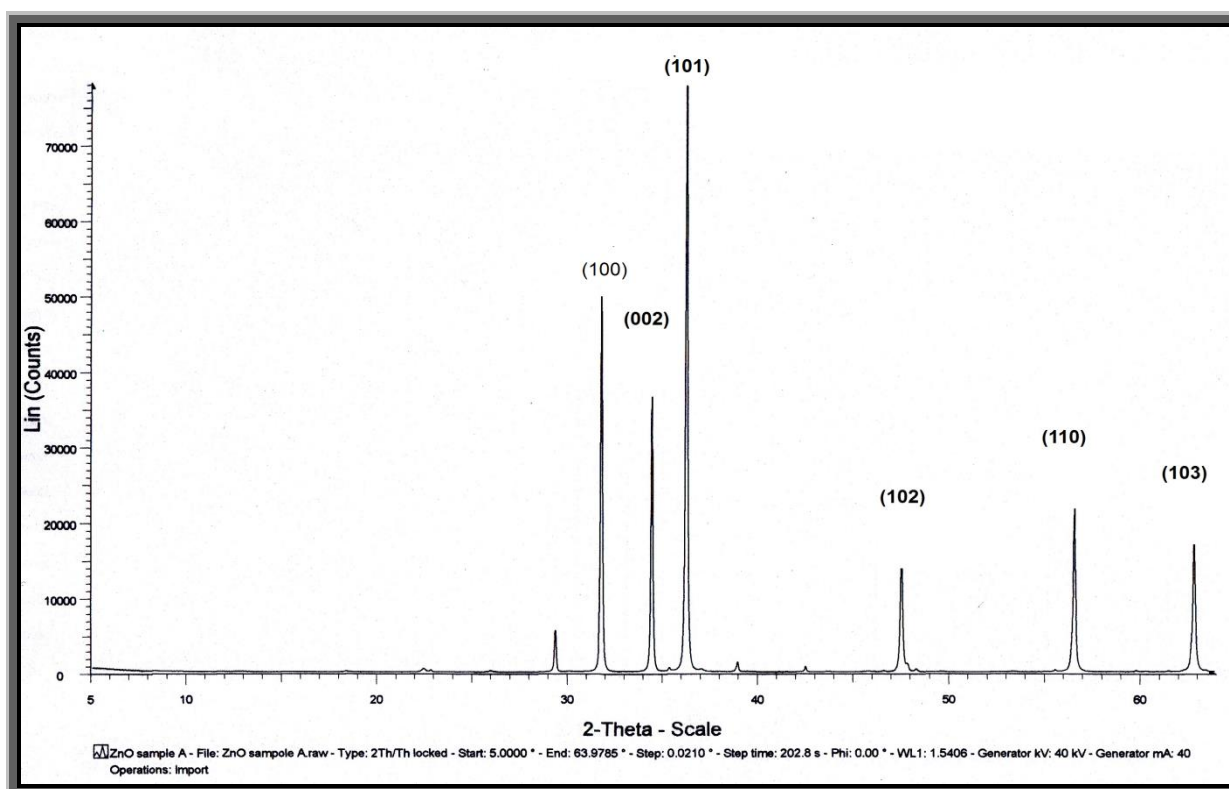
(b) calcined at 450 °C

Figure (4-1) XRD patterns of ZnO calcined at (a) 350 °C, (b) 450 °C

Figures (4-1) (a) and (b) show the XRD patterns of ZnO samples calcined at 350 °C and 450 °C respectively It is very clear that the major reflections between 30°and 40° (2θ values) indicate more crystalline regions in the zinc oxide sample, also the less intense peaks at 48°, 57°, 63° and 70° (2θ values) indicate the high crystallinity of ZnO samples. The detailed analysis of the XRD and the assignments of various reflections are given in the Tables (4-1-a) and (4-1-b).

Table (4-1-a) Strongest three peaks (calcined at 350 °C)

No.	Peak No.	2 Theta (deg)	d(Å)	FWHM (deg)	Intensity (counts)
1	3	36.2477	2.4762	0.19540	4674
2	1	31.7648	2.8147	0.19800	2683
3	2	34.4213	2.6033	0.19680	1980

Table (4-1-b) Strongest three peaks (calcined at 450 °C)

No.	Peak No.	2 Theta (deg)	d(Å)	FWHM (deg)	Intensity (counts)
1	3	36.4078	2.732	0.129	78000
2	1	31.9307	2.943	0.1209	51000
3	2	34.5833	2.869	0.1184	37000

Particle size calculation from x-ray diffraction of ZnO

From this study, considering the peak at degrees, average particle size has been estimated by using Debye-Scherrer formula (2-2).

(a) for sample calcined at 350 °C :

D =41.86 nm

(b) for sample calcined at 450 °C :

D =66.19 nm

So the average particle sizes of the ZnO calcined at 350 and 450 °C are about 41.86 and 66.19 nm respectively, which demonstrate that the average particle sizes increased as the calcining temperature increased. During the calcining the diffusion of particle to particle followed by the formation of grain boundary and the closing of voids and neck growth proceeds rapidly but powder particles remain discrete. The structure recrystallizes and particles diffuse into each other. Isolated pores tend to become spheroidal and densification continues at a much lower rate.

In addition, it also demonstrates that the ZnO calcined at lower temperatures contains some non-crystals and has smaller crystallite size. This result is identical to the result obtained by Liqiang Jing et al (2002) in their preparation and characterization of ZnO ultrafine particles [12]. They estimate values of D for the ZnO calcined at 320, 430 and 550 °C to be 12.1, 17.9 and 25.3 nm, respectively.

4-2-2 XRD pattern of CuO powder

Copper bicarbonate is calcined at (a) 350 and (b) 450 °C for 2 hours. The XRD patterns of the synthesized CuO powder are shown in Figure (4-2) (a) and (b) for those calcined at 350 °C and 450 °C respectively.
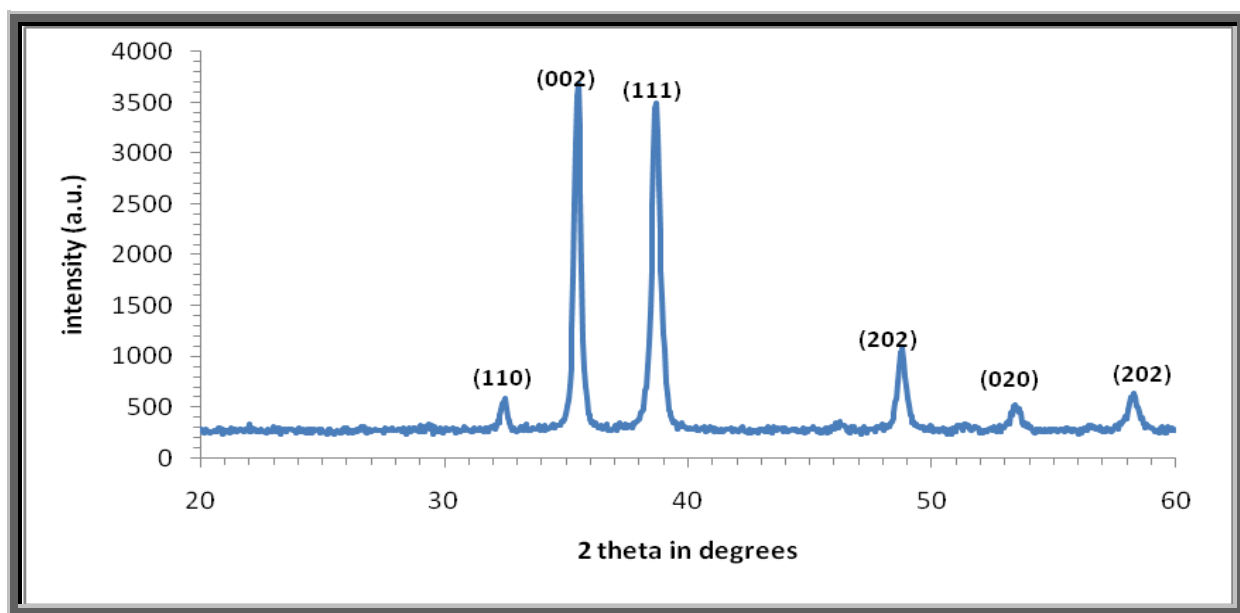
(a) calcined at 350 °C
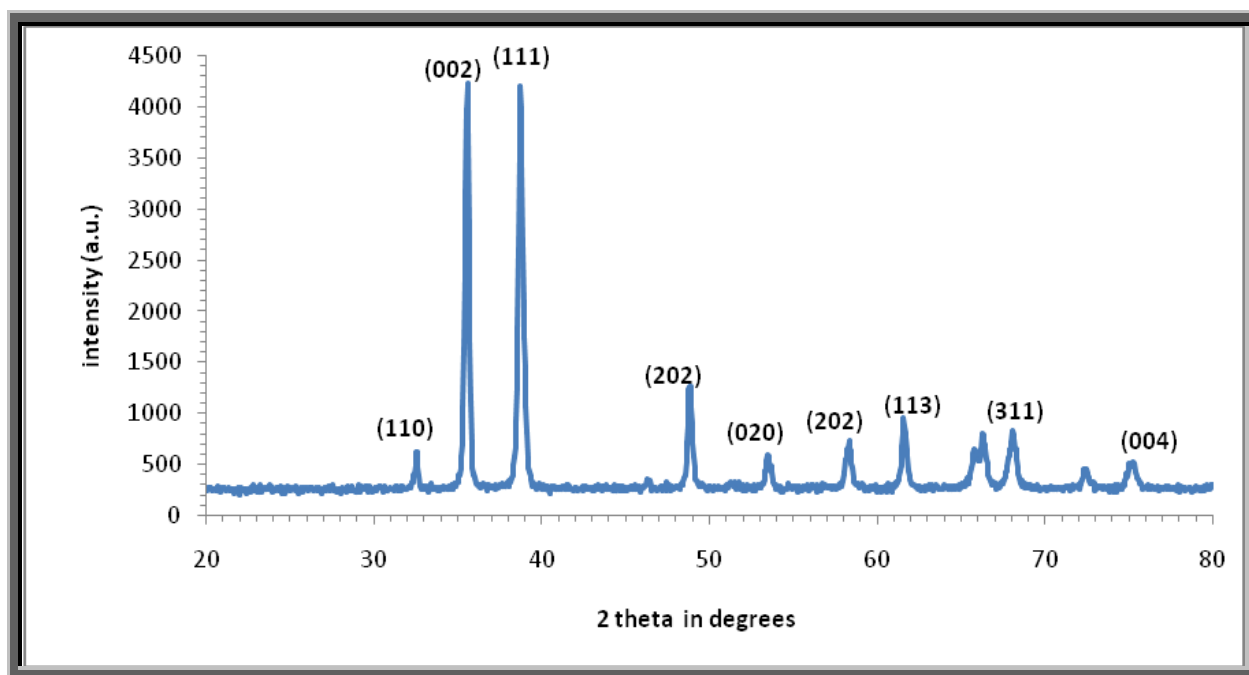
(b) calcined at 450 °C

Figure (4-2) XRD patterns of CuO calcined at (a) 350 °C (b) 450 °C

In Figure (4-2) the crystal planes of (110), (002) and (111) belong to monoclinic system. All diffraction data are in good agreement with JCPDS files No.961011195, (a = 4.6700 Å , b = 3.4300 Å and c = 5.1200Å) and no other phases are detected, and the diffraction peaks are sharp with the crystal growing completely with high purity.

From figure (4-2) (a) and (b) one can see that the XRD patterns of CuO samples calcined at 350°C and 450°C respectively it is very clear that the major reflections between 30° and 40°(2θ values) indicate more crystalline regions in the copper oxide sample; besides the less intense peaks at 48.7°, 53.4° and 57.8° (2θ values) indicate the high crystallinity of CuO samples. The detailed analysis of the XRD and the assignments of various reflections are given in the Table (4-2-a) and (4-2-b).

Table (4-2-a) Strongest three peaks (sample calcined at 350°C)

No.	Peak No.	2 Theta (deg)	d(Å)	FWHM (deg)	Intensity (counts)
1	2	35.4851	2.52772	0.31720	2345
2	3	38.6944	2.32514	0.36800	2248
3	4	48.7530	1.86635	0.34590	580

Table (4-2-b) Strongest 3 peaks (sample calcined at 450°C)

No.	Peak No.	2 Theta (deg)	d(Å)	FWHM (deg)	Intensity (counts)
1	2	38.7294	2.32312	0.29120	2714
2	3	35.5433	2.52372	0.27830	2712
3	4	48.8098	1.86431	0.28160	749

The XRD pattern of figure (4-2) which is identical to the single-phase CuO with a monoclinic structure, no peaks of impurity are identified. This indicates that the synthesis of CuO is of high purity. The broadening of the peaks indicates that the crystal size is small.

Particle size calculation from x-ray diffraction of CuO

by using Debye-Scherrer formula (2-2):

(a) for sample calcined at 350 °C :

D =26.83 nm

(b) for sample calcined at 450 °C :

D =29.44nm

Calculations based on Scherrer's equation lead to mean particle size values of 26.83 nm for the sample calcined at 350°C and of 29.44nm for the sample calcined at 450 °C. This, however demonstrates that the average particle size increased as the calcining temperature increased. This result agrees with the result obtained in the preparation of zinc oxide.

4-2-3 XRD pattern of Fe_2O_3 powder

X-ray diffraction patterns that represent the general behavior of the sample annealed in the temperature of 200^oC will be shown. This sample has been prepared by the previously described method. The major XRD peak was obtained at $2\theta = 33.16$ while the second major peak is obtained at $2\theta = 35.66$. For various samples belonging to this range of annealing temperature, the relative intensity of these two major peaks lay between 70 to 80 %. The other observed peaks are at $2\theta = 40.88$, 49.72, and 54.06. The relative intensities of the two major peaks and the other smaller peaks that are observed suggest strongly that alpha Fe_2O_3 is the major phase in this material. The lattice constants so obtained for this set of alpha Fe_2O_3 nanoparticles are a = b = 5.0355 Å and c = 13.7471 Å. Figure (4-3) shows x-ray diffraction of Fe_2O_3.
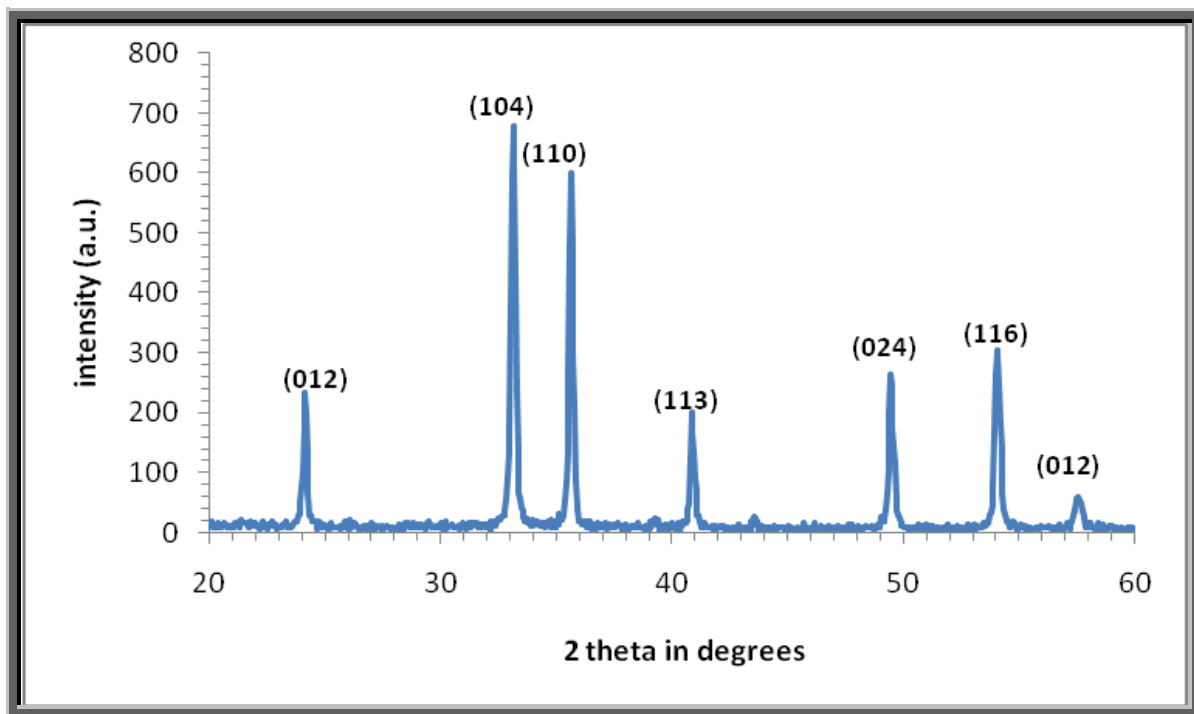
Figure (4-3) XRD patterns of Fe_2O_3 prepared and annealed at 200 °C

The crystal planes of (110), (104) and (012) belong to hexagonal system. The crystal parameters are a = 5.035 Å and c = 13.747 Å. All diffraction data are in good agreement with JCPDS files No.962101168, no other phases are detected, and the diffraction peaks are sharp, with crystal growing completely to high purity. Table (4-3) shows data of strongest three peaks:

Table (4-3) Strongest three peaks (Fe_2O_3 prepared and annealed at 200°C)

No.	Peak No.	2 Theta (deg)	d(Å)	FWHM (deg)	Intensity (counts)
1	2	33.1693	2.6987	0.23170	451
2	3	35.6666	2.5152	0.21890	368
3	4	54,0686	1.6947	0.23000	242

Fe$_2$O$_3$ particle size calculation from x-ray diffraction

Average particle diameter D is obtained from the main peaks using Scherrer's formula (2-2) for the peak width broadening as a function of the size of the particles.

D =34.75 nm

In the current sol-gel method of preparation we observe that the size of the particles depends on three parameters which are : dilution of the solutions, concentration of the citric acid solution, and the annealing temperature of the dried gel.

4-2-4 Ferrites characterization from x-ray diffraction

X-ray diffractometer is used to identify the types of ferrites from their crystalline phases. The characteristic pattern of the samples is compared with ICDD-JCPDS (The International Centre for Diffraction Data-Joint Committee on Powder Diffraction Standards) standard pattern for crystals identification. Peak intensity is often examined to quantify the crystalline compound as it represents all the scattering of specific compound detected, thus related to both structure and composition of the compound. Internal standard method is one of the quantitative methods [73].

Generally, XRD can be used to characterize the crystallinity of nanoparticles, which gives the average diameters of all the nanoparticles. The precipitated fine particles are characterized by XRD for structural determination and estimation of crystallite size. The lattice constant (a) is computed using the 'd' value and with their respective (h k l) parameters. Same ferrites (F3, F4, C1, C2, C3, C4, C5, C6) prepared for the present work are phase analyzed by standard XRD and are shown in figure (4-4).
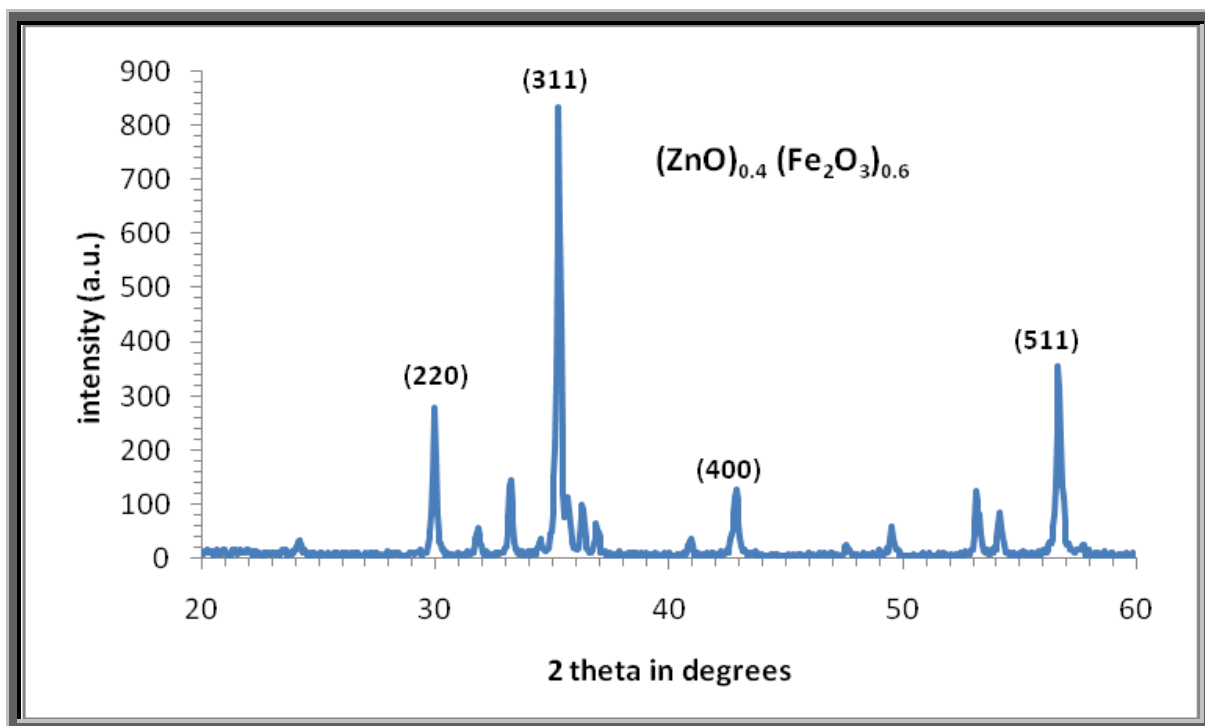
F3
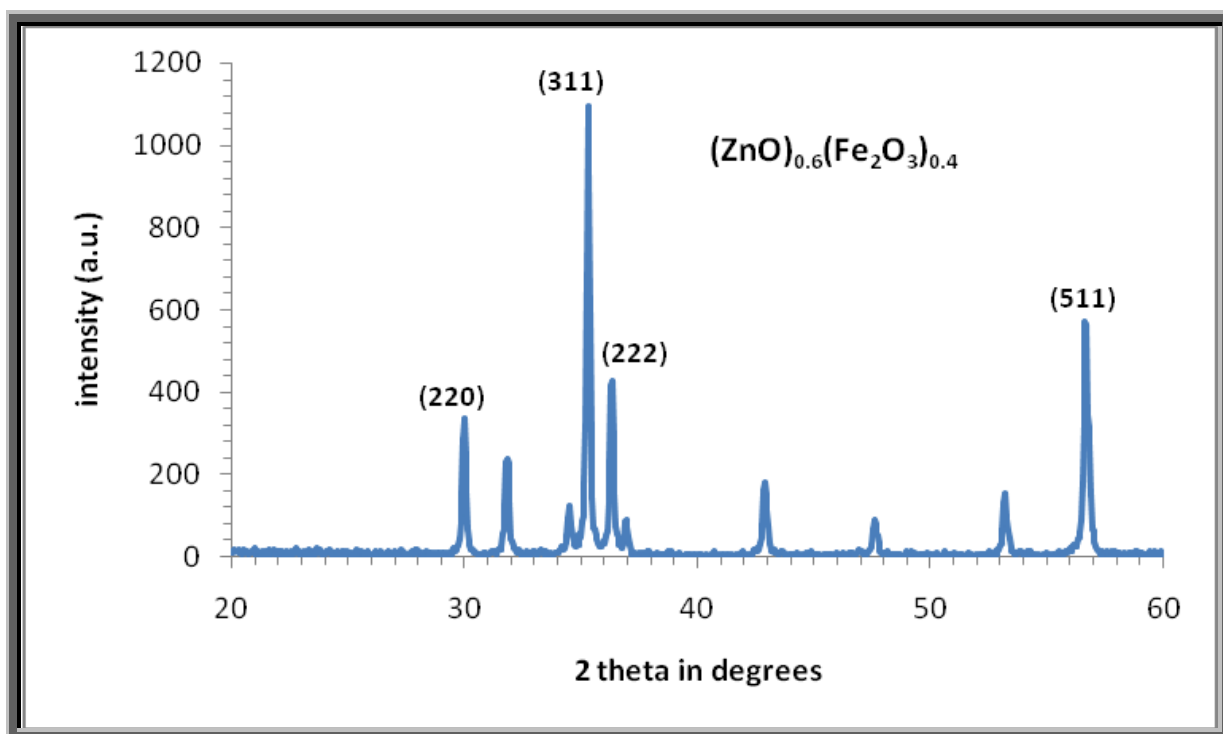
F4

Figure (4-4-a) XRD pattern of (F3,F4) ferrites sintered at 1000 °C for 4 hours
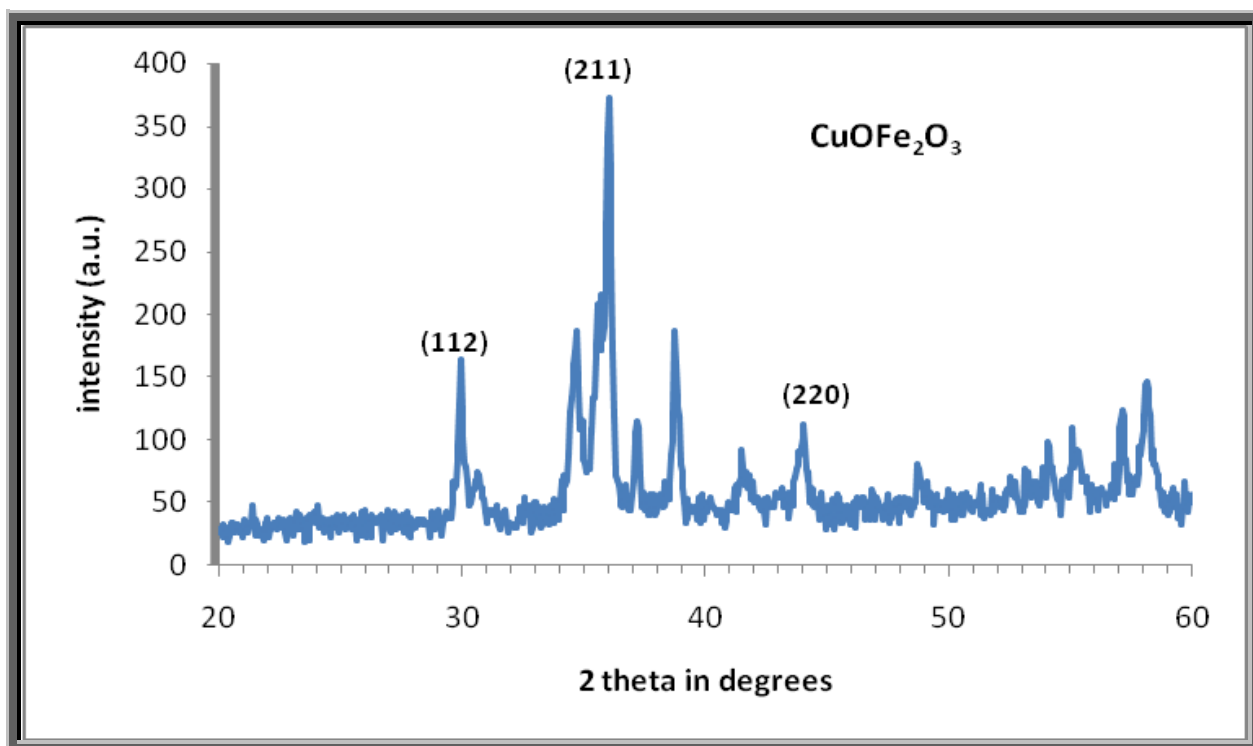
C1
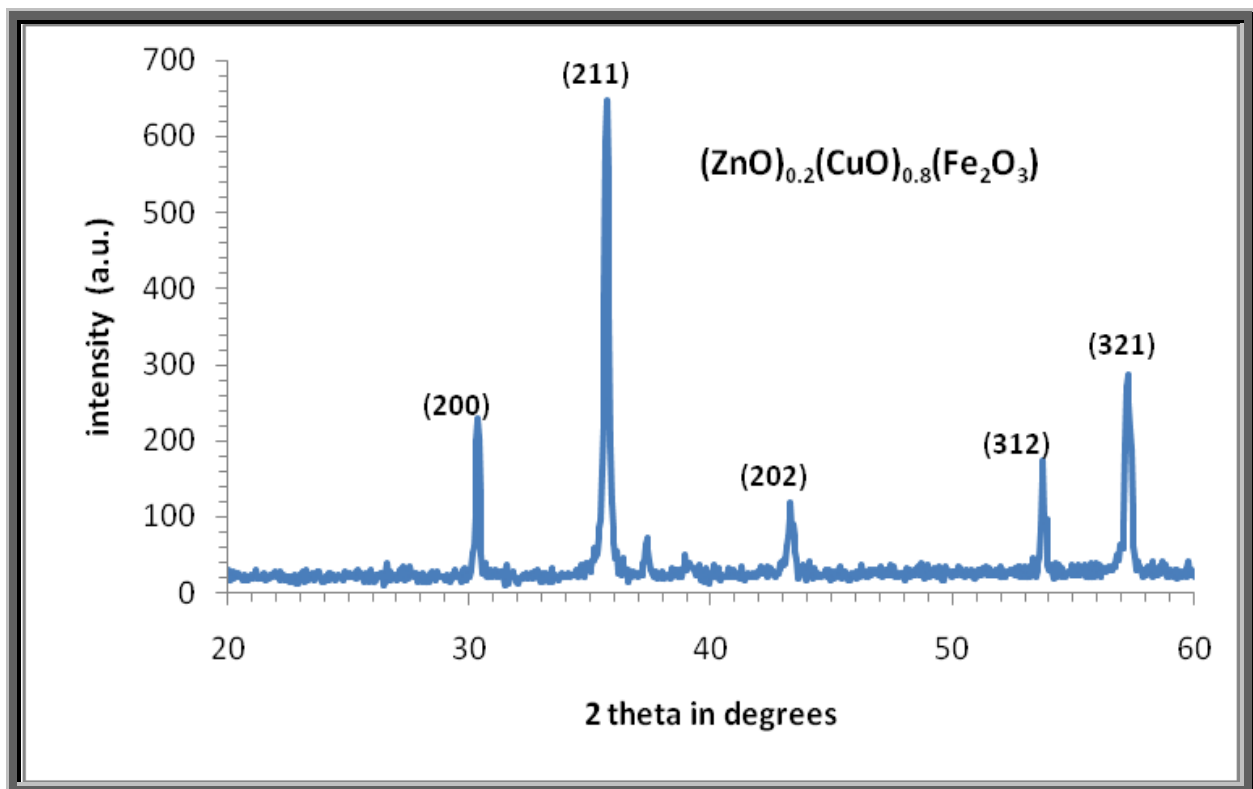
C2

Figure (4-4-b) XRD pattern of (C1,C2) ferrites sintered at 1000 °C for 4 hours
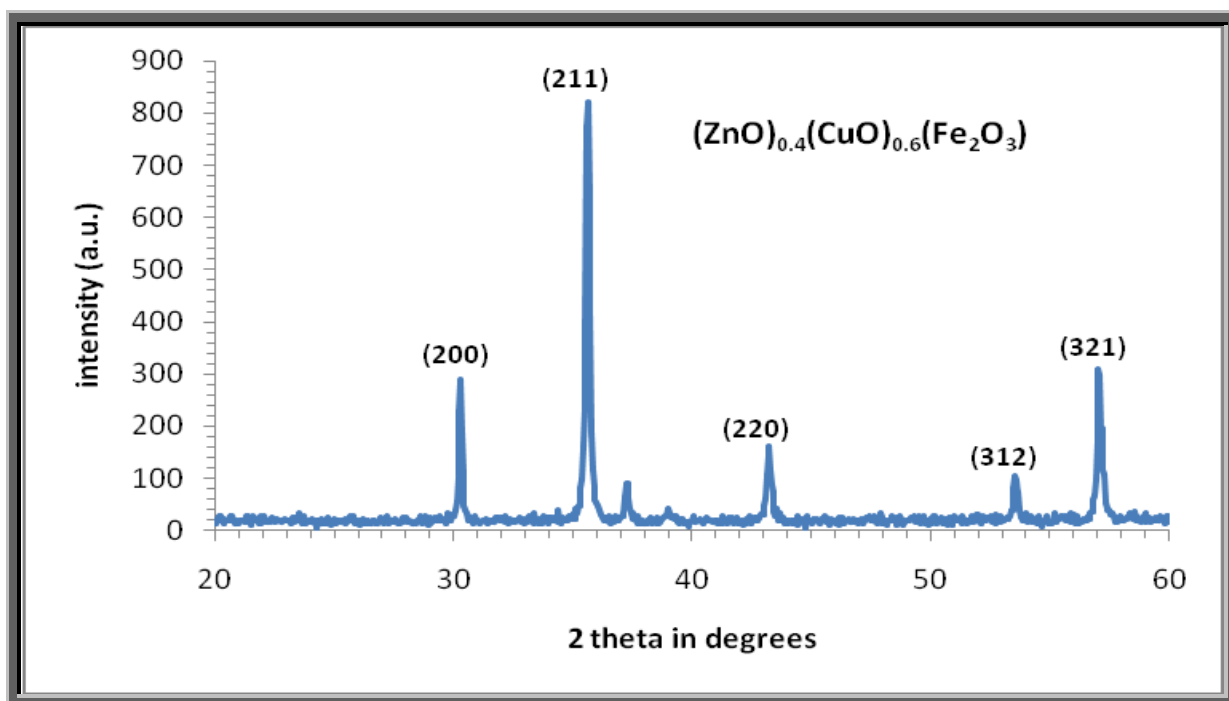
C3
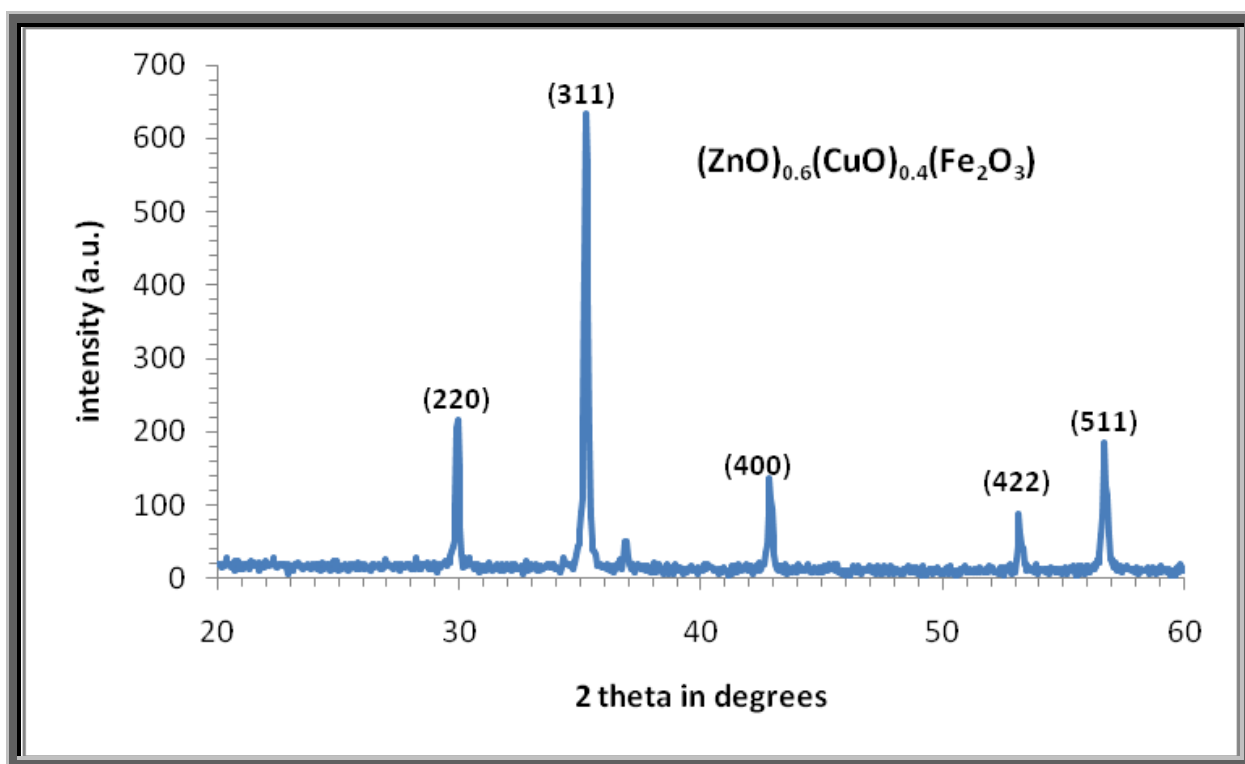
C4

Figure (4-4-c) XRD pattern of (C3,C4) ferrites sintered at 1000 °C for 4 hours
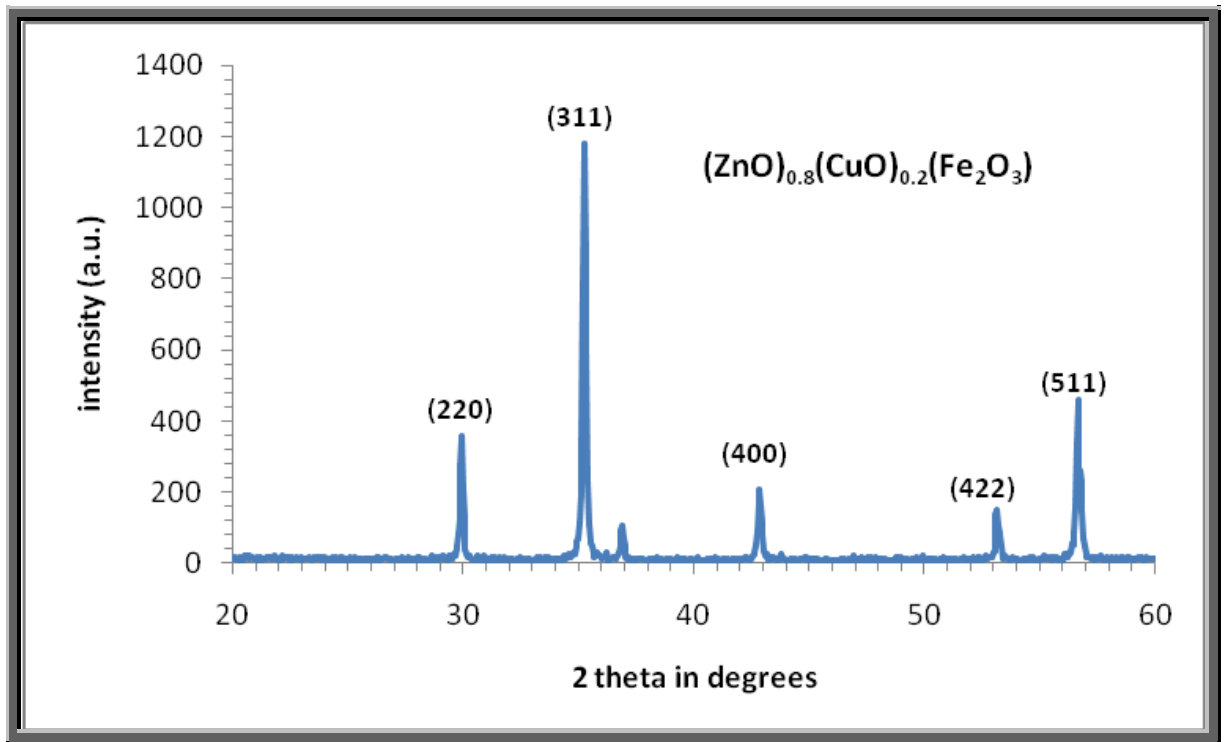
C5
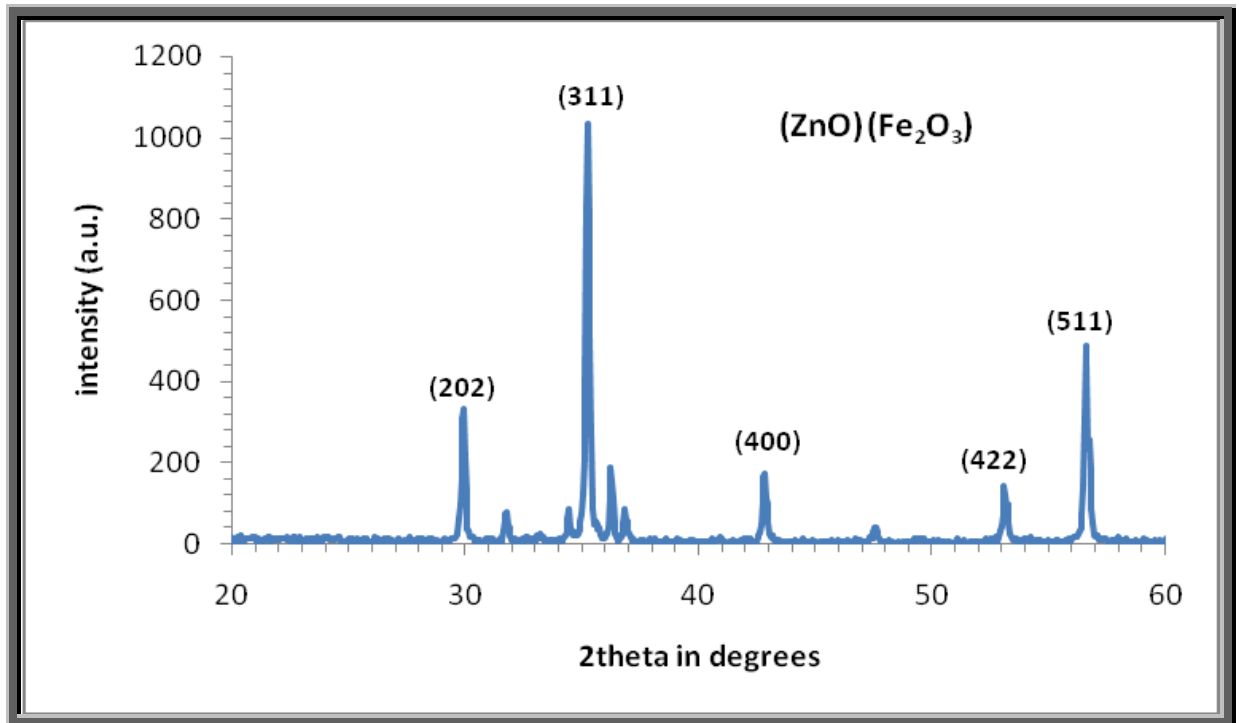
C6

Figure (4-4-d) XRD pattern of (C5,C6) ferrites sintered at 1000 °C for 4 hours

The lattice parameters and crystallite size of the sintered ferrite specimens are evaluated from XRD analysis. The broad peaks in the XRD patterns indicate a fine particle nature of the particles. Table (4-4) shows the XRD data of ferrites sintered at 1000°C.

Table (4-4) XRD data of ferrites calcined at 1000 °C (Strongest 3 peaks)

1000 °C			
Sample	2 Theta (deg)	d(Å)	FWHM (deg)	Intensity (counts)
F_3	35.3224	2.53899	0.16930	582
	56.6785	1.62274	0.18190	285
	30.001	2.97591	0.16620	197
F_4	35.3332	2.53824	0.15680	807
	56.6861	1.62254	0.16910	493
	36.3438	2.46995	0.16460	311
C_1	36.0389	2.49014	0.28610	216
	35.5874	2.52069	0.37700	99
	34.6613	2.58589	0.42870	87
C_2	35.7064	2.51256	0.20370	453
	57.2534	1.60780	0.20160	227
	30.3765	2.94017	0.17560	150
C_3	35.6567	2.51595	0.17740	596
	57.0912	1.61199	0.17300	247
	30.3173	2.94578	0.15390	178
C_4	35.2827	2.54176	0.16550	470
	29.9582	2.98027	0.15680	144
	56.7054	1.62203	0.17980	141
C_5	35.2766	2.54219	0.15600	840
	56.6633	1.62314	0.16310	346
	29.9667	2.97944	0.15660	222
C_6	35.2672	2.54284	0.17030	734
	56.6277	1.62407	0.15840	424
	29.9553	2.98055	0.17010	230

Most modern magnetically soft ferrites have a cubic spinel structure. The $ZnO_X(Fe_2O_3)_{1-X}$ and $(ZnO_X CuO_{1-X} Fe_2O_3)$ ferrites are sintered at 1000 °C for 4 hours. XRD patterns show that a single phase $ZnOFe_2O_3$ ferrite with the cubic spinel structure and all the samples demonstrate the high crystalline structure. The formation of a spinel crystal structure has been noted on the basis of diffraction peaks corresponding to Miller indices of (220) and (311), this result is identical to the result obtained by J.M. Yang and F.S. Yen (2008)[20]. Which confirms the formation of cubic spinel structure. Figure (4-4-a) illustrates ferrrites (F3,F4) of cubic spinel structure, the results obtained by XRD are in good agreement with the JCPDS card (22-1012). Table (4-5) shows the particle size of $ZnOFe_2O_3$ ferrites:

Table (4-5) particle size of $ZnOFe_2O_3$ ferrites

Sample	2 Theta (deg)	d(Å)	FWHM (deg)	Particle size(nm)	Cubic a(Å)
F_3	35.3224	2.53899	0.16930	50.362	8.421
F_4	35.3332	2.53824	0.15680	54.296	8.428

In ferrite $Zn_X(Fe_2O_3)_{1-X}$, the particle size increases when ZnO increases. The lattice constant (a) is found to increase with the increase in zinc oxide concentration. The lattice parameter (a) of the cubic structure samples is determined by using the relation (3-2).

In $(ZnO_XCuO_{1-X} Fe_2O_3)$ ferrites, the solid interaction between CuO and Fe_2O_3, leading to the formation of copper ferrite, begins only above 800°C to 1000°C. Depending on the cation distribution among the interstitial sites of the spinel structure, copper ferrite crystallizes either in a tetragonal or cubic symmetry[54]. A single phase is formed for the sample with x = 0 ,($CuOFe_2O_3$). The diffraction peaks of Fe_2O_3 disappear completely but a small amount of CuO remains as second phase beside the tetragonal copper ferrite, for(x = 0, 0.2, 0.4) figure (4-4) illustrates ferrites (C1,C2,C3) single phase of tetragonal copper. The

samples show all the characteristic peaks of ferrite material with most intense peak (211),which confirms the formation of tetragonal structure ferrite. This result is identical to the result obtained by Kenfack Flaurance in the study of Cu-Ni-Fe-O system (2004)[54].

In $ZnO_XCuO_{1-X} Fe_2O_3$ ferrites for (x = 0.6, 0.8, 1), the samples show all the characteristic peaks of ferrite material with most intense peak (311), which confirms the formation of cubic spinel structure. The results obtained by XRD are in good agreement with the JCPDS card (34-0425). The particle size of ferrite sample is calculated using Scherrer's formula and is shown in table (4-6) together with lattice parameters .

Table (4-6) particle size of ferrites and lattice parameters

Sample	2 Theta (deg)	d(Å)	FWHM (deg)	particle size (nm)	Cubic a(Å)	Tetragonal a,c(Å)
C_1	36.0389	2.49014	0.28610	29.82		a=8.273, c=1.173
C_2	35.7064	2.51256	0.20370	41.867		a=5.880,c=0.955
C_3	35.6567	2.51595	0.17740	49.64		a=5.892, c=0.954
C_4	35.2827	2.54176	0.16550	51.481	8.430	
C_5	35.2766	2.54219	0.15600	54.352	8.431	
C_6	35.2672	2.54284	0.17030	50	8.434	

From the above data, it turns out that in ferrite ($ZnO_X CuO_{1-X} Fe_2O_3$) the lowest value of the particle size at x=0, ($CuOFe_2O_3$) without ZnO ,and the particle size increases when ZnO increases .In ferrite C6 as x = 1 the particle size of (50 nm) with formula ($ZnOFe_2O_3$) without CuO. The lattice constant (a) is found to increase with the increase in zinc oxide concentration. In tetragonal structure ferrite, the lattice parameters (a,c) are calculated using the relation[59].

$$d_{hkl=\frac{1}{(\frac{h^2+k^2}{a^2}+\frac{l^2}{c^2})^{1/2}}}$$

4-3 Scanning electron microscope (SEM) test

The morphology and image of powder samples are done by scanning electron microscope (SEM) type VEGA//EasyProbe which is a favorable combination of a scanning electron microscope.

4-3-1 SEM of ZnO powder calcined at 350 °C

The SEM images of the ZnO sample prepared by precipitation methods and calcined at 350 °C are shown in figure (4-5).
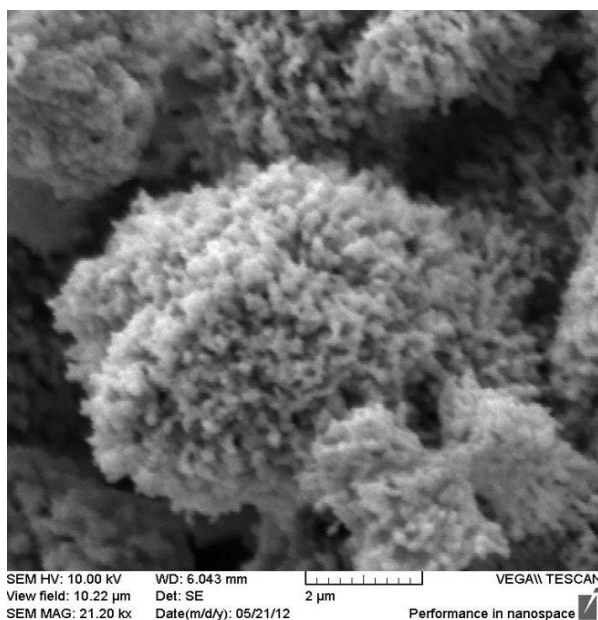
Figure (4-5) SEM images of ZnO powders calcined at 350°C

The figure above shows that a network formation and agglomeration has taken place. The study of SEM micrograph reveals less number of pores with smaller lump size.The SEM micrographs clearly shows the microstructural homogeneity and remarkably dense mode of packing of grains of ZnO nanoparticles with minimum porosity.

4-3-2 SEM of CuO powder calcined at 350 °C

Figure (4-6) shows the SEM image of the synthesized CuO sample prepared and calcined at 350°C. In which homogeneous system with agglomerates of submicronic particles is observed.
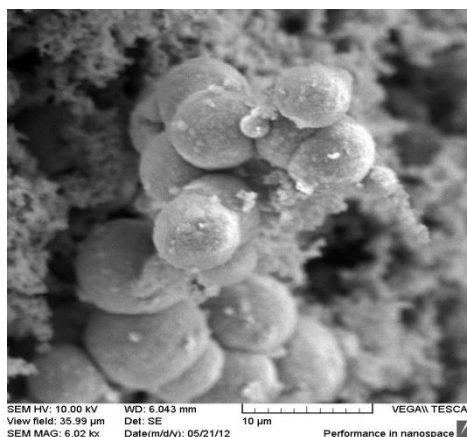
Figure (4-6) SEM image of CuO powders calcined at 350

It can also be observed that the powders are composed of non-agglomerated spherical particles, with the formation of soft agglomerates with irregular morphology constituting the quite fine particles. The study of SEM micrographs reveals a less number of pores with smaller lump size. This result is similar to the result obtained by Yu Li (2008) [74], in the Synthesis of Copper (II) Oxide Particle for Hydrogen Generater catalysts. Which is shown in figure (4-7) SEM image of CuO.
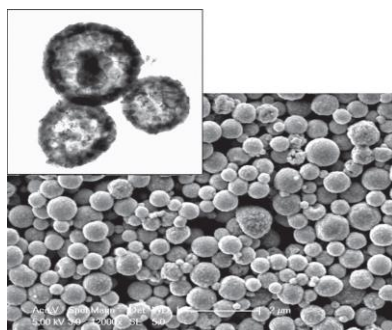
(4-7) SEM image of CuO[74].

We can also see from the above image a spherical particles of CuO [74].

4-3-3 SEM of CuO powder calcined at 450 °C

Figure (4-8) shows the SEM images of CuO sample prepared and calcined at 450°C, where we can observe that the powders are composed of non-agglomerated flower shape nanoparticle CuO.

SEM HV: 10.00 kV	WD: 6.048 mm		VEGA\\ TESCAN
View field: 21.88 µm	Det: SE	5 µm	
SEM MAG: 9.90 kx	Date(m/d/y): 05/21/12		Performance in nanospace
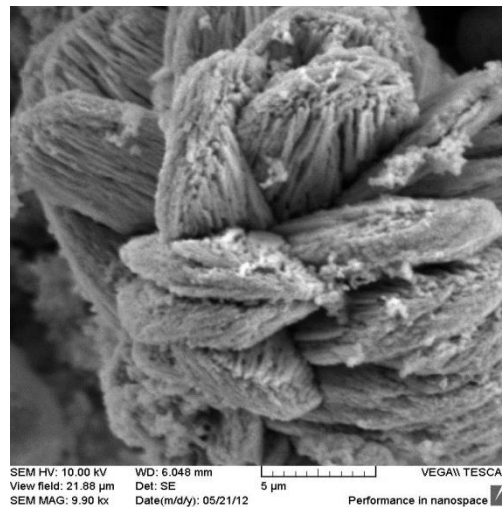
Figure (4-8) SEM images of CuO powders calcined at 450°C.

This result is similar to the result obtained by Li Zhang et al (2011) [75]. Figure (4-9) Shows SEM image of CuO with flower nanoparticle shape formation.
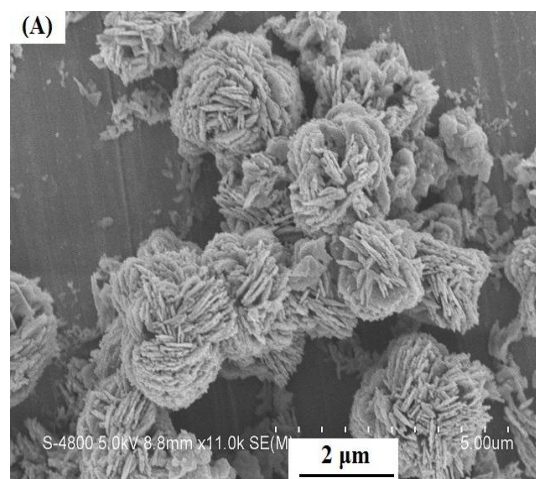
Figure (4-9) CuO flower nanoparticle [75].

SEM image reveals that a large number of CuO flower shape are formed.

4-3-4 SEM of Fe$_2$O$_3$nano particle prepared by sol-gel method

Figure (4-10) shows the SEM image of Fe$_2$O$_3$ powder annealed at 200 °C.
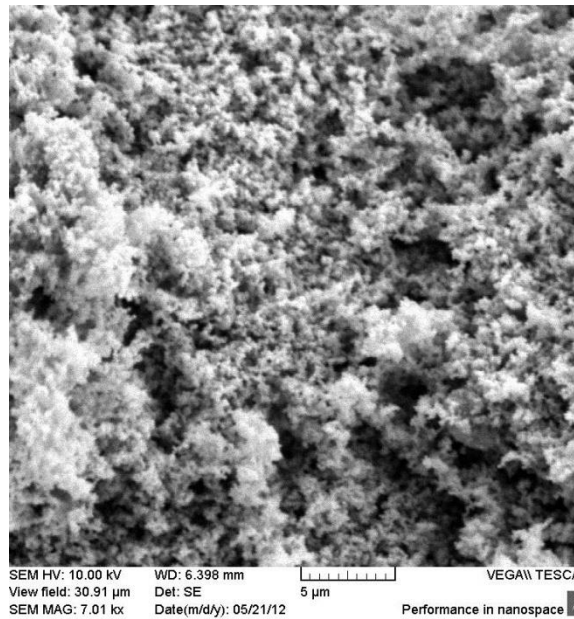
Figure (4-10) SEM image of Fe$_2$O$_3$ powders annealed at 200 °C.

Scanning electron microscopy (SEM) micrograph image of Fe$_2$O$_3$ shows a homogeneous system with agglomerates of submicronic particles. SEM micrographs of Fe$_2$O$_3$ also reveal a great decrease of particle size, and a loss of the original morphology of the particles. It also reveals a decrease in calcinations temperature resulting to particles being finer and more uniform as we observe in figure. The resulting powder consists of small irregularly shaped agglomerates.

4-3-5 SEM of ferrites sintering at 1000 °C

Figure (4-11) shows the SEM images of $ZnO_X(Fe_2O_3)_{1-X}$ and $(ZnO_X CuO_{1-X} Fe_2O_3)$ ferrites sintered at 1000°C for 4 hours.
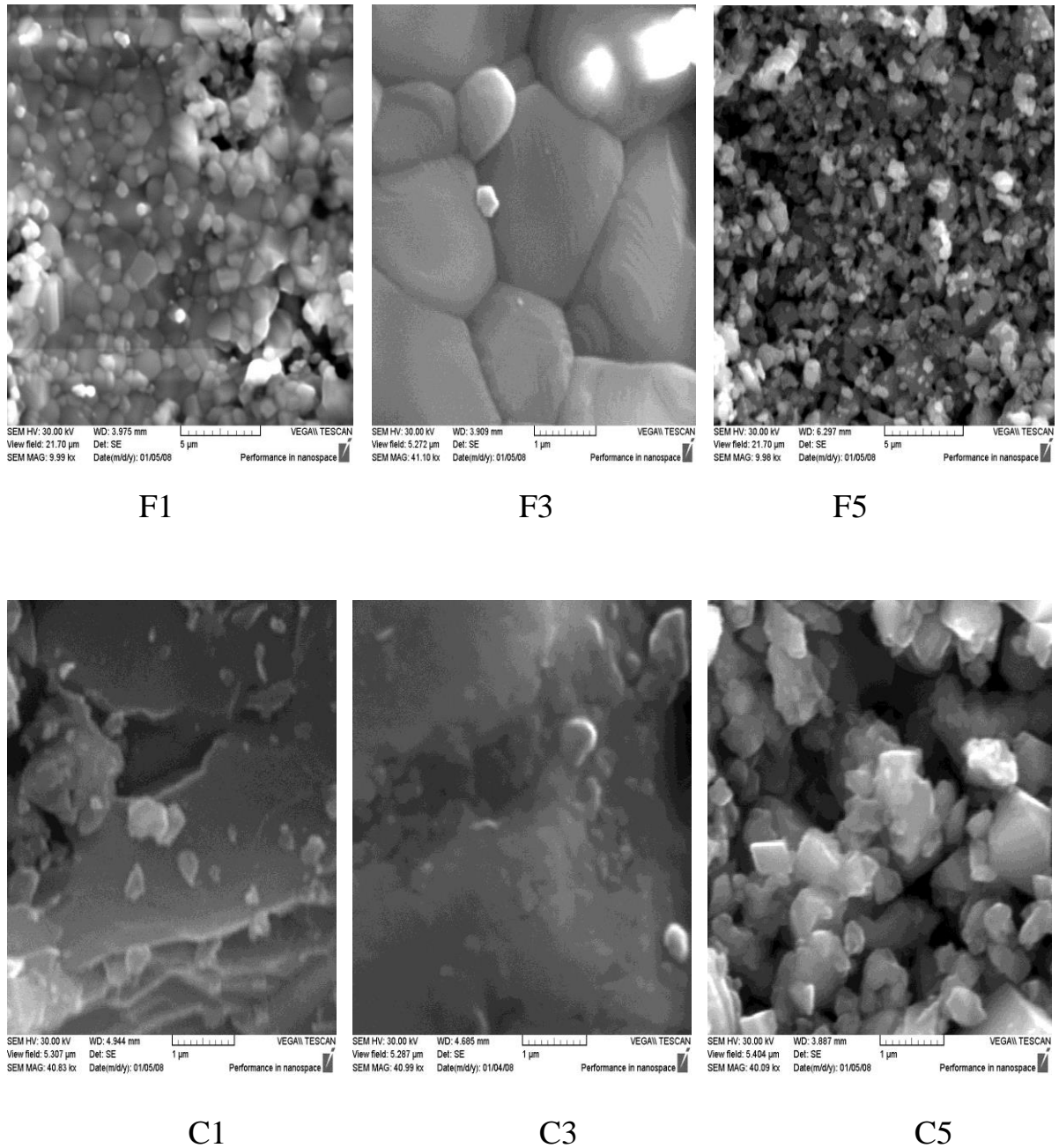
F1   F3   F5

C1   C3   C5

Figure (4-11) SEM images of ferrites (F1,F3,F5,C1,C3,C5) sintered at 1000 °C

Scanning electron microscope (SEM) applied to samples sintered at 1000°C is used to determine the lump size. From the micrograph, we can observe the formation of soft agglomerates with irregular morphology constituting the quite fine particles. The study of SEM micrographs reveals a less number of pores with smaller lump size, and a homogeneous system with agglomerates of submicronic particles. Since the ceramic method involves sintering of the stoichiometric mixtures at high temperatures, the crystallites are in order of micrometer with relatively smooth surface. The aggregate of crystallites of various sizes indicates a size distribution in the micrographs. The variation in size of the particles among the different samples is due to the difference in processing temperatures. When the ferrite powders with more crystalline content are used for samples sintered at high temperatures, the local shrinkage speed is much higher than the densification speed of the ceramics.

SEM micrograph of Fe_2O_3 pellet shows the grain boundary of the sample (F1,F3) being sintered at 1000°C. The grains are more or less spherical in shape and there is grain size distribution over different samples prepared by the ceramic method. The rate of grain growth and the resultant microstructure depend in a complex way on many factors, such as the sintering temperature, the oxygen partial pressure, and stoichiometry.

4-4 Density test

Calculation of ferrites density at different temperatures.

Experimentally,density measurements are performed using Archimedes' principle. The errors associated with this method derive mainly from thermal, surface effects pore presence and specimen size. Density of the sintered samples is measured by Archimedes method using distilled water as fluid medium. The apparent density is shown in table (4-7).

Table (4-7) apparent density of ferrites

Sample	Density g/cm^3 at 800°C	Density g /cm^3 at 900°C	Density g /cm^3 at 1000°C
F_1	4.631	4.711	4.821
F_2	4.450	4.507	4.780
F_3	3.655	4.208	4.521
F_4	3.365	3.593	3.809
F_5	3.362	3.843	4.312
F_6	3.020	3.439	3.833
C_1	3.971	4.579	4.734
C_2	3.318	3.935	4.892
C_3	3.941	4.280	4.451
C_4	3.988	4.288	4.895
C_5	3.227	3.876	4.321
C_6	3.236	3.962	4.861

There is an increase in the density and shrinkage of the sintered pellets with an increase of, time and temperature, but the porosity shows otherwise. This table confirms that the density properties increase with the increase of the sintering time and temperature.

4-5 Calculation of porosity from actual sintered density at 1000 °C

The X-ray density (Ideal density (DX)) of the samples has been computed from the values of lattice parameters using the formula (3-1).

The apparent density is calculated by Archimedes method (Actual density (D)) and the calculation of porosity using the formula (2-5). Porosity of ferrite is shown in table (4-8).

Table (4-8) porosity of ferrites

Sample	X-ray density (DX) g/cm^3	Actual density (D) g/cm^3	D/DX	1-D/DX	Porosity %
F3	5.3	4.521	0.853	0.147	14.7
F4	5.3	3.809	0.719	0.281	28.1
C4	7	4.895	0.699	0.301	30.1
C6	7	4.861	0.694	0.306	30.6

The data in table (4-8) clarify that the value of porosity varies between 14-30 % and its value is related to the particle size. Moreover, the change in the porosity for all investigated samples is due to the change in the X-ray density; another reason might be the difference in the melting point of the oxides used, i.e. the melting point of CuO (1326 °C) is lower than that of Fe_2O_3 (1566 °C).

The difference in sintering procedures used for each method also lead to a change in the number of pores, which is smallest in the ceramic method as the result of individual grains coming closer to each other which cause an increase in the effective area of grain-to-grain contact.

4-6 Mechanical test (Hardness)

Another mechanical property which is important to consider is "hardness", which is a measure of a material resistance to localized plastic deformation (a small dent or a scratch). Early hardness tests are based on natural minerals with a scale constructed solely on the ability of one material to scratch another that is softer. Vickers hardness (V.H) is used to measure the hardness of ferrite samples. The hardness of ferrites is shown in table (4-9).

Table (4-9) Vickers hardness test of ferrites

Sample	$V.H$ Sintered at 800°C	$V.H$ Sintered at 900°C	$V.H$ Sintered at 1000°C
F2	210	218	223
F3	217	221	230
F5	253	261	269
C1	265	271	280
C3	312	319	323
C5	321	332	339

Ferrites are dense, homogeneous magnetic materials made by mixing iron oxides with elements of metals such as manganese, zinc, nickel and copper. Table (4-9) shows the dependence of ferrite hardness on the temperature of the heat treatment. It seems that the amount ferrite hardness increases at about 900°C and near 1000 °C . The hardness value of a ferrite system also depends on the metal content. The hardness value increases with the increase in metal content. In ferrite (F2,F3,F5) hardness increases when ZnO increases ,as previously mentioned in ferrites (C1,C3,C5) hardness. The decrease in the hardness of ZnOCuO Fe$_2$O$_3$ ferrite system is attributed to the lower hardness value of CuO as compared to the base metal in the system .

4-7 Electrical resistivity measurement of ferrites

Resistivity of ferrites is known to depend upon the purity of the starting materials and the preparation details such as sintering temperature. The electrical resistivity of ferrites is shown in table (4-10).

Table (4-10) The electrical resistivity of ferrites

Symbol	Electrical Resistivity (Ω.cm) at 800°C	Electrical Resistivity (Ω.cm) at 900°C	Electrical Resistivity (Ω.cm) at 1000°C
F2	7.5×10^6	4.1×10^6	1.5×10^6
F3	4.7×10^6	1.3×10^6	0.7×10^6
F5	2.8×10^6	1.1×10^6	0.2×10^6
C1	8.5×10^4	6.2×10^4	4.7×10^4
C3	9.5×10^4	7.3×10^4	4.9×10^4
C5	0.1×10^5	8.2×10^4	5.4×10^6

Table (4-10) lists the variations of the electrical resistivity measured at room temperature and the values of resistivity of ferrites of different compositions sintered at various temperatures. According to the above arguments, the resistivity of the ferrites is expected to decrease with the increasing sintering temperature. However, a reverse trend is observed in the present work for sintering temperatures to about 1000°C. This indicates that some factors other than those considered above are also important in determining the resistivity of ferrite ceramics. The grain size, grain boundaries, porosity and stoichiometry are important factors in this regard. That is why samples sintered at lower temperatures which have smaller grain sizes exhibit higher values of resistivity, that resistivity of a polycrystalline material, in general, increases with the decreasing grain size. Smaller grains imply larger number of insulating grain boundaries which act as barriers to the flow of electrons. Smaller grains also imply smaller grain-to-grain surface contact area and therefore a reduced electron flow. Higher values of resistivity for ZnO ferrites have lower zinc contents. The decrease in resistivity in samples sintered above 1000 °C is attributed to the formation of Fe^{2+} phase. The formation of Fe^{2+} gives rise to

electron hopping between Fe^{2+} and Fe^{3+} ions which brings about a reduction in resistivity [76].At higher sintering temperatures, loss of zinc takes place due to volatilization, zinc volatilization at high temperatures results in the formation of Fe^{2+} ions there by increasing the electron hopping and reducing the resistivity.

High resistivity ferrites with low eddy current losses are required from the technological applications point of view. The electrical resistivity of ferrites has been normally found to increase on doping or substituting for other oxides. The electrical resistivity is increased due to the increasing of the separation between the magnetic ions whereas the number of charge carriers remains unchanged.

4-8 Hysteresis loop measurement of ferrites

The hysteresis loop is, in fact, a state of magnetization of a solid material registered as a function of the strength and direction of the magnetizing field. The exhibited loops suggest that the nano ferrite powders are basically superparamagnetic materials ,which means that each nano particle is a single magnetic domain individually characterized by spontaneous magnetization (ferromagnetic). Figure (4-12) shows the hysteresis loop of (F3)ferrites.

f	=	20000	Hz	H[A/m]	B[T]	B[T]	H coil (N1) :	5		
Hmax	=	450	A/m	10	0.035	-0.026	B coil (N2) :	5	Tested by:	AL-Tahaddie co.
Bmax	=	0.115	T	20	0.039	-0.02	H range :	± 2.5 V	Job for :	
Formf.B=		1.07		50	0.05	2137e-6	B range :	± 2.5 V	Shape :	RING
Br	=	0.031	T	100	0.064	0.038	Waveform :	Sine	Material :	
Hc	=	46	A/m	200	0.084	0.075	Amplitude :	± 2.76 V	Info 1 :	F304/53
Ps	=	34.8	W/kg	500			No. averages:	80	Info 2 :	
µamp	=	203		1000			Period :	800 Pt.	Info 3 :	
				2000			Area :	10.35 mm²		
				5000			Length :	23.56 mm		
				10000					Test No. :	REMACOMP C100A
T real =		30	°C							

F3 at 900 °C

f	=	50	Hz	H[A/m]	B[T]	B[T]	H coil (N1) :	5		
Hmax	=	448	A/m	10	0.033	-0.023	B coil (N2) :	5	Tested by:	AL-Tahaddie co.
Bmax	=	0.113	T	20	0.038	-0.015	H range :	± 2.5 V	Job for :	
Formf.B=		1.04		50	0.049	0.011	B range :	± 0.1 V	Shape :	RING
Br	=	0.028	T	100	0.064	0.043	Waveform :	Sine	Material :	
Hc	=	35.5	A/m	200	0.084	0.074	Amplitude :	± 4.42 V	Info 1 :	F304/53
Ps	=	0.08	W/kg	500			No. averages:	80	Info 2 :	
µamp	=	200		1000			Period :	800 Pt.	Info 3 :	
				2000			Area :	10.35 mm²		
				5000			Length :	23.56 mm		
				10000					Test No. :	REMACOMP C100A
T real =		30	°C							

F3 at 1000 °C

Figure (4-12) hysteresis loop of (F3) ferrites sintering at 900, 1000 °C
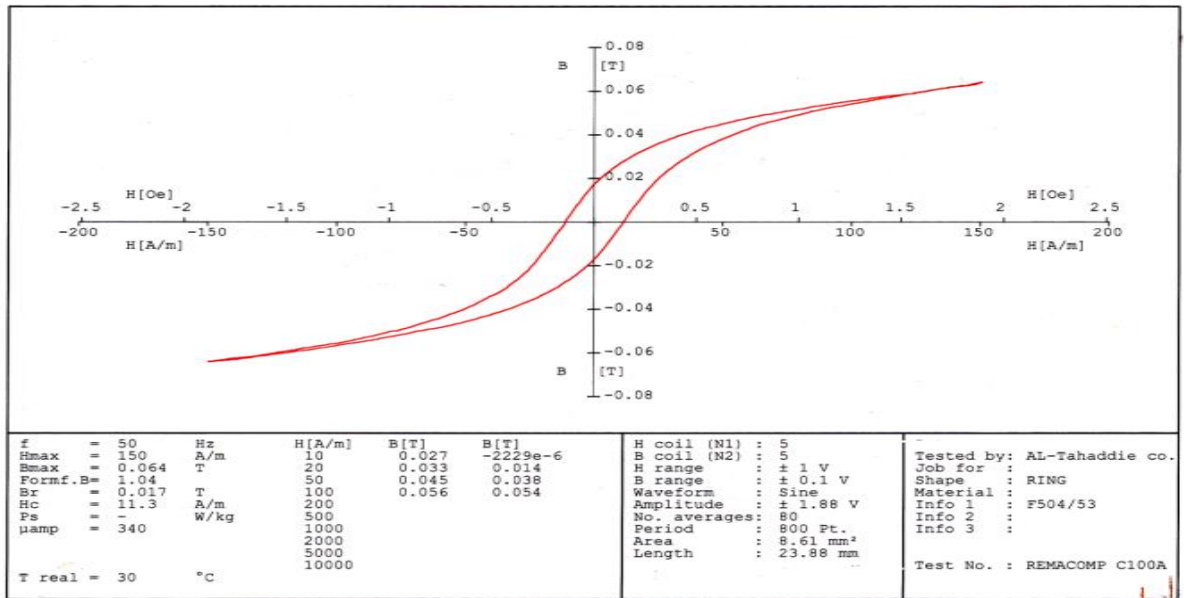
F5 at 900 °C
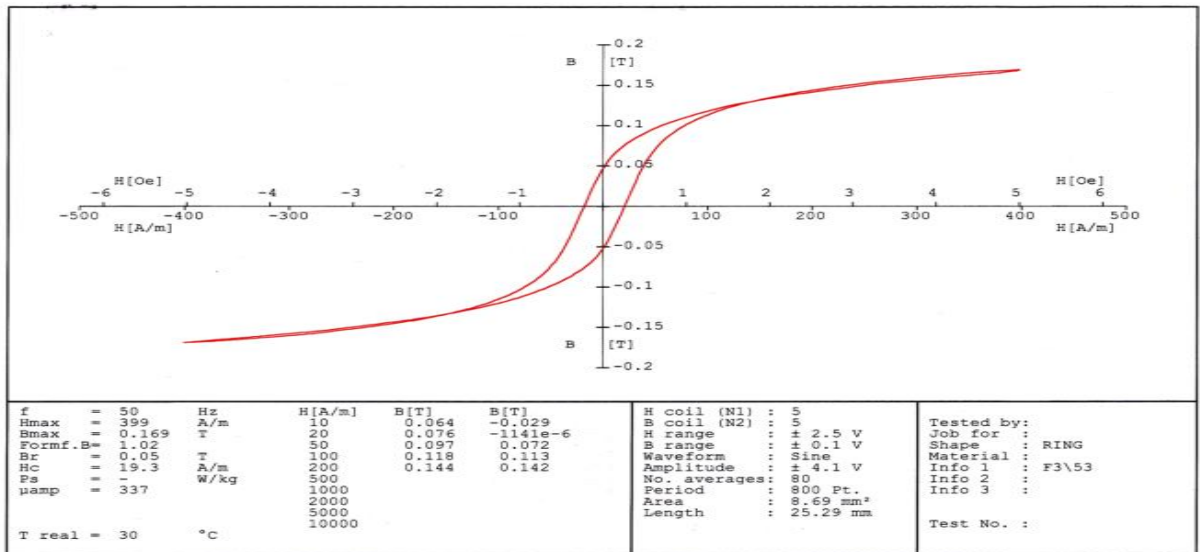
F5 at 1000 °C

Figure (4-13) hysteresis loop of (F5) ferrites sintering at 900, 1000 °C.

The figures above shows narrow hysteresis loop for F3, F5 ferrite at 1000 °C. Also it showes narrow hysteresis loop when ZnO increases for F5 ferrite, because of the insulating properties of ZnO material which cause to the resistance increases and eddy currents decrease, and thereby improving the magnetic properties. For the sample F3 which sintered at 900 °C the value of remnant magnetization (Br) was 0.031 T ,and the Coercive force Hc=46 A/m ,but for the same sample sintered at 1000 °C it seemed that Br and Hc decreased

to Br =0.028 T ,Hc=35.5 A/m respectively with the sintering temperatures increase. for the sample F5 it showed an inverse characteristics with the sintering temperatures increase these are Br =0.017 T ,Hc=11.3 A/m at 900 °C and Br =0.05 T, Hc=13.3 A/m at 1000 °C

Figure (4-14) shows the hysteresis loop of (C3) ferrites.

C3 at 900 °C
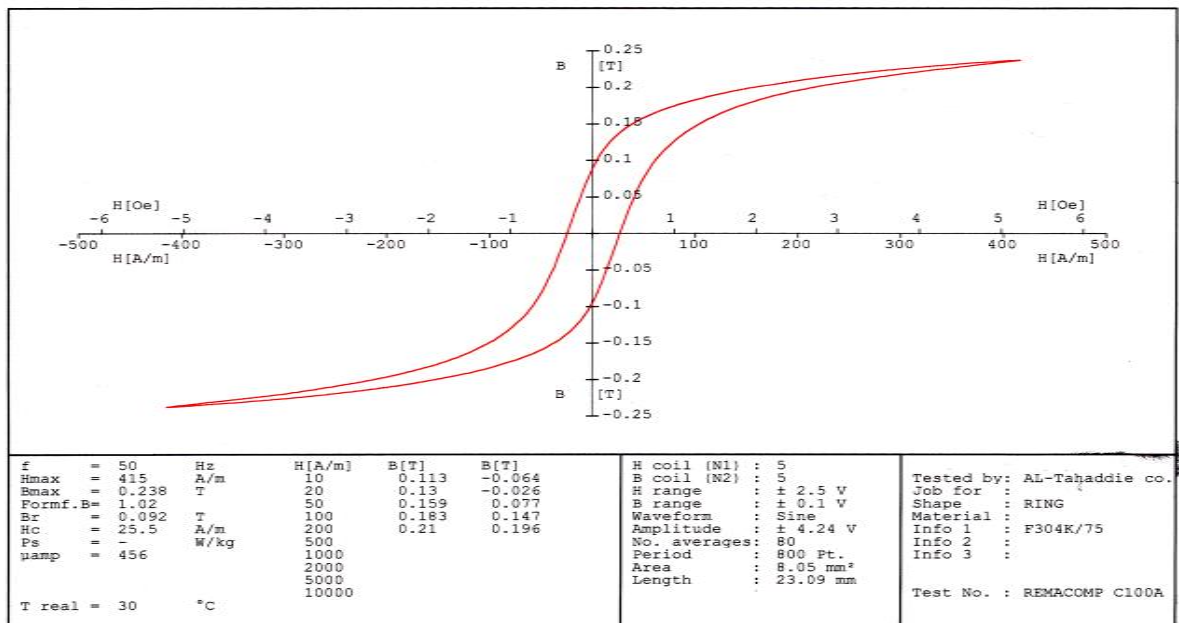
C3 at 1000 °C

Figure (4-14) hysteresis loop of (C3) ferrites sintering at 900,1000 °C

f	=	50	Hz	H[A/m]	B[T]	B[T]
Hmax	=	426	A/m	10	0.041	-0.032
Bmax	=	0.132	T	20	0.047	-0.025
Formf.B=		1.05		50	0.06	2928e-6
Br	=	0.037	T	100	0.076	0.047
Hc	=	44.7	A/m	200	0.099	0.091
Ps	=	-	W/kg	500		
µamp	=	246		1000		
				2000		
				5000		
				10000		
T real =	30	°C				

H coil (N1) : 5
B coil (N2) : 5
H range : ± 2.5 V
B range : ± 0.1 V
Waveform : Sine
Amplitude : ± 4.33 V
No. averages: 80
Period : 800 Pt.
Area : 11.76 mm²
Length : 24.82 mm

Tested by: AL-Tahaddie co.
Job for :
Shape : RING
Material :
Info 1 : f2/53
Info 2 :
Info 3 :

Test No. :

C6 at 900 °C

f	=	50	Hz	H[A/m]	B[T]	B[T]
Hmax	=	416	A/m	10	0.064	-0.042
Bmax	=	0.157	T	20	0.072	-0.02
Formf.B=		1.03		50	0.087	0.048
Br	=	0.055	T	100	0.104	0.089
Hc	=	27.2	A/m	200	0.126	0.122
Ps	=	-	W/kg	500		
µamp	=	299		1000		
				2000		
				5000		
				10000		
T real =	30	°C				

H coil (N1) : 5
B coil (N2) : 5
H range : ± 2.5 V
B range : ± 0.1 V
Waveform : Sine
Amplitude : ± 3.91 V
No. averages: 80
Period : 800 Pt.
Area : 10.46 mm²
Length : 22.15 mm

Tested by: AL-Tahaddie co.
Job for :
Shape : RING
Material :
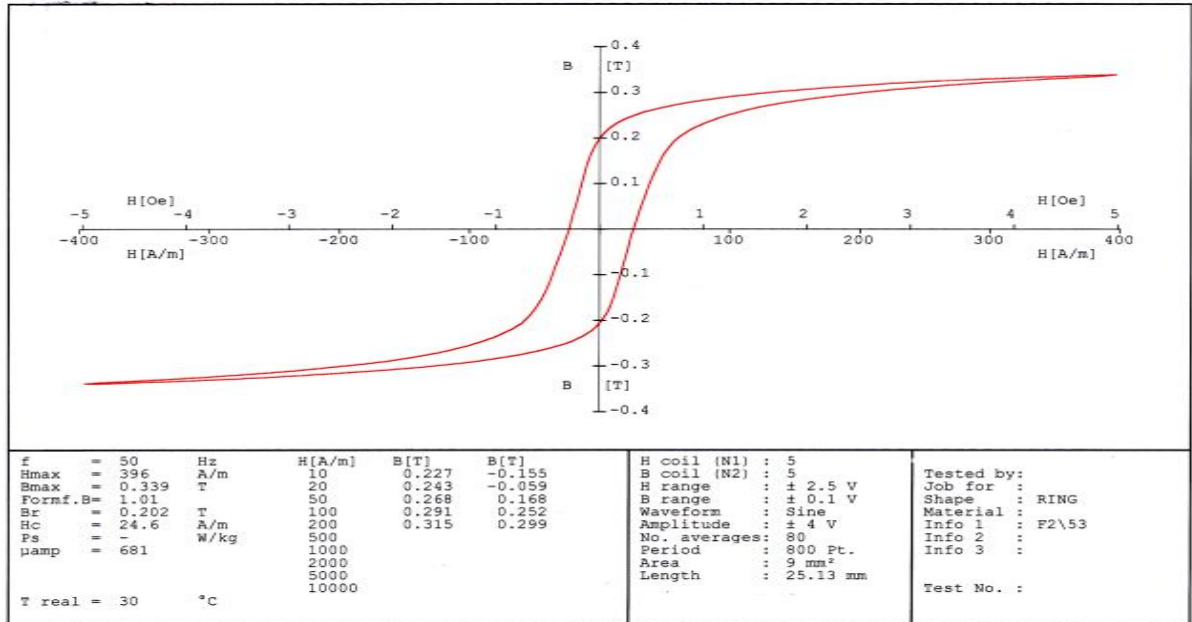Info 1 : F104K/53
Info 2 :
Info 3 :

Test No. : REMACOMP C100A

C6 at 1000 °C

Figure (4-15) hysteresis loop of (C6) ferrites sintering at 900,1000 °C

The figure above shows narrow hysteresis loop for C3, C6 ferrite at 1000 °C, and narrow hysteresis loop for C6 ferrites compared to that of C3 by the increasing in ZnO and decreasing in CuO percentage, and due to insulating properties of ZnO material which cause to resistance increases and eddy currents decrease ,thereby improving the magnetic properties.For the sample C3 sintered at 900 °C the value of remnant magnetization (Br) is 0.202 T, and the Coercive force Hc=24.6 A/m, but for the same sample sintered at 1000 °C it seemed that Br decreased 0.092 T, and Hc=25.5 A/m, it showed Br decrease when sintering temperatures increased.for the sample C6 it showed Br =0.037 T ,Hc=44.7 A/m at 900 °C and Br =0.05 T , Hc=13.3 A/m at 1000 °C

1-2 Literature Review

The history of powder metallurgy and the art of metals and ceramics sintering are intimately related. Sintering involves the production of a hard solid metal or ceramic piece from a starting powder. (PM) according to DeGramo, "While a crude form of iron powder metallurgy existed in Egypt as early as 3000 B.C, and the ancient Incas made jewelry and other artifacts from precious metal powders, mass manufacturing of (PM) products did not begin until the mid-or late- 19th century". In these early manufacturing operations, iron was extracted by hand from metal sponge following reduction and was then reintroduced as a powder for final melting or sintering. By 1860 the fusion method became very popular and almost replaced the powder metallurgy process for making platinum products, because the latter method was found to be quicker and cheaper. Another advancement in the powder metallurgy took place with the manufacture of metallic objects deliberately made porous so that it could be impregnated with lubricants. Several patents were taken including one for the production of bronze materials with graphite around 1910 .Hence, considerable developments took place in the field of powder metallurgy during the late 19th and early 20th century. The production of cemented carbides started in 1922 which revolutionised the machining and metal working industry. From this work many other products developed such as heavy alloys, cemented multicarbides, contact materials etc. using the principle of liquid phase sintering or infiltration techniques. From the sintered porous bronze bearing, other development of products such as porous filters, electrodes etc. and metal-non-metal aggregates such as friction materials took place. Modern applications of powder metallurgy techniques include the processing of ferrites, garnets, piezoelectric materials etc. For electronic industry, beryllium, super alloys and titanium alloys for aircraft and aerospace and a variety of fuel elements for nuclear reactors [8].

In powder metallurgy or ceramics, it is possible to fabricate components which otherwise would decompose or disintegrate. All considerations of solid-liquid phase changes can be ignored, so powder processes are more flexible than

casting, extrusion, or forging techniques. Controllable characteristics of products prepared using various powder technologies include mechanical, magnetic and other unconventional properties of such materials as porous solids, aggregates, and intermetallic compounds competitive characteristics of manufacturing processing (e.g., tool wear, complexity, or vendor options) also may be closely regulated [9].

It is hardly possible to trace the first usage of zinc oxide – Various zinc compounds were widely used by early humans, in various processed and unprocessed forms, as a paint or medicinal ointment, but their exact composition is uncertain. From the 12th to the 16th century zinc and zinc oxide were recognized and produced in India using a primitive form of the direct synthesis process. From India, zinc manufacture moved to China in the 17th century. In 1743, the first European zinc smelter was established in Bristol, United Kingdom [10].

In the recent times, most zinc oxide was used in the rubber industry. In the 1970s, the second largest application of ZnO was photocopying. High-quality ZnO produced by the "French process" was added into the photocopying paper as a filler. This application was, however soon displaced [11].

In 2002, Liqiang Jing et al [12] prepared ZnO ultrafine particles by the thermal decomposition method of the precursor, zinc carbonate hydroxide. The structure and properties of the prepared ZnO were studied using TEM, XRD, Raman, XPS and UV–Vis absorption spectroscopy. It was found that the prepared ZnO exhibited obvious quantum size effect and surface effect. In addition, there were many active species on the surface of ZnO such as oxygen deficiencies and hydroxyls, both of which can improve its photocatalytic activity.

CuO nanoparticles were prepared in 2002, by Hui Wang et al[13] using microwave irradiation. CuO nanoparticles with an average size of 4 nm have been successfully prepared by microwave irradiation, using copper (II) acetate and sodium hydroxide as the starting materials and ethanol as the solvent. The CuO nanoparticles are characterized by using techniques such as X-ray powder diffraction, transmission electron microscopy. The prepared CuO nanoparticles have regular shape, narrow size distribution and high purity. The band gap is estimated to be 2.43 eV according to the results of the optical measurements of the CuO nanoparticles.

Precipitation method was used in 2004, Junwu Zhu et al[14] to prepare CuO nanoparticle by a novel quick-precipitation method where highly dispersed copper oxide (CuO) nanoparticles with an average size of 6 nm. The prepared CuO nanoparticles were characterized by X-ray diffraction (XRD), transmission electron microscopy (TEM), UV–Visible absorption spectroscopy. The results show that the prepared CuO nanoparticles have high dispersion and narrow size distribution. The influence of reaction conditions on morphology of CuO nanocrystals was discussed. Spherical, ellipsoidal and needle-shaped CuO nanocrystals could be obtained simply by varying the reaction temperature and controlling the addition of sodium hydroxide.

Aljosa Kosak et al [15] prepared MnZn-ferrite nanoparticles in 2004. Manganese zinc ferrite nanoparticles were prepared using precipitation in reverse microemulsion system consisting of hexadecytrimethy ammonium bromide (CTAB) as a surfactant, butanol as a cosurfactant,
hexanol as an oil phase and an aqueous solution of metal sulfates. Tetramethy ammonium hydroxide (TMAH) served as the precipitating agent. The influence of the microemulsion`s composition on the nature of the spinel product was studied. The synthesized nanoparticles were characterized by using transmission electron microscopy (TEM), X-ray diffractometry (XRD), specific surface area and magnetometry.

In 2006, Kinnari Parekh et al [16] prepared $Mn_{0.5}Zn_{0.5}Fe_2O_4$ ferrite nanoparticles. A ternary system of $Mn_{0.5}Zn_{0.5}Fe_2O_3$ has been synthesized for the first time using thermal decomposition of metal acetylacetonate in the presence of a high temperature boiling point solvent and fatty acids. Unlike the results of synthesis of this material by other techniques, they obtain nearly monodispersed nanoparticles, rendering them ideal for applications like in hyperthermia. The crystal structure and morphology of the particles obtained using X-ray diffraction (XRD) and transmission electron microscopy (TEM) are those of a single phase spinel structure with no other impurity phases. The particles are of 7 nm average diameter, with a very narrow (<10%) size distribution. The oleic acid surfactant on the particles shows a 28% weight loss in thermo-gravimetric analysis (TGA), which corresponds to a mono layer thickness of the coating. magnetic measurements show the particles to be superparamagnetic with a characteristic blocking temperature of around 50 K.

CuO nanoparticle was prepared in 2007,by Zhanhu Guo et al[17] both unmodified cupric oxide (CuO) nanoparticles and those functionalized with a bi-functional coupling agent methacryloxy propyltrimethoxy silane (MPS) were used to fabricate vinyl-ester resin polymeric nanocomposites. The nanoparticle functionalization was observed to have a significant effect on the physical properties of the cupric oxide filled vinyl-ester resin nanocomposite. Thermal degradation study by thermo-gravimetric analysis (TGA) showed increased thermo-stability in the functionalized-nanoparticle-filled vinyl-ester resin nanocomposites as compared with the unmodified-nanoparticle-filled counterparts. The more uniform particle dispersion and the chemical bond between nanoparticle and vinyl-ester resin were found to contribute to the increased thermal stability and enhanced tensile strength.

Yan Zhu and Yingxue Zhou [18] prepared ZnO nanoparticles in 2008, by the one step solid-state reaction using $ZnSO_47H_2O$ and NaOH as the reagents. By adjusting the molar ratio of the reagents, the unwanted component $Zn(OH)_2$, which is the intermediate product of the reaction, can be fully removed in the final product, and the preparation of pure ZnO nanoparticles are achieved at room temperature. The X-ray diffraction pattern and transmission electron microscopic observations show that these nanoparticles are of hexagonal phase ZnO mostly in round shapes with a minority of rod shape with a mean grain size of about 40 nm.

Manganese-Zinc ferrite was produced in 2008 by Saw Mya Ni and Kay Thi Lwin [19] for electronic applications. Ceramic ferrites are magnetic materials composed of selected oxides with iron oxides. The most common commercial soft magnetic materials are spinel ferrites. The Manganese-Zinc ferrite is preferred for lower frequency applications less than 2 MHz where as Ni-Zn ferrite is preferred for higher frequency, generally for power transformers, power inductors and general power applications. The micro structure and properties of ceramic ferrites depend critically upon the processing conditions. The physical properties and sintering characteristics of, the most ($Mn_{1-x}Zn_xFe_2O_4$) have been carried out for equimolar composition, x =0.5, at three sintering conditions; three sintering temperatures (1100,1200 & 1300 °C) and three sintering times (1, 2 & 3 hr).The X-ray diffraction analysis and scanning electron microscopy were used for phase identification of manganese Zinc ferrites. The physical properties, density and shrinkage of the sample pellets have been studied by dimensional method and the porosity by boiling water method.

In the same year J.M.Yang and F.S. Yen [20] have studied evolution of intermediate phases in the synthesis of zinc ferrite nanopowders by the tartrate precursor method. The advanced electronic applications of zinc ferrite ($ZnFe_2O_4$) material are considered to require improvement in the powder processing, particularly, meticulous particle control in the nanometer range,

stoichiometry and phase purity. The variation of the intermediate phases, crystallite size and chemical composition of the products at different calcination temperatures have been investigated by X-ray diffraction (XRD), Fe^{2+} content analysis, transmission electron microscopy (TEM) and energy dispersive spectrometry (EDS) techniques. Results show that the stoichiometry and phase purity of the resultant zinc ferrite nanopowders have been noted to be highly influenced by their intermediate phases. A single phase, approaching the desirable stoichiometric zinc ferrite nanoparticles,is noted to be possibly prepared by an annealing treatment of the precursor gel powders at 350 °C for 4 hours.

ZnO nanostructures were prepared in 2009 by Doungporn Yiamsawas et al [21] by solvothermal method. This technique is based on thermal decomposition of organometallic compound in organic solvent and has been successfully applied for the synthesis of various types of nanosized metal oxide with large surface area, high crystallinity and high thermal stability.An interesting correlation between aspect ratio of the ZnO products and physical properties of the solvent was observed and presented in this work. The size and morphology for different environmental conditions were investigated. The different environments during ZnO preparation led to the different morphology with width and length in the range of 8.9-69 nm and 68-108 nm respectively. The TEM image clearly reveals that the lattice spacing is about 0.52 Å corresponding to the (001) plane of hexagonal structured ZnO.

D.Sibera et al[22] in 2009 have studied the synthesis and characterization of ZnO doped with Fe_2O_3. They compare two methods of synthesis of nanocrystallline zinc oxide. The synthesis was carried out using microwave assisted hydrothermal synthesis and traditional wet chemistry method followed by calcination. The phase composition of the samples was determined using X-ray diffraction measurements. Depending on the chemical composition of the samples, hexagonal ZnO, and/or cubic $ZnFe_2O_4$ were identified. The morphology of the materials was characterized by using scanning electron

microscopy. Two different structures of agglomerates were observed   to be a hexagonal structure (corresponding to zinc oxide) and spherical (corresponding to spinel phase).The effect of the iron oxide concentration on specific surface area and density of the samples was determined.

Nickel Copper Ferrite was prepared by Y L N Murthy et al [23] in 2009. Nano size nickel copper ferrite powders ($NiCuFe_2O_4$) have been prepared by coprecipitation method. The resulting powders were characterized by X-ray diffraction (XRD),Scanning electron microscope (SEM).The results showed nanosize nickel copper ferrite (35.65nm).The powders showed extensive XRD line broadening and size of crystals observed from the XRD line broadening was 35.65 nm at 1000°C.

In 2010, Shen Xiao-Yi et al [24] prepared ultrafine zinc oxide powder by hydrothermal method with zinc acetate and sodium hydroxide as raw materials, while polyethylene glycol employed as dispersant agent, ultrafine zinc oxide powder was synthesized by hydrothermal method. Influence of NaOH concentration on morphology of ZnO powder was studied. The synthesized ZnO powder looked like flower cluster and consisted of micro rods with hexagonal morphologies. The crystal structure and optical property of the prepared powder were also characterized by using XRD, UV-visible absorption spectrum and photoluminescence spectra, the results indicate that ZnO powder is of hexagonal wurtzite structure and well crystallized with high purity.There is a strong excitation absorption peak at 300 nm in UV-visible absorption spectrum and the blue shift exists obviously.

Kuryliszyn-Kudelska et al[25] In 2010 have studied the magnetic properties of ZnO nanocrystals doped with Fe_2O_3 in the magnetic of   5 to 70 wt%. The nanocrystals were synthesized by wet chemical method. The detailed structural characterization was performed by means of X-ray diffraction and micro-Raman spectroscopy measurements. The results of systematic measurements of magnetic AC susceptibility as a function of temperature and frequency are presented. They observed different types of magnetic behavior for

ZnO samples doped with low content of Fe_2O_3. The results of low-field AC susceptibility are satisfactorily explained by superparamagnetic model including inter-particle interactions, as the increase of magnetic Fe_2O_3 content, the spin-glass-like behavior is observed.

CuO Powders was prepared in 2010 by Zhenyu Du and X.B Sun [26] by direct precipitation method using $CuSO_4$ and NaOH. Then $Cu(OH)_2$ precursor was calcined in muffle furnace at 400℃ for 2h in order to obtain CuO particle. The analysis of the factors affecting the CuO, the optimum conditions for the synthesis of nano-CuO with the direct-precipitation method was studied. Then they analyzed phase composition and crystal structure of samples using XRD and calculated the average grain size of samples by Scherrer formula, and observed and analyzed by TEM to characterize the morphology and the particle size.

In 2010, R. Justin Joseyphus et al [27] investigated superparamagnetic particle size limit of Mn-Zn ferrite nanoparticles synthesised through aqueous method. $Mn_{0.67}Zn_{0.33}Fe_2O_3$ nanoparticles with size ranging from 20 to 80 nm have been synthesized using the modified oxidation method. The Curie temperature for all the samples are found to be within 630 ± 5 K suggesting that there is no size-dependent cation distribution. Mossbauer studies on the nanoparticles synthesis suggest that the critical particle size limit for superparamagnetism is about 25 nm at 293 K.

Precipitation method was used by Amrut. S. Lanje et al [28] in 2010 to prepare CuO nanoparticles. They have studied Synthesis and optical characterization of copper oxide nanoparticles using copper acetate as a precursor and NaOH as a stabilizing agent. This gives a large scale production of CuO nanoparticles easily. X-ray diffraction pattern (XRD) reveals single phase monoclinic structure. Scanning electron microscopy (SEM) showed the rectangular morphology of the prepared CuO nanoparticles. The transmission electron microscopy (TEM) showed 5-6 nm size of prepared CuO nanoparticles.

Photoluminescence (PL) showed band edge emission at 398 nm and green emission at 527 nm. The band edge-absorption peak is found to be at 355 nm.

In 2011, Deepak Bhalla et al [29] presented Mn-Zn soft ferrites manufactured by powder metallurgy and overall output yield of its plant. The efforts have been made to synthesize the crucial parameters which are responsible for better material preparation, pressing and sintering. By adopting these recommendations, The rejection rate is substantially reduced and the variation in magnetic properties is less. Data, which give more uniformity in bigger lots and are responsible for more uniform magnetic properties, have been discussed. Simple, quality-control instruments and their measurement methods which can be incorporated for stage inspection have been explained. Improved pressing, sintering, porosity, density and permeability relationship have been drawn in addition to sintering method to obtain better sintered density and high permeability in ferrites.

CONCLUSIONS

1- The average particle size has been estimated using Debye-Scherrer formula with the average particle sizes being increased as the calcining temperature increases.

2- $[ZnO_X(Fe_2O_3)_{1-X}]$ soft ferrites have a cubic spinel structure, and the particle size increases when ZnO increases. The lattice constant (a) is found to increase with the increase in zinc oxide concentration.

3- Zinc copper ferrite ($ZnO_XCuO_{1-X} Fe_2O_3$) crystallizes either in a tetragonal or cubic symmetry.

4- SEM micrographies show that a network formation of the ZnO has taken place with less number of pores with smaller lump size.

5- SEM images of the synthesized CuO sample with spherical particles is obtained for the sample calcined at 350°C.

6- We can observe that the powders are composed of non-agglomerated flower synthesis of CuO for the sample calcined at 450°C .

7- There is an increase in the density and shrinkage of the sintered pellets with an increase of the sintering conditions such as time and temperature.

8- The ferrite hardness increases with the increasing of the sintering temperatures.

9- The resistivity of the ferrites is observed to decrease with the increase in sintering temperature.

Future work

1-The use of other techniques to prepare (ZnO, CuO, Fe_2O_3) for different nano-forms.

2- Preparing ferrites with ratios of (0.1, 0.3, 0.5) oxides.

3- Sintering of ferrites at temperatures (1100,1200) °C.

4- Using TEM tests for ferrites to know the granular size in smaller size.

5- Test of the thermal conductivity and dielectric constant for the prepared ferrites.

References

[1] G. George," Properties of Ferrite", Demand Media ,(1999).

[2] C.Heck, " Magnetic Materials and their Applications" London: Butterworth, (1974).

[3] R.L.Orban,"New research directions in powder metallurgy "Romanian Reports in Physics, Vol. 56, No. 3, P. 505 - 516,(2004).

[4] S.P.Gubin, Y.u. Koksharov, G. B. Khomutov, G. Y. Yurkov" Magnetic nanoparticles: preparation, structure and properties" Russian Chemical Reviews 74 (6),p. 489 – 520,(2005).

[5] I.Chicinas," Soft magnetic nanocrystalline powders produced by mechanical alloying routes"Journal of optoelectronics and advanced materials,Vol. 8,No. 2, p. 439 – 448,(2006).

[6] A.Lagashettya, V.Havanoorb, S.Basavarajab, S.D.Balajib, A.Venkataramanb," Microwave-assisted route for synthesis of nanosized metal oxides" Science and Technology of Advanced Materials 8,p. 484–493, Elsevier Ltd,(2007).

[7] F.Li, L.Wang, J.B.Wang, Q.G.Zhou, X.Z.Zhou, H.P.Kunkel, G.Williams, " Site preference of Fe in nanoparticles of $ZnFe_2O_4$" J.Magn.Mater., p. 268-332(2004).

[8] P.Ramakrishnan,"History of powder metallurgy" Indian journal of history of science,18(1),p.109-114(1983).

[9] M.Khan, "The Importance of Powder Particle Size and Flow Behavior in the Production of (PM) Parts for Soft Magnetic Applications" Intern.J. Powder Metallurgy and Powder Tech. 16 (2),p.123–130 (1980).

[10] General information of zinc from the national institute of health, WHO, and international zinc association accessed 10 March (2009).

[11] F.Porter, "Zinc Handbook: Properties, Processing, and Use in Design. CRC Press" (1991).

[12] L.Jing, Z.Xu, J.Shang, X.Sun, W.Cai, H.Guo,"The preparation and characterization of ZnO ultrafine particles" Materials Science and Engineering A332 ,p.356–361,(2002).

[13] H.Wang, J.Xu, J.Zhu, H.Chen," Preparation of CuO nanoparticles by microwave irradiation" Journal of Crystal Growth 244,p. 88–94,(2002).

References

[14] J.Zhu, D.Li, H.Chen, X.Yang, L.Lu, X.Wang,"Highly dispersed CuO nanoparticles prepared by a novel quick-precipitation method" Materials Letters, vol.58, p. 3324-3327 (2004).

[15] A.Kosak, D.Makovec, M.Drofenik," The preparation of MnZn-ferrite nanoparticles in awater/CTAB, 1-butanol/1-hexanol reverse microemulsion" phys. stat. sol.(c)1, No. 12, p. 3521–3524,WILEY, (2004).

[16] K.Parekh, R.V. Upadhyay, L. Belova, K. V. Rao,"Ternary monodispersed $Mn_{0.5}Zn_{0.5}Fe_2O_4$ ferrite nanoparticles: preparation and magnetic characterization" Nanotechnology, Vol.17, N.24, (2006).

[17] Z.Guo, X.Liang, T.Pereira, R.Scaffaro, H.T.Hahn,"CuO nanoparticle filled vinyl-ester resin nanocomposites:Fabrication,characterization and property analysis" Composites Science and Technology 67,p. 2036–2044, (2007).

[18] Y.Zhu, "Preparation of pure ZnO nanoparticles by a simple solid-state reaction method" China, Appl. Phys. A 92, p.275–278,(2008).

[19] S.Ni, K.Lwin, "Production of manganese-zinc ferrite cores for electronic applications" World academy of science, engineering and technology 46,(2008).

[20] J.Yang, F.Yen," Evolution of intermediate phases in the synthesis of zinc ferrite nanopowders prepared by the tartrate precursor method" Journal of alloys and compounds 450, p.387–394, (2008).

[21] D.Yiamsawas, K.Boonpavanitchakul, W. Kangwansupamonkon,"Preparation of ZnO nanostructures by solvothermal method" Journal of microscopy society of thailand 23(1), p. 75-78. (2009).

[22] D. Siberaa, R.Jedrzejewskia, J.Mizerackib, A. Preszb, U.Narkiewicza, W.Łojkowskib," Synthesis and Characterization of ZnO Doped with Fe_2O_3- Hydrothermal Synthesis and Calcination Process" Proceedings of the III national conference on nanotechnology nano,V.116, (2009).

[23] Y.Murthy, I.Viswanath, T.Rao, R.singh, "Synthesis and characterization of Nickel Copper Ferrite" International journal of chemtech research , Vol.1, No.4, p. 1308-1311, (2009).

[24] S.Xiaoyi, Z.Yuchun, Z.Yanhui," Preparation and characterization of ultrafine zinc oxide powder by hydrothermal method" Trans. Nonferrous Met. Soc. China 20,p. 236-239, (2010).

References

[25] K.Kudelskaa, B.Hadzicb, D.Siberac, L.Kilanskia, N.Romcevicb , M.Romcevicb, U.Narkiewiczc, W.Dobrowolskia," Nanocrystalline ZnO doped with Fe_2O_3— magnetic and structural properties"International school and conference on the physics of semiconductors, Vol. 119 (2011).

[26] Z.Xihua, X.Min,"Preparation of Nanoscale CuO Powders"Advanced materials research,Vol.113, P.1770-1773, (2010).

[27] R. Joseyphus, A. Narayanasamy, B. Jeyadevan, K. Shinoda, K.Tohji, " Superparamagnetic particle size limit of Mn-Zn ferrite nanoparticles synthesised Through Aqueous Method" Sendai, p.980-8579, Japan (2010).

[28] A. Lanje, S. Sharma, R. Pode, R. Ningthoujam," Synthesis and optical characterization of coppe oxide nanoparticles" Advances in applied science research 1(2), p. 36-40, (2010).

[29] D. Bhalla, S. Aggarwal, G. Govil, I. Kakkar," Manufacturing of manganese-zinc soft ferrite by powder metallurgy" The open materials science journal 4, p. 26-31, (2010).

[30] J. Behera "Synthesis and characterization of ZnO nanoparticles"MSc thesis, National Institute of Technology, India,(2005).

[31] T. Theivasanthi, M. Alagar " X-Ray Diffraction Studies of Copper Nanopowder" Department of Physics, PACR Polytechnic College,India (2010).

[32] K. Zadeh, B. Fry "Nanotechnology-Enabled Sensors " springer, Australia (2008).

[33] C. Raab, M. Simko,U. Fiedeler, M. Nentwich, A. Gazso" Production of nanoparticles and Nanomaterials" Institute of technology assessment of the austrian academy of sciences, No. 006en ,(2011).

[34] A. Bandyopadhyay," Nano materials" New age international publishers, New Delhi, (2008).

[35] N. Goswami, D. Sharma "Structural and optical properties of unannealed and annealed ZnO nanoparticles prepared by a chemical precipitation technique" Physica E:low-dimension nanostructure,vol. 42, p.1675-1682, (2010).

[36] Dti, "Nanoparticle technology: production and application development" A mission to Russia and Ukraine. (2005).

References

[37] A. Hernandezbattez , R. Gonzalez, J. Viesca, J. Fernandez, J. Diazfernandez, A. MacHado, R. Chou, J. Riba, "CuO, ZrO_2 and ZnO nanoparticles as antiwear additive in oil lubricants" Wear ,Vol. 265, P.422-428, (2008).

[38] C. Klingshirn, B. Meyer, A. Waag, A. Hoffmann, J. Geurts," Zinc Oxide: From Fundamental Properties Towards Novel Applications" Sprinerg-verlag berlin heidelberg (2010).

[39] M. Morales, "Fabrication and study of ZnO micro-and nanostructures" MSc thesis, Wright state university (2007).

[40] S. Baruah, J. Dutta, "Hydrothermal growth of ZnO nanostructures" Sci. Technol. Adv. Mater.,Vol. 10, P.013001 (2009).

[41] C . Klingshirn, "ZnO: Material, Physics and Applications" ChemPhysChem, 8(6), p.782-803 (2007).

[42] E. Wiberg, A. Holleman, " Inorganic Chemistry" Elsevier,(2001).

[43] K. Takahashi, A. Yoshikawa, A. Sandhu "Wide Band gap Semiconductors" Springer-Verlag Berlin Heidelberg (2007).

[44] U. Ozgur, I. Alivov, C. Liu, A. Teke, A. Reshchikov, S. Dogan, V. Avrutin, J. Cho, "A comprehensive review of ZnO materials and devices" Journal of applied physics 98,Vol. 98, P.103 (2005).

[45] C. Look, W. Hemsky, R. Sizelove, "Residual Native Shallow Donor in ZnO" Journal physical review letters, Vol. 82, P.2552-2555, (1999).

[46] A. Janotti, G. Van De Walle, "Hydrogen multicentre bonds" Nature Material 6(1), P.7-44 (2007).

[47] H. Kato, M. Sano, T. Yao "Growth and characterization of Ga-doped ZnO layers on a-plane sapphire substrates grown by molecular beam epitaxy" Journal of crystal growth,Vol. 239, P.538-543, (2002).

[48] J. Dwarkadas " Copper (II) oxide" Sanghvi college of Engineering , (2011).

[49] G. Aixia, G. Wang, X. Zhang, B. Fang, " Synthesis of CuO nanoflower and its application as a H_2O_2 sensor" Indian academy of sciences, Bull. Mater. Sci.,Vol. 33, No. 1, P. 17-20, (2010).

References

[50] J. Forsyth, S. Hull ,"The effect of hydrostatic pressure on the ambient temperature structure of CuO" J. phys.:Condens. Matter, Vol. 3, No.28,(1991).

[51] B. Al-Maiyaly "Study the Effect of Annealing and Doping by Halogens on the Optical and Electrical Properties of Fe_2O_3 & Co_3O_4 Oxide Films and Their Mixture" PhD Dissertation, Baghdad University, College of Education (2007).

[52] S. Gautam, S. Kumar, P. Thakur, K. Chae1, R. Kumar, B. koo ,C. Lee "Electronic structure studies of Fe doped ZnO nanorods by x-ray absorption fine structure" Journal of physics D: Applied physics,V.42, No.17,(2008).

[53] C. Barry; N. Grant "Ceramic materials: science and engineering" Springer,(2007).

[54] K. Flaurance." Complex oxides of the system Cu-Ni-Fe-O:synthesis parameters, phase formation and properties" The faculty of mathematics and natural sciences of the dresden university of technology, (2004).

[55] U. Ghazanfar,"Preparation and characterization of ferrite materials for practical applications" university of the Punjab,Lahore, Pakistan (2005).

[56] E. Snelling,"Soft ferrites,properties and application" Butterworth and Co,(publishers) L.T.d, Londn,(1988).

[57] V. Petkov, T. Ohta, Y. Hou, Y. Ren," Atomic-Scale Structure of nanocrystals by High-Energy X-ray Diffraction and Atomic Pair Distribution Function Analysis Nanoparticles" J. Phys. Chem. C 111,p. 714-720,(2007).

[58] H. Keller," X-ray Diffraction" University stuttgart fakultat for mathematic and physic, advanced practical course, (2011).

[59] J.Connolly," Elementary Crystallography for X-Ray Diffraction" Introduction to X-Ray powder diffraction, Spring, (2012).

[60] A. Goldman, "Modern ferrite technology "Van nostrand reinhold, New York,(1990).

[61] K. Batoo, M. Ansari"Low temperature-fired Ni-Cu-Zn ferrite nanoparticles through auto-combustion method for multilayer chip inductor applications"Nanoscale Research Letters 7, p. 112, Springer, (2012).

[62] M. Ahmed, N. kasha, S. Dek1" Preparation and characterization of nanometric Mn ferrite via different methods" Nanotechnology 19, p.6(2008).

References

[63] R. Morjan, S. Prasalovich" Magnetic Hysteresis" chalmers university of technology (2003).

[64] E.Pcos, A.G. " Ferrites and accessories" Siferrit material N87,(2006).

[65] A. sinha,"powder metallurgy", 2nd Ed.,Dhanpat Ral&Sons, Delhi, (1987).

[66] D.Garmo's," Materials and Processes in Manufacturing";Wiley, 10th Edition, (2007).

[67] D. William, "material science and engineering an introduction" John wiley &son ,Inc , p.676-681, (2000).

[68] L. Mark, M. Weaver " Powder Metallurgy" Chapter 7, Reading: p. 449,(2011).

[69] S. Feldbauer," Advances in Powder Metal Sintering Technology", Abbott Furnace Company, St. Marys, PA 15857.

[70] S. Nath, D. Chakdar, G. Gope " Synthesis of CdS and ZnS quantum dots and their applications in electronics" Nanotrends- A journal of nanotechnology and its application,02(03) (2007).

[71] B. Hall, D. Zanchet, D. Ugarte "Estimating nanoparticle size from diffraction measurements" Journal of applied crystallography, Vol. 33, Part 6 (2000).

[72] J.Serway "Physics for scientists and engineers with modern physics" seventh Edition ,(2008).

[73] H. Cheng, J. En, W. Vong, H. Ta, Y. Liang "Porous ferrite synthesis and catalytic effect on benzene Degradation" International journal of the physical sciences, Vol. 6(4), p. 855-865, (2011).

[74] Y. Li "Synthesis of Copper(II) Oxide Particle and Detection of Photoelectrochemically Generated Hydrogen" Chemical Engineering, University of California, Davisin (2008).

[75] L. Zhang, F. Yuan, X. Zhang, L. Yang" Facile synthesis of flower like copper oxide and their application to hydrogen peroxide and nitrite sensing" Chemistry Central Journal, Vol.5, p.75 (2011).

[76] A. Verma, T. Goel, R. Mendiratta, R. Gupta" High-resistivity nickel zinc ferrites by the citrate precursor method" Journal of Magnetism and Magnetic Materials 192 ,p.271-276 (1999).

References

References

References

Republic of Iraq
Ministry of Higher Education and
Scientific Research
University of Diyala
College of Science
Department of physics

Preparation and characterization of some nano metal oxides and their ferrites

Submitted by

Zena Mohammad Ali Abbas Rasool Al-Bana

In partial fulfillment for the requirement of the Degree of
Master of Science in Physics

Supervised by

Assistant Professor　　　　　　　　　　Assistant Professor

Dr. Tahseen H. Mubarak　&　Dr. Karim H.Hassan

2012 م　　　　　　　　　　　　　　　　　ه **1433**